CARBON-13 IN HYDROLOGICALLY-CLOSED SYSTEMS: EXPERIMENTATION AND MODELING

By

Alyssa Joy Olson

Submitted in Partial Fulfillment
of the Requirements for the

Masters of Science in Hydrology

New Mexico Institute of Mining and Technology
Department of Earth and Environmental Science

Socorro, New Mexico

May, 2002

ABSTRACT

Information about quaternary paleoclimatology has been dominated by marine and ice core records, but these data do not provide direct information on mid-latitude continental paleoclimate. However, one source of continental records is sediments deposited in closed-basin lakes. Data on $\delta^{13}C$ and $\delta^{18}O$ measured in calcite from closed-basin lake sediments suggest a relationship, or covariance between these isotopes. As the $\delta^{18}O$ becomes enriched so does the $\delta^{13}C$ during the hydrologically closed periods of the lake's history. Covariation of $\delta^{13}C$ and $\delta^{18}O$ has been considered diagnostic of closed-basin lacustrine sediments, but the mechanism of this covariation remains controversial. The main factors that affect $\delta^{18}O$ in a closed-basin lake are vapor exchange and hydrologic balance. On the other hand, the mechanisms for $\delta^{13}C$ variation in closed lacustrine basins are not clearly understood. Several hypotheses, including vapor exchange, hydrologic balance, lake productivity, and CO_2 degassing have been put forward to explain $\delta^{13}C$ variation but none have been tested experimentally.

This work involves experimentally determining the effects of CO_2 degassing on carbon isotope evolution. The hypothesis is that in alkaline lakes, the exchange of CO_2 with the atmosphere, as a function of lake volume, dominates the carbon isotope dynamics. Verification of this hypothesis will allow the carbon isotope history of such

lakes to be modeled, thereby enhancing the value of the paleoenvironmental records obtained from lacustrine carbonates.

In a series of simple experiments, we approximated a closed-basin lake using three chemically different solutions; a deionized water control, a Na-HCO_3 solution and a Ca-Na-HCO_3-Cl solution. The solutions were allowed to evaporate in three large tanks. Once the final evaporation point was reached, deionized water was added in a series of five steps until returning to the original volume.

The dissolved inorganic carbon $\delta^{13}C$ and $\delta^{18}O$ measurements in both the Na-HCO_3 and Ca-Na-HCO_3-Cl solutions indicated different covariant trends during different stages of the experiment. The calcite that precipitated in the Ca-Na-HCO_3-Cl solution also showed a covariant trend for these isotopes. The final $\delta^{13}C$ values in both solutions confirmed the absence of biological productivity. The covariation observed in both solutions was a direct result of the geochemical evolution of the solution. The ^{18}O isotopes showed an evolution consistent with Rayleigh distillation. The ^{13}C isotopes, however, appeared to be driven mostly by CO_2 exchange with the atmosphere, which could be calculated with a carbon exchange and degassing model rather than with Rayleigh distillation.

ACKNOWLEDGEMENTS

This work was funded in part by Geological Society of America, Grant No. 6511-99 for isotope measurements. The author respectfully wishes to thank the following people and groups for their contributions and support: Fred Phillips, Ph.D., Andy Campbell, Ph.D., Rob Bowman, Ph.D., D. Mike Chapin, Sam Earman, Barret Cole, Dr. Phillips' Research Group, Jan Hendrix, Ph.D., and Andrew Wolfsberg at Los Alamos National Laboratory. The New Mexico Bureau of Mines Chemistry Labs; Barb Popp and Lynn Branvold for their assistance with chemical analysis and New Mexico Bureau of Mines for XRD analysis. I wish to acknowledge the support and example of my father, Tom Olson, who made the pursuit of an advanced education possible. Tim Callahan, husband; thank you for always being supportive and understanding.

TABLE OF CONTENTS

Page

LIST OF TABLES

Page

LIST OF FIGURES

Page

1. INTRODUCTION

In recent decades, quaternary paleoclimatology research has been dominated by the study of marine and ice core records, but these records do not provide direct information on mid-latitude continental paleoclimate. Lake cores have been identified as a potential source for this information. In the course of research in this area, an interesting relationship has been identified between $\delta^{13}C$ and $\delta^{18}O$ in the primary carbonate sediments present in the some of the lake cores (Stuiver, 1970; Fritz, et. al, 1975; Spencer, et. al, 1984; Gasse, et. al, 1987; Gasse and Fontes, 1989; Talbot, 1990; Johnson et. al, 1991). The relationship is a linear covariant trend between $\delta^{13}C$ and $\delta^{18}O$. A similar covariation has been observed in the biological deposits from closed-basin lakes (Talbot, 1994).

Talbot (1990) presented an extensive review of the information collected from modern hydrologically closed and open lakes and proposed the following criterion for discriminating between open versus closed conditions. If a strong correlation coefficient for the linear covariation ($R^2 > 0.7$) is found between the $\delta^{13}C$ and $\delta^{18}O$ data pairs measured from carbonate sediment samples, then the lake was probably hydrologically closed during the period that the samples were deposited. If the data show a weak correlation coefficient ($R^2 < 0.7$) then the lake was most likely open during that period. The distinction between open and closed-basin lakes is important because evaporation is

the only outflow mechanism in a hydrologically closed lake whereas open lakes have multiple outflows for example, evaporation and river outflow. Modern closed-basin lakes such as Lake Turkana (Kenya), the Great Salt Lake (Utah, USA), Van (Turkey), Natron-Magadi (Kenya-Tanzania), Lake Bostumtwi (Ghana), and Rukwa (Tanzania) have covariant correlations greater than 0.7, while modern open lakes such as Henderson Lake (USA), Huleh (Israel), Greifensee (Switzerland), Lobsifensee (Switzerland) and Little (Canada) have correlations less than 0.7 (Talbot, 1990). Talbot (1990) examined core records from six different ancient lacustrine basins and applied the criterion obtained from modern lakes in order to decide if the ancient lakes were open or closed. Such an indicator potentially has widespread application to interpreting continental paleoclimate records. While covariation of $\delta^{13}C$ and $\delta^{18}O$ may often be diagnostic of closed-basin lacustrine sediments, the mechanism causing the covariance remains poorly understood.

The mechanism for $\delta^{18}O$ enrichment is generally accepted as being due to hydrologic balance and evaporation. Oxygen -16 is preferentially removed during evaporation, causing the lake water to become enriched in oxygen-18. This also leads to enrichment of carbonate ions with respect to oxygen-18.

There are at least two mechanisms that can enrich $\delta^{13}C$ in the lake. One is biological and the other geochemical. The most commonly cited hypothesis to explain $\delta^{13}C$ enrichment in shrinking closed-basin lakes is related to increased biological productivity (McKenzie, 1984; Benson, 1995; Li et. al, 1997); it states that evaporation results in increased concentrations of nutrients in the remaining lake water, leading to a period of increased biological production. Biological organisms preferentially

incorporate the carbon-12 relative to carbon-13, causing the dissolved inorganic carbon in the lake water to become enriched in carbon-13 and thus the primary carbonate deposited is heavier. Periods of increased biological productivity strongly influence the carbon isotope composition of the lake water. The biological increase in productivity may be due to either periods of increased evaporation or decreased freshwater input. At the same time, the geochemical mechanism is important. The lake is evaporating and becoming more alkaline. This also causes the pH to increase. The increase of pH causes degassing of CO_2 from the lake, preferentially removing carbon-12 and enriching the lake water in carbon-13.

These two mechanisms are sometimes referred to as the coupled evaporation-productivity effect (McKenzie, 1984; Benson, 1995; Li et. al, 1997). It is important to uncouple the evaporation-productivity effect in closed-basin lake systems. It is critical to clarify the relative contributions of evaporation and productivity to the formation and maintenance of a covariant trend in order to understand the isotopic records of lakes. Many lakes in the southwestern United States show strong linear covariance between the carbon-13 and oxygen-18 isotopes, but do not exhibit evidence of high biological productivity. This suggests that increased biological productivity may not always be a necessary component of the covariant trend. Owens Lake, California, is an example of a lake where the evaporation component may outweigh productivity, because cores show less than 3% total organic carbon (Smith, 1997).

The two mechanisms for carbon-13 enrichment described above have been discussed extensively; however, experimental testing demonstrating the cause of covariance between ^{18}O and ^{13}C has been very limited. The objective of the work

described here was to test the extent of covariant fractionation of oxygen-18 and carbon-13 that could be produced by evaporation and carbon dioxide degassing in a hydrologically closed system without the influence of biological productivity. Experiments were designed to examine the hypothesis that the degassing of carbon dioxide from a body of water undergoing evaporation is sufficient to enrich $\delta^{13}C$ and create a covariant trend in the primary carbonate sediments and the in remaining solution. The experiments consisted of evaporating three solutions: 1) a sodium bicarbonate solution that was free of calcium, 2) a bicarbonate solution containing calcium that was intended to precipitate calcite, and 3) a deionized water solution used as a control. The effects of refilling a lake were mimicked by rehydrating the experimental solutions with deionized water.

2. METHODS

2.1. Experimental Design

The design of the experiment consisted of two phases, evaporation and hydration of three chemically different solutions. The hydration refers to the addition of deionized water to the remaining solution in the tanks. Large tanks were used to mimic a shallow lake environment where the surface area was large relative to the depth. The experiment closely imitated a natural closed-basin lake setting with two important differences: 1) little to no wind velocity across the surface of the solution, and 2) the residence time for the solution was much shorter than in closed-basin lakes. A closed-basin lake will have a residence time on the order of years, compared to the 6-month duration of this experiment. However, the tanks represented a truly closed-basin hydrological system where the only outflow was by evaporation.

Each tank was made of heavy-duty plastic, so there were no interactions between the tank material and the solutions. The deionized water tank was 18 x 41 centimeters and the two chemical solution tanks were 28 x 55 centimeters. Prior to the addition of any fluid, the volume to depth relations of the tanks were calibrated in 2-liter increments by means of volumetric additions of 2-liters of water. An additional soft plastic ruler was

added to the tank the sides of the tank to refine the volume measurements below 2-liter increments.

Fifty liters of deionized water, purchased from The Water and Ice Store of Socorro, New Mexico, were placed in each of the three tanks in the Drip Lab room. A copy of the routine chemical analysis of the water was obtained (Table 1) and ions of interest to the experiment, such as calcium or bicarbonate, were negligibly low in concentration. The control tank contained only deionized water and was not used in the phase-two hydration, but continued to evaporate. The chemicals were added to the water in each tank and mixed in place. The Na-HCO_3 solution tank was mixed to a target concentration of 0.5 g/L of sodium bicarbonate ($NaHCO_3$). The target mass of sodium was 6845 mg, the measured mass was 7000 mg giving an error of -2.5%. The sodium measurements were made according to the method described in section 2.4.1. The $NaHCO_3$ was off-the-shelf Arm and Hammer Baking Soda, which had a light $\delta^{13}C$ (-19‰), an identifiably different signature from atmospheric $\delta^{13}C$ (~-7‰). The Ca-Na-HCO_3-Cl solution tank was mixed to a target concentration of 0.5 g/L of sodium bicarbonate (using the same Arm and Hammer soda) and 0.5 g/L of calcium chloride ($CaCl_2 \cdot 2H_2O$). The target mass was 6845 mg of sodium, the actual measured mass was 6766 mg, giving an error of 1.15%. The calcium chloride source was Aldrich Chemicals, Catalog number 22,350.6, Lot No. 06108TW. The concentrations of the Ca-Na-HCO_3-Cl solution were chosen so that the solution was initially saturated with respect to calcite, and thus within the first few evaporation steps the solution would be supersaturated, and a precipitate would form. The target mass of calcium was 6849 mg and the measured mass

after mixing was 3700 mg, suggesting that even though calcite precipitate was not visible in the solution, that calcium was being removed even at the initial mixing. All three of the solutions were allowed to evaporate until the fraction of original water remaining (f) was below 0.1 and the carbonate (CO_3) concentration in solution was at least 60 percent of the bicarbonate (HCO_3). Overall, twenty-three samples each were taken from the Ca-Na-HCO_3-Cl and Na-HCO_3 solutions during the five months of the evaporation process and twenty-eight samples from the deionized water during the six-month experiment.

Analysis	PPM	Analysis	PPB	Analysis	PPB
Chloride (Cl)	<1.0	**Arsenic (As)**	<4	**Zinc (Zn)**	26
Sulfate (SO_4)	<2	**Cadmium (Cd)**	<0.6	**Be**	<0.5
Nitrate (NO_3)	0.29	**Copper (Cu)**	11		
Fluoride (F)	<0.2	**Iron (Fe)**	3		
Sodium (Na)	<0.05	**Lead (Pb)**	<1		
Potassium (K)	<0.02	**Manganese (Mn)**	3		
Magnesium (Mg)	<0.03	**Silica (SiO_2)**	14 ppm		
Calcium (Ca)	<0.01	**Silver (Ag)**	<1		
pH	5.5	**Conductivity ($\mu mhos/cm^2$)**	10		

Table 1 Water quality analysis for the source of deionized water used in all phases of the experiment. Analysis performed and reported by the New Mexico Bureau of Mines and Natural Resources Chemistry Laboratory.

During the hydration phase, intended to mimic a refilling lake, deionized water was added back to the Na-HCO_3 and Ca-Na-HCO_3-Cl tanks in five steps returning the solution to the original 50 liters. For each step, approximately 12 liters of deionized water, from the same source, and purged with nitrogen gas for at least 6 hours to remove dissolved CO_2, was added to the remaining evaporate solution. The dissolved CO_2 was removed from the water prior to addition so that the new solution would pull in

atmospheric CO_2 and the isotopic and geochemical changes associated with absorption of could be observed. The tanks were allowed to reach a steady pH value before a new addition was made, which generally took five days. Over the five days, approximately two liters of solution were lost to evaporation, resulting in a net addition of 10 liters to each of the two tanks. A sample was collected from each tank after the solutions reached a steady pH value and before a new addition was made. Overall, five samples were taken during the month-long hydration phase of the experiment, bringing the total number to twenty-eight for the Na-HCO_3 and Ca-Na-HCO_3-Cl solutions.

A Davis Weather Monitor (model no. 7440) and later a Davis Perception II (model no. 7400) were installed near the tanks for most of the experiment to record weather conditions. Temperature, relative humidity, and barometric pressure were measured every 30 minutes. Two breaks in the weather record were due to failure of the first monitor and a power surge to the replacement monitor. Temperature, relative humidity, and barometric pressure figures are presented in Appendix E. Cardboard covers were put in place on the walkway guard rails approximately six inches above the tanks to help limit contamination from dust and other airborne debris and to limit light that might encourage the growth of organisms.

2.2. Sampling and Sample Preservation

The following procedure was used for each sampling during both the evaporation and hydration phases of the experiment. First, the cardboard covers were removed. The water levels at both the 2-liter calibration marks and the plastic ruler marks were recorded. All polyurethane sample bottles, (previously washed, rinsed with dilute nitric

acid and deionized water, and allowed to dry), were labeled with the sample number, tank name, and analyses to be performed. The pH meter and the electrical conductivity meter were calibrated, and the respective measurements from each tank were recorded. Using 100 mL Nalgene syringes that were dedicated to each tank, water samples were removed. Each sample contained 175 mL and was split into sub-samples: 100 mL was used for carbon-13 and oxygen-18 analysis of carbonate ions in solution, 50 mL for measurement of alkalinity, 5 mL for oxygen-18 and deuterium associated with the water molecules, and 20 mL for sodium and calcium analysis. The cardboard covers were then returned to their previous position.

The same procedure was used for the hydration phase. Once the pH measurements began to cluster around a single value, the samples were collected, and the deionized water was added. The water volume was recorded prior to sampling, both before the water addition and after the water addition. The water used for the additions was stored in 50-liter carboys. Approximately 20 liters were transferred to a 20-liter carboy and bubbled with nitrogen gas for approximately six hours to reduce the amount of dissolved CO_2 in the solution. This water was then added slowly back to each tank through a Nalgene tube to reduce mixing with the atmosphere prior to contact with the solution. Once the deionized water had been added, pH measurements were made every few minutes for 1.5 hours and then every couple of days until the measurements began to cluster around a similar point.

Calcite precipitate samples were periodically collected from the evaporating solution of Na-Ca-HCO_3-Cl. Plastic trays commonly used for weighing chemicals were placed at the bottom of the tank and allowed to gather precipitating calcite. The trays

were removed and the precipitate rinsed onto filter paper with deionized water. The filter paper, Gelman Science Tuffryn Membrane Filters, .47 mm, .45µm, (Catalog number 66223, lot numbers 501308 and 81346), and the precipitate was oven dried at 100°C, and allowed to cool. The precipitate was weighed and stored in sealed plastic containers until analysis.

Samples collected for analysis of carbon-13 and oxygen-18 of the carbonate ions in solution were preserved according to the procedure given by Fritz (1980). The pH of the 100 mL was quickly adjusted to above 10 with the addition of 1mL of 1 M sodium hydroxide (NaOH). The sodium hydroxide solution was prepared by adding 4.0 g of NaOH pellets (Fisher catalog number 8-315; lot number 7208600) to 100 mL of deionized water. Then, fifteen grams of barium chloride ($BaCl_2$ Fisher, catalog number B-33), was added to the sample. After mixing, a barium carbonate ($BaCO_3$) precipitate soon formed and was allowed to settle for at least 48 hours. The solution was then filtered using Gelman Science Tuffryn Membrane Filters, .47 mm, .45µm, (Catalog number 66223, lot numbers 501308 and 81346). The filtrate was oven dried at 100°C, allowed to cool, weighed, and stored in sealed plastic containers until analysis. The recovered filtrate weights are listed in Appendix B.1. The 5-mL samples used for oxygen-18 and deuterium analyses were placed in a 30-mL glass sample vial with a Poly-Seal screw cap for storage until analysis. The rest of the samples were reserved for alkalinity (50 mL), and sodium and calcium (20 mL) analysis and stored in 125-mL Nalgene bottles in a refrigerator until analysis.

2.3. Isotopic Analysis

All samples prepared by the methods described below were run on the Finnigan MAT Delta E mass spectrometer located in the Stable Isotope Laboratory at New Mexico Tech. Samples were compared to the appropriate standard gas produced by Oz Tech Trading Corporation. The final isotopic data are in Appendix C.4. and the intermediate processing data are in Appendix C.1. and C.2.

2.3.1. Oxygen-18 (Water) Analysis by CO_2/H_2O Equilibration Methods

The determination of the oxygen-18 in H_2O in a water sample requires equilibration with CO_2 gas with a known isotopic value. The method described here follows the method of Cohn and Urey (1938) with the pre-evacuated container modifications described by Socki et al. (1992). The equilibration was done in evacuated blood vials that were filled with approximately 150 µmol of cleaned CO_2 gas. The amount of gas in the equilibration vessel was determined by using a mercury manometer and the following empirical equation that was derived for this laboratory setup:

$$CO_{2\ \text{Blood Reaction Vessel}} = 0.002 * (P_{\text{Manometer}})^2 + 6.4292 * (P_{\text{Manometer}}) \qquad (1)$$

where $P_{manometer}$ is the difference in height on the two sides of the manometer and $CO_{2\ \text{Blood Reaction vessel}}$ is the amount of gas in µmol. The gas was cleaned by forcing it through a water trap surrounded by solid CO_2 and alcohol and then into a CO_2 trap surrounded by liquid nitrogen where the non-condensable gases were removed using a vacuum pump. A sample of 1 mL was put into the reaction vessel using a 1-mL medical syringe. The cleaned CO2 is reheated and added to the reaction vessel along with the water sample.

The vessels containing samples and cleaned CO_2 gas were placed in a water bath with a known constant temperature and shaken for 4 hours at a speed of ~300 Hz to promote equilibration.

Once the sample was equilibrated, the CO_2 was extracted on a glass vacuum extraction line. Again, the water trap and the CO_2 trap were used to clean and capture the sample gas. The percent yield of CO_2 was calculated by comparing the quantity of CO_2 gas extracted from the blood reaction vessel to the quantity of CO_2 gas introduced into the blood reaction vessel prior to equilibration.

The raw data from the mass spectrometer gives the final oxygen-18 ($\delta^{18}O^f$) of the water. The initial oxygen-18 ($\delta^{18}O^i$) value of the water was determined from the set of equations given by Campbell and Larson (1998) for a water dominated system:

$$\delta^{18}O^{i}_{H_2O} \text{ (Inital Water)} = \delta^{18}O^{f}_{H_2O} - \Delta_{CO_2 \rightarrow H_2O} \qquad (2)$$

where $\Delta_{CO2 \rightarrow H2O}$ is the temperature-dependent fractionation

$$\Delta_{CO_2 \rightarrow H_2O} = -0.021 * (10^6 / T^2) + 17.994 * (10^3 / T) - 19.97 \qquad (3)$$

and T is temperature in Kelvin.

2.3.2. Deuterium (Water) Analysis Methods

The analysis of deuterium employed the liberation of hydrogen gas by the reaction of water with elemental zinc at high temperatures, following the method of Coleman et al (1982). Solid zinc (300 mg) was loaded in reaction vessels and slightly heated under a vacuum to remove any water vapor. The vessels were allowed to cool and 3 μL of the sample was placed into the reaction vessel using micropipet. This created an 83:1 molar

ratio between the zinc and the sample, thus eliminating the potential for fractionation of the hydrogen gas. The reaction vessel and the water sample were quickly frozen with liquid nitrogen. Any atmospheric gases introduced to the reaction vessel during the introduction of the micropipett were removed under vacuum. The samples were returned to air temperature and then baked at approximately 450°C for 30 minutes. The reaction vessels were allowed cool to air temperature, and then placed directly on the mass spectrometer for analysis. Three standards, prepared in the same manner as the samples, were also measured to provide the correction equation. The standards used here were VSMOW (Vienna Standard Mean Ocean Water), SLAP (Standard Light Antarctic Precipitation), and GISP (Greenland Ice Sheet Precipitation). The correction was determined by plotting the actual values versus the measured values and determining the equation of the best-fit line.

There is some fractionation but by keeping the water-to-zinc ratio constant, the fractionation is constant. The water standards are measured under the same conditions effectively canceling out the fractionation effects.

2.3.3. Carbonate analysis by CO_2 Extraction

Analysis of the barium carbonate precipitate and calcite precipitate required reaction with 100% phosphoric acid in a vacuum. The reaction was as follows

$$3BaCO_3 + 2H_3PO_4 \leftrightarrow 3Ba^{2+} + 2PO_4^{3-} + 3H_2O + 3CO_2 \qquad (4)$$

The carbon was evolved into carbon dioxide gas and was measured directly; however, the measured oxygen isotope composition must be corrected. For these analyses, one batch of acid was used and the acid fractionation factor (AFF) was 10.4‰. The AFF accounts

for the one third of oxygen fractionated in the formation of water molecules. The oxygen-18 was calculated according to the following relationship

$$\delta^{18}O_{\text{Actual}} = \delta^{18}O_{\text{Measured}} - AFF \quad (5)$$

A special reaction vessel was used to conduct the reaction. The glass reaction vessel had a divider at the bottom so that a known amount of sample can be placed on one side and the phosphoric acid on the other. The vessel was then sealed and placed under a vacuum for at least four hours, then the vessel was removed from the vacuum and "tipped" to allow the acid to cross over the divider and react with the sample. This reaction was allowed to proceed for at least eight hours. The evolved gas was then cleaned and measured as described in Section 2.3.1.

2.4. Chemical Analysis

2.4.1. Sodium and calcium analysis

Sodium and calcium analysis was conducted on a Video 12 (atomic adsorption/atomic emission) spectrophotometer. The spectrometer and the standards were maintained by the New Mexico Bureau of Mines and Natural Resources Chemistry Labs. Calcium was analyzed at a wave length of 422.7 nm. Sodium was analyzed at either 589.6 or 332 nm depending on the concentration of the sample. A standard curve was recorded so the concentrations of the samples could be directly reported by the instrument. The machine was programmed to take five measurements and compute the average concentration based on the accepted calibration curve. Duplicates were performed on dilutions.

2.4.2. Alkalinity determinations

The alkalinity determinations were made according to titration method 2320 B., found in The Standard Methods of Water and Waste Water Analysis, [1996].

Standarizing the Acid

Standard sulfuric acid was used as the titrant. A 1-liter solution of 0.1 N H_2SO_4 was made by mixing 2.8 mL of concentrated reagent grade sulfuric acid with 997.2 mL of deionized water. The acid was standardized against 40 mL of 0.05 N Na_2CO_3 solution mixed with 60 mL of deionized water. The solution was titrated to a pH of 5.0 and then boiled gently for five minutes under a watch glass. The solutions were allowed to cool to room temperature, cover condensate on the watch glass was rinsed into beaker, and titrated to the pH inflection point of 4.5. The normality, N was calculated according to

$$N = \frac{A * B}{53.00} * C \qquad (6)$$

where, A is the Na_2CO_3 weighed into 1-L flask, B is the mL of Na_2CO_3 solution taken for titration, and C is the mL for acid used. The normality for the acid used in these titrations was determined to be 0.09 after doing the standardization in duplicate.

Measuring the Samples

The pH meter, an Orion model 250A (serial number 010457) with a replaceable sealed probe, model number 910DN, was calibrated using Orion pH buffer solutions, pH 10 (catalog number 911060) and pH 7 (catalog number 910760). An Orion pH 4.0 buffer was used as a check solution for the low end of the curve. A 50 mL aliquot of the sample was measured into a beaker and placed on a stir plate. The pH meter was placed in the sample for the initial pH measurement. The sample was gently stirred to reduce

excessive mixing with the atmosphere or degassing. Once equilibrium was established, the sample was titrated immediately, allowing only for equilibration of the added acid addition, to endpoints of 8.3 and 4.5. The amount of acid was recorded and the total phenolphthalein alkalinity or carbonate alkalinity was calculated according to

$$\text{Alkalinity, eq / L} = \frac{A * N}{S} \qquad (7)$$

where, A is the amount of acid used in the titration, mL, N is the normality of acid, eq/L, and S is the amount of sample titrated, mL.

2.4.3. pH and Electrical Conductivity determinations

To determine the pH of the water tanks over the course the evaporation, the following procedure was followed. The pH meter was calibrated using Orion pH buffer solutions, pH 10 and pH 7. To obtain a pH measurement from within the tanks, the probe was gently agitated in the solution, avoiding unnecessary atmospheric mixing but sufficient to obtain a representative measurement. When the meter had stabilized, the value was recorded.

The electrical conductivity of the solution was determined using a YSI 85 Oxygen Conductivity Salinity & Temperature meter. This probe was placed in the solution in a manner similar to the pH measurement. Equilibrium was assumed when the reading stabilized around one value. The meter calibration was occasionally checked using 124 and 1186 μS/cm solutions. A complete listing of all chemical analyses is presented in Appendix D.

2.4.4. Confirmation of Calcite Precipitate in the Ca-Na-HCO_3-Cl solution

Calcite was first observed in the Ca-Na-HCO_3-Cl solution at f = 0.95. The precipitate did not immediately settle out to the bottom of the tank. Instead it formed a surface film that adhered to the sides of the tanks and any instrumentation or sampling device inserted into the solution. A flocculant was used to induce settling of the precipitate for sample collection. The use of a flocculant is a standard procedure in the preparation of field samples for carbon-14 analysis (Fritz, 1980). The flocculant, Percol, was added one time to the Ca-Na-HCO_3-Cl solution during the evaporative phase of the experiment at an f = 0.89. Percol is a Poly(DiallyDimethylammonium Chloride) and was mixed 2.5 g Percol to 500 mL deionized water. The addition of the 500 mL Percol solution did cause the calcite produced during the subsequent portion of the experiment to flocculate and settle. Calcite samples were collected and analyzed at f = 0.87, 0.62, 0.41, and 0.02. The weights of calcite precipitate collected are listed in appendix B.1.,Table 4.

X-Ray Diffraction (XRD) measurements of the collected precipitate were made by the New Mexico Bureau of Mines. The samples were determined to be calcite with trace amounts of vaterite, a polymorph of calcite. Kim et al. (1997) noted the common occurrence of vaterite-calcite mixtures when nitrogen gas was bubbled through aqueous solutions. The bubbling of N_2 gas through solutions caused degassing of CO_2, which is similar to the degassing processes found in evaporating solutions. The degassing of CO_2 that occurred during the evaporative phase of the experiment is the most likely cause of trace amounts of vaterite in the collected precipitate. Precipitation of calcite was not observed during the hydration phase of the experiment.

3. CONCEPTUAL AND BACKGROUND INFORMATION

This section describes the expected interactions for chemical and isotopic constituents during the evaporation and hydration of the control deionized water, Na-HCO_3 and Ca-Na-HCO_3-Cl solutions.

3.1. Chemical Interactions during the Experiment

Conservative components of the experimental solutions should become concentrated with the removal of water and the subsequent hydration steps should dilute these components. The Na^+ ions in the Na-HCO_3 solution should be conservative because there was no potential for loss though precipitation of solid phase or through volatilization. The only deviations from the expected concentration during evaporation and subsequent dilution during the hydration should be due to the removal of mass from sampling. These small differences should be apparent in the sodium and electrical conductivity data. The HCO_3^-, and CO_3^{2-} ions should increase due to the evaporation and decrease due to degassing of carbon dioxide. For the Ca-Na-HCO_3-Cl solution, Ca^{2+}, HCO_3^- and CO_3^{2+} should increase due to the evaporation but be countered by decreases due to the precipitation of calcite and degassing of carbon dioxide; only the sodium and the chloride ions should be conservative. The electrical conductivity of the Ca-Na-HCO_3-Cl solution should decrease during the hydration due to the decrease in ionic strength.

The expected response for the pH is a steady increase over the course of evaporation. Initially, the Na-HCO_3 solution and the Ca-Na-HCO_3-Cl solution were both supersaturated with respect to the atmospheric partial pressure of carbon dioxide and should rapidly degas the excess carbon dioxide in order to arrive at equilibrium with atmospheric CO_2. This would cause a rapid early increase in the pH. The Ca-Na-HCO_3-Cl solution should begin to deviate from the pH data of the Na-HCO_3 solution because of the expected calcite precipitation. The precipitation of calcite will tend to drive the pH down according to the following reaction

$$Ca^{2+} + HCO^{-}{}_3 \rightarrow CaCO_3(Calcite) + H^{+} \quad (8)$$

Eventually, equilibrium between the decrease in pH caused by precipitation and the increase caused by degassing should be established.

The alkalinity of the Ca-Na-HCO_3-Cl solution should not follow a pattern similar to that of the Na-HCO_3 solution. Instead, the precipitation of calcite should cause the removal of carbonate (CO_3^{2-}). This should decrease the alkalinity as the water evaporates and calcite forms. The alkalinity during the hydration process should be diluted from the initial values because of the changes in solution composition during evaporation and the increase in solution volume.

3.2. Isotopic Interactions

3.2.1 Oxygen and Hydrogen (Water) Isotopes during Evaporation

Concentration of oxygen and hydrogen isotopes are expected follow a Rayleigh distillation pattern during the evaporation of the solutions. The concept of Rayleigh

distillation was originally developed by Lord Rayleigh in the early twentieth century to describe the distillation of a two-component system. To qualify as a Rayleigh process, different components of a system must move from one reservoir to another at different rates. The original formulation of Rayleigh distillation only considers the movement of isotopes in one direction without back-equilibration of the isotope. A modified version of the Rayleigh equation must be used if isotopes can move back and forth between reservoirs.

The Rayleigh equation for isotopic fractionation during the evaporation process under zero humidity, with movement in only one direction, is

$$\delta_f = \delta_i + \varepsilon(\ln f) \tag{9}$$

where δ_f is the isotopic value at any time, δ_i is the initial isotopic value, ε is the enrichment factor, and f is the fraction of the evaporating liquid remaining in the system. Over the course of evaporation, the lighter isotopes will preferentially move from the liquid phase to the gas phase. The simple Rayleigh equation can be used to calculate the enrichment during the course of evaporation. Any deviations of measured data from this calculated trend can generally be accounted for using corrections for the effects of humidity and temperature changes.

Humidity and temperature corrections factors have been developed by several authors. The temperature dependence of the enrichment factor for oxygen-18 moving between water and the atmosphere is given by Friedman and O'Neil (1977)

$$10^3 \ln \alpha_{l-v} = -(1.137(10^6 * T^{-2}) - 0.4156 * (10^3 * T^{-1}) - 2.0667) \tag{10}$$

where $10^3 \ln \alpha_{l\text{-}v}$ is equivalent to the equilibrium enrichment factor, ε, for isotope movement from liquid to vapor, and T is the temperature in Kelvin. The liquid-to-vapor enrichment of deuterium as a function of temperature is given by Gilath and Gonfiantini (1983)

$$10^3 \ln \alpha_{l-v} = -(24.844 * (10^6 * T^{-2}) - 76.248 * (10^3 * T^{-1}) + 52.612) \quad (11)$$

Both Equations (10) and (11) were derived in an earlier study (Majzoub ,1971).

As described by Clark and Fritz (1997), water vapor leaving the surface of the solution enters a completely saturated layer that is typically only a few microns thick. This layer is assumed to be in isotopic equilibrium with the surface of the liquid reservoir. Directly above this layer is a transition zone, where the humidity changes from 100% to a value in equilibrium with the bulk atmosphere. This type of non-equilibrium evaporation process must have a modified enrichment factor, ε, to account for this kinetic effect. Clark and Fritz (1997) employed the following equation

$$\varepsilon_{l-v} = \varepsilon_{l-v} + \Delta\varepsilon_{bl-v} \quad (12)$$

where l-v refers to the standard liquid-vapor interface, bl-v refers to the interface between the boundary layer and the bulk atmosphere, and, Δε is the term that accounts for the kinetic effects. Gat (1981) describes the equations for the average Δε at any relative humidity, h.

$$\Delta\varepsilon_{bl-v}{}^{18}O = 14.2 * (1 - h) \quad (13)$$

$$\Delta\varepsilon_{bl-v}D = 12.5 * (1 - h) \quad (14)$$

Equations (9) through (14) should provide a calculated set of data that matches the measured set of data from the evaporation phase of the experiment. However, the experimental work of Gat (1981) was conducted in a controlled laboratory setting where wind velocities should be at a minimum. The parameters 14.2 and 12.5 in equations (13) and (14) account for low wind velocities and should provide an upper bound for the data in this experiment. The work of Merlivat and Jouzel (1979) was intended to describe an environment similar to an ocean setting where wind velocities are high and $\Delta\varepsilon_{bl\text{-}v}$ is given as,

$$\Delta\varepsilon_{bl-v} = \frac{1}{\alpha_{lv}} * \frac{1-k}{1-kh} - 1 \tag{15}$$

where k is 18.3‰ for oxygen and 16.8‰ for deuterium and is based on the following relationship based on enrichment (ε_k), wind velocity (u_*), kinematic viscosity (ν), von Karman Constant (X), diffusion (D), and elevation above the water surface (z),

$$k = \frac{(\varepsilon_k + 1)^{\frac{1}{3}} - 1}{(\varepsilon_k + 1)^{\frac{2}{3}} + \frac{\ln(\frac{u_* z}{30\nu})}{13.6\chi(\frac{\nu}{D})^{\frac{2}{3}}}} \tag{16}$$

While the formulation of Gat (1981) provided an upper bound, this relationship from Merlivat and Jouzel describes the lower bound where diffusion-driven fractionation will be limited. The room where my experiment was conducted should be between these two bounds since the wind velocities were somewhere above the control of a laboratory environment and well below the turbulent velocities above the ocean or a lake.

3.2.2. Oxygen and Hydrogen (Water) Isotopes during Hydration

The hydration of both chemical solutions will be a mixing problem with respect to the oxygen and deuterium isotopes. The isotopic ratios of the input water and original solution ratios as well as the volumes are known, so the new mixed solution isotopic ratios should follow this equation:

$$\delta_{nm} = \chi_s * \delta_s + (1 - \chi_i) * \delta_i \tag{17}$$

where δ is the isotopic ratio, χ is the volume fraction, the subscripts nm, s, and i represent the new mixture, the original solution, and the input solution, respectively.

3.2.3. Relationship to the Global Meteoric Water Line

A correlation between the isotopic enrichments of oxygen-18 and deuterium in water was first documented by Craig (1961). The equation is now accepted as standard and is:

$$\delta D = 8 * \delta^{18}O + 10 \tag{18}$$

where δD is the measured deuterium value in per mille, and, δ^{18}O is the measured oxygen-18 value in per mille. This equation represents the Global Meteoric Water Line (GMWL). Oxygen-18 and deuterium ratios in precipitation (rain) should follow the GMWL, but deviations from the line will result as the water is affected by different processes. The waters in this experiment should initially have values that correspond to the GMWL, but the evaporation process will cause the subsequent measurements to form a different line. Generally, evaporation from a surface water body will produce a deviation from the GMWL with a slope of six. This deviation represents evaporation of the isotopes in an environment assuming a relative humidity of 85% (Clark and Fritz,

1997). The evolution of oxygen-18 and deuterium in this experiment should evolve away from the GMWL with a slope less than six because of an expected relative humidity less than 85%.

3.2.4. Covariant Trends between oxygen-18 and carbon-13

This work is primarily concerned with evaluating the possible influence of carbon dioxide degassing on generating covariant trends between oxygen-18 and carbon-13 in calcite precipitated in closed-basin lakes and in the dissolved carbon species. The carbon isotope evolution in this experiment should be driven by CO_2 degassing, as both solutions are initially supersaturated with respect to P_{CO2}, and the evaporation-driven increases of pH will also cause the solution to degas CO_2.

The final value of carbon-13 in equilibrium with the atmosphere should be between 1 and 3‰, unless modified by photosynthetic activities, in which case the value may be as heavy as 6‰ (Li et al., 1997). Both carbon-13 and oxygen-18 in the carbonate ion should follow a Rayleigh-distillation pattern of enrichment leading to a covariant trend in the solution. If the CO_2 degassing hypothesis is correct, the result should be a strong covariant trend. The R-squared value should be greater than or equal to the suggested 0.7 (Talbot, 1990).

3.2.5. Enrichment Factors of Carbon-13 between Bicarbonate and Gaseous Carbon Dioxide

This section discusses the enrichment that should occur during the fractionation of carbon-13 from bicarbonate to degassed carbon dioxide. In this experiment, the carbon isotope composition was measured on the total dissolved inorganic carbon as described in

section 2.2. Direct isotopic measurements of the bicarbonate species or the carbon dioxide degassing from the solution were not made; therefore, these calculations must be made using a mass balance approach on the entire data set. Initially, each measurement of carbon isotope ratio is converted into a mass (mol) using the known amount of water in the solution at each sampling time (corrected for mass removal via sampling). Then, at each experimental sampling point, the distribution of carbonate species is solved using six equations and assuming chemical equilibrium. Alkalinity in this case equals the total alkalinity measured by titration as described in section 2.4.2. The total alkalinity is equal to $[HCO_3^-]+2[CO_3^{2-}]$, where [] represents moles.

$$HCO_3^- = \text{Alkalinity} - 2 * \text{Carbonate Alkalinity} - OH^- \tag{19}$$

$$CO_3^{2-} = 2 * \text{Carbonate Alkalinity} - 2 * OH^- \tag{20}$$

$$OH^- = \frac{10^{-14}}{10^{-pH}} \tag{21}$$

$$H_2CO_3 = \frac{HCO_3^- * H^+}{10^{-3.5}} \tag{22}$$

$$CO_2(aq) = \frac{H_2CO_3}{10^{2.8}} \tag{23}$$

$$C_T = HCO_3 + CO_3^{2-} + H_2CO_3 + CO_{2aq} \tag{24}$$

where $10^{-3.5}$ is the equilibrium constant for the dissociation of carbonic acid (H_2CO_3), and $10^{2.8}$ is the equilibrium constant for protonation of dissolved CO_2. Once the distribution of carbon has been found, then the ratio of carbon-13 to carbon-12 at each sampling point can be found.

$$\left(\frac{\delta^{13}C_{Sample}}{1000} + 1\right) * \left(\frac{^{13}C}{^{12}C}\right)_{\text{Standard}} = \left(\frac{^{13}C}{^{12}C}\right)_{\text{Sample}} \tag{25}$$

The $\delta^{13}C_{sample}$ is the bulk isotope measurement of the sample and $(^{13}C/^{12}C)_{standard}$ is the experimentally determined carbon isotope ratio for the isotopic standard (PDB, PeeDee Belemite carbon standard) equal to 0.0112372 (Craig, 1957). Assuming the total amount of carbon in the system consists of 98 to 99% carbon-12, the amount of carbon-13 in the sample can be determined according to the next equation.

$$\frac{^{13}C(mol)}{^{12}C(mol)} * C_T(mol) = {}^{13}C(mol) \tag{26}$$

Once the total carbon-13 has been determined, then the distribution of carbon-13 among the carbon species can also be solved. A linear system of four equations with four unknowns is written based on the following relationship,

$$\varepsilon_{a-b} \cong \delta_a - \delta_b \tag{27}$$

where, δ_a and δ_b represent two different reservoirs. This equation assumes that $\delta_b/10^3 <<$ 1. Using known enrichment factors, the calculated carbon-12 molar amounts in each carbonate species, and the known value of the standard material, R_{std}, the following system of equations is written.

$$\varepsilon_{H_2^{13}CO_3 \to H^{13}CO_3} = H_2{}^{13}CO_3 * \frac{1000}{H_2{}^{12}CO_3 * R_{std}} - H^{13}CO_3 * \frac{1000}{H^{12}CO_3 * R_{std}} + 0_{CO_3} + 0_{CO_{2(aq)}} = -9 \tag{28}$$

$$\varepsilon_{H^{13}CO_3 \to {}^{13}CO_3} = 0_{H_2CO_3} + H^{13}CO_3 * \frac{1000}{H^{12}CO_3 * R_{std}} - {}^{13}CO_3 * \frac{1000}{{}^{12}CO_3 * R_{std}} + 0_{CO_{2(aq)}} = 1 \tag{29}$$

$$\varepsilon_{H_2{}^{13}CO_3 \to {}^{13}CO_{2(aq)}} = H_2{}^{13}CO_3 * \frac{1000}{H_2{}^{12}CO_3 * R_{std}} + 0_{HCO_3} + 0_{CO_3} - {}^{13}CO_{2(aq)} * \frac{1000}{{}^{12}CO_{2(aq)} * R_{std}} = 1 \tag{30}$$

$$Total^{13}C = H_2{}^{13}CO_3 + H^{13}CO_3 + {}^{13}CO_3 + {}^{13}CO_{2(aq)} \tag{31}$$

The mass of carbon-13 in each species is determined using this system of equations. A FORTRAN90 code called Gausstest was modified from a code written by Hahn (1996). The codes are listed in Appendix F.

The distributions of carbon-12 and carbon-13 were solved for the Na-HCO_3 solution using equations (28) to (31). Using this information, the R values for bicarbonate can be calculated by the following equation.

$$R_{HCO_3} = \frac{H^{13}CO_3}{H^{12}CO_3} \tag{32}$$

For the Na-HCO_3 solution, the amount of CO_2 degassed at each experimental sampling point in the experiment can be determined by assuming that any decrease in total carbon was due to degassing. The decrease should be equal to the amount of CO_2 degassed. This can be calculated for both carbon-12 and carbon-13. The calculation of the R value is therefore identical to equation (32) modified for CO_2(g) instead of HCO_3^-. With both R_{HCO3} and the R_{CO2}, the enrichment factor relating the isotopic composition of dissolved carbon to the carbon dioxide reservoir in the atmosphere is calculated by,

$$\varepsilon_{A\to B} = (\frac{R_A}{R_B} - 1) * 1000 \tag{33}$$

Enrichment factors were calculated using equations fitted to the data rather than using actual point-to-point data differences. This method was employed because data scatter around the trends caused extreme variability in the point-to point calculated enrichment factors. Using these smooth fitted curves, the final enrichment factors were calculated for both the intermediate sampling points and cumulative points.

The distribution calculations for carbon-12 and carbon-13 species in the bulk Ca-Na-HCO_3-Cl solution were treated the same as the Na-HCO_3 solution (equations (19) -

(32)). The major difference from the Na-HCO_3 solution was that there were two sinks for carbon, carbon dioxide degassing and calcite precipitation, rather than degassing alone. After the calculations for carbon isotope distribution, the amount of calcite that precipitated during the evaporation phase was inferred from the reduction of calcium concentration between each sampling period. The calculated total carbon loss from the system during evaporation included the loss of carbon to calcite precipitation. The cumulative calcite precipitation was calculated from the decrease of calcium measured in solution during the evaporation. Therefore, the loss of carbon to degassing of carbon dioxide to the atmosphere can be calculated. From this point, the enrichment calculations proceed identically to the calculations for the Na-HCO_3 solution.

The calculations of enrichment factors between carbon dioxide and bicarbonate during the hydration differ from the calculations made during the evaporation in one regard. The increase in carbon is assumed to be due to absorption of carbon dioxide from the atmosphere with a $\delta^{13}C$ of -7‰. The calculations to solve for the distribution of carbon-12 and 13 and the fractionation factors are the same for the hydration phase as the evaporation phase.

The expected equilibrium enrichment factor of bicarbonate relative to atmospheric carbon dioxide is ±7.9‰ (Mook, et al., 1974). The sign depends upon the direction of isotope movement, negative for carbon dioxide degassing, positive for carbon dioxide sorption.

3.2.6. Isotopic Differences between Oxygen-18 Reservoirs

The difference in the oxygen isotopic composition between reservoirs, referred to as the isotopic difference, is given by,

$$\Delta_{ab} = \delta_a - \delta_b \tag{34}$$

where Δ is the isotopic difference, δ_a and δ_b are isotopic ratios for each reservoir a and b. The two reservoirs considered are water and carbonate ions. The bulk carbon reservoir must be considered because $\delta^{18}O$ was measured only on the bulk carbonate using the barium chloride precipitation method (section 2.2.). In the carbon-13 enrichment calculations, the enrichment factors between individual carbon species can be used with the alkalinity data to solve the distribution of carbonate. There is not enough experimental data on the fractionation of oxygen in carbonate species for a similar detailed calculation with the oxygen-18 bulk carbonate measurements, so the isotopic difference will be evaluated instead. The isotopic difference can approximate an enrichment factor assuming that $\delta_b/1000 << 1$.

Usdowski et al. (1991) published fractionation factors for oxygen isotope exchange between water and different carbonate species at a temperature of 19°C (Table 2). The average temperature during the evaporation phase was 15.7°C and it is not known if application of their results to this temperature is appropriate. These enrichment factors are provided for comparison to the isotopic differences that will be calculated from the data.

Direction of Fractionation	Fractionation Factor	Enrichment Factor
$\alpha_{CO2\rightarrow H2O}$	1.0579	56.29
$\alpha_{CO2\rightarrow CO2g}$	1.0148	14.69
$\alpha_{H2CO3\rightarrow H2O}$	1.0395	38.74
$\alpha_{HCO3\rightarrow H2O}$	1.0351	34.50
$\alpha_{CO3\rightarrow H2O}$	1.0184	18.23
$\alpha_{H2CO3\rightarrow CO2}$	0.9825	-17.66
$\alpha_{HCO3\rightarrow CO2}$	0.9784	-21.84
$\alpha_{CO3\rightarrow CO2}$	0.9626	-38.12

Table 2 Oxygen-18 fractionation factors at 19°C from Usdowski et al. (1991).

The enrichment factors in Table 2 are calculated assuming that ε_{ab} is approximately equal to $-\varepsilon_{ba}$, and that the enrichment of oxygen-18 from water to bicarbonate is –34.5‰ (T = 19°C).

Applying this information to the evaporation and hydration phases for the two solutions, the average isotopic difference between the oxygen in water and the oxygen in carbonate ions should be -34‰. The average isotopic difference may shift toward the -18‰ value of water-to-carbonate as the concentration of carbonate increases at the later stages of evaporation.

4. DATA AND PRELIMINARY INTERPRETATIONS

4.1. Chemical Evolution of the Solutions

4.1.1. Sodium and Calcium Data

The evaporation of the water from the experimental solutions caused an increase in the concentration of sodium. The data collected showed an exponential increase in sodium during evaporation. The changes in sodium concentration were also calculated with the PHREEQC geochemical code (Appendix G.6.). The model calculation concentrated sodium by removing the same molar quantity of water at each step. The data and the calculations for the Na-HCO_3 solution evaporation are in good agreement (Figure 1). The same trends are seen in the Ca-Na-HCO_3-Cl solution evaporation where the concentration of sodium increases as the water evaporates. Again, the data and the model are in good agreement with each other (Figure 2). The sodium data was also used to refine the fraction of water remaining data (Appendix J.).

The measured sodium from the hydration of the Na-HCO_3 solution compares well with the evaporation sodium measurements (Figure 1). The model calculation closely follows the general trend of hydration. The same agreement between the hydration and evaporation data is seen in the sodium data from the Ca-Na-HCO_3-Cl solution (Figure 2) and in the calculation from the geochemical model.

Interpretation of the calcium data from the evaporation phase of the Ca-Na-HCO_3-Cl solution is more difficult (Appendix N). The data show (Figure 3) at least two distinct periods when calcium was being removed, two periods when calcium was increasing, and one period when the concentration appears constant. The first drop in the calcium concentration occurred at fraction of water remaining (f) of 0.95. The calcium concentration returned to the initial value at f = 0.85 suggesting that the calcium was not precipitating during this period. The concentration leveled off between f = 0.85 and f = 0.60. The calcium concentration decreased again at f = 0.60 and continued until f = 0.30. Between f = 0.30 and f = 0.15 there appeared to be an increase in calcium concentration. Calcium concentration then continued to decrease until the completion of the evaporative phase of the experiment. The hydration data (Figure 3) show a continued decrease that is probably due to dilution as the solution returns to the original f, rather than continued precipitation of calcite. New calcite formation was not observed during the hydration process.

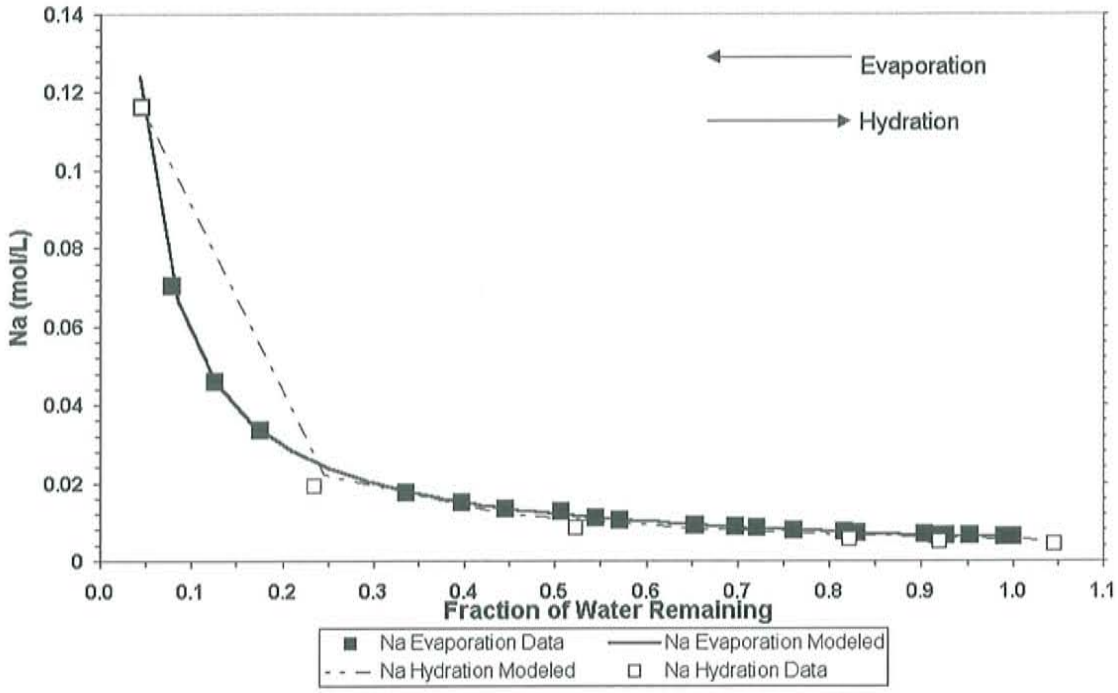

Figure 1 Sodium data measured from the evaporating Na-HCO_3 solution in solid black squares. The PHREEQC modeled sodium concentrations are drawn with a solid black line. The hydration data are open squares with the PHREEQC modeled concentrations drawn with a dashed line

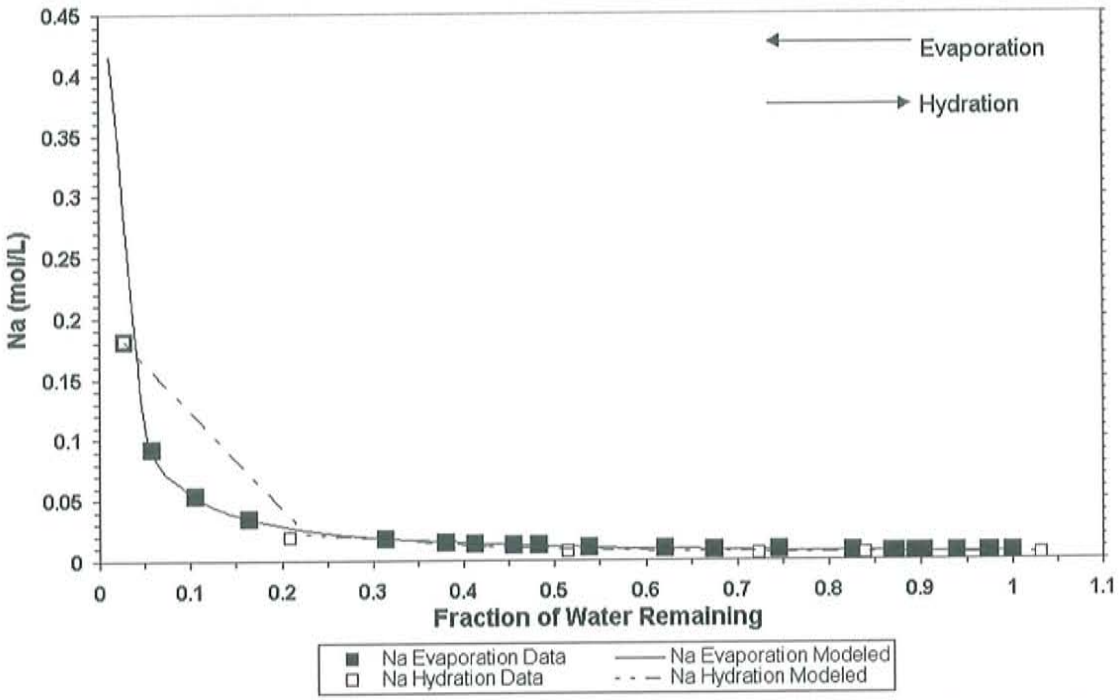

Figure 2 Sodium data measured from the evaporating Ca-Na-HCO_3-Cl solution in solid black squares. The PHREEQC modeled sodium concentrations are drawn with a solid black line. The hydration data are open squares with the PHREEQC modeled concentrations drawn with a dashed line.

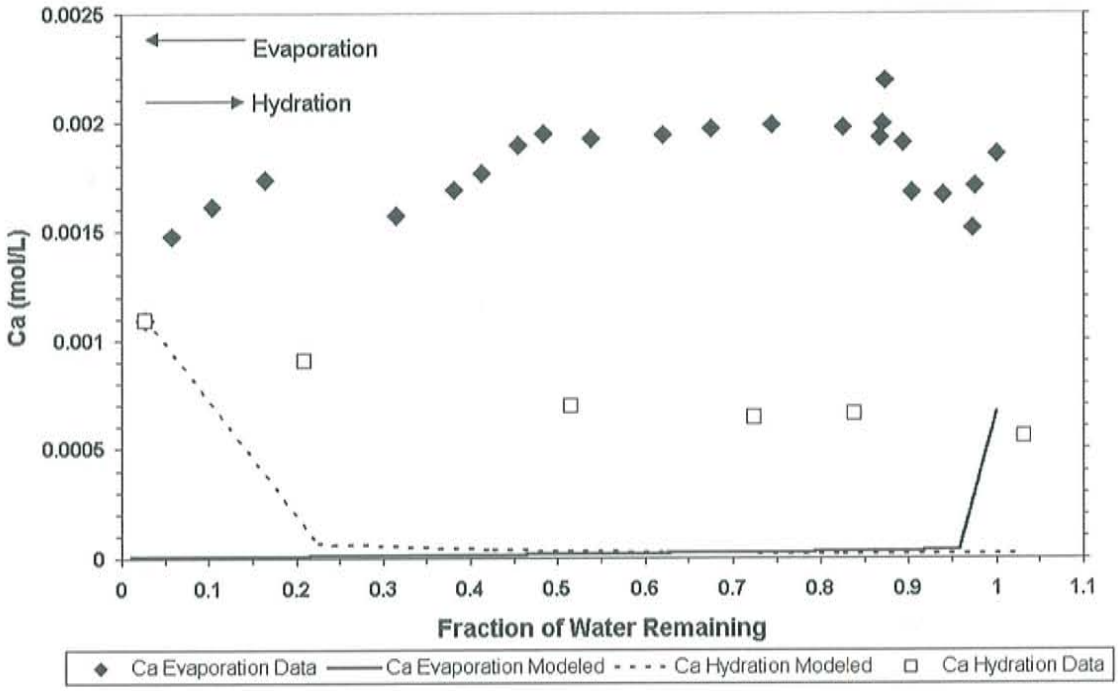

Figure 3 Calcium concentration measured from the evaporating Ca-Na-HCO_3-Cl solution in solid black squares. The PHREEQC modeled calcium concentrations are drawn with a solid black line. The calcium concentrations measured during hydration are open squares with the PHREEQC modeled concentrations drawn with a dashed line.

4.1.2. pH and Electrical Conductivity Data

The pH measurements from the Na-HCO_3 solution show an early increase in pH consistent with initial degassing of CO_2 from the solution (Figure 4). Then, the pH steadily increased for the duration of the evaporation phase. The observed changes in pH were quite different from the model-calculated changes. The initial early rise in pH was slightly delayed relative to the model calculation and the subsequent decrease was smaller in the model than observed from the data. Between f = 0.87 and 0.3, the pH was well below the evaporative-driven PHREEQC calculation. The PHREEQC calculation

initially required that the solution evaporate in equilibrium with a P_{CO2} of $10^{-3.5}$. Only at f < 0.4, was the calculation of the pH increase consistent with the data. An alternative PHREEQC calculation with the atmospheric CO_2 equal to an elevated value of $10^{-3.1}$ provides a better overall fit to the data (Figure 4). Further analysis of the uncertainty bounds on the individual pH measurements indicates that the solutions were most likely in equilibrium with standard atmospheric P_{CO2} (i.e., $10^{-3.5}$ atm). (Appendix M)

The measurements during the hydration phase for the Na-HCO_3 solution (Figure 4) generally overlap with the evaporation phase data. The pH model calculation for the Na-HCO_3 solution shows that the expected pH was higher than the actual measurements. This is similar to the evaporation calculation of pH. Although, the pH data overlap for both evaporation and hydration phases suggesting a dilution process, they are both lower than calculated for a solution in equilibrium with atmospheric CO_2. The alternative calculation of the hydration pH with an elevated P_{CO2} of $10^{-3.1}$ intersects with all but one of the data points.

The pH data from the Ca-Na-HCO_3-Cl solution (Figure 5) shows a decrease at the onset of calcite precipitation. The pH rose sharply after the addition of the Percol at an f =0.9 and then gradually increased during the remainder of the experiment. This gradual increase probably represents a balance between the precipitation effects and the evaporation effects. Because the pH gradually increased over the experiment, the evaporation effects proved to be a stronger mechanism for pH change than the precipitation effects. Similar to the Na-HCO_3 solution, the model-calculated pH is much higher than the measured pH over much of the experiment. Unlike the Na-HCO_3 solution, the pH data in the Ca-Na-HCO_3-Cl solution were not matched by the model at

any point. The calculated curves were able to capture the trends of pH change in each of the solutions but not the proper magnitude. Similar to the Na-HCO_3 solution, an alternative PHREEQC calculation with a higher atmospheric CO_2 was required to fit the pH data in the early and middle stages of the evaporation. The atmospheric CO_2 value that best fit the data was $10^{-2.8}$, contrary to the $10^{-3.1}$ for the Na-HCO_3 solution. The apparent increase in PCO2 results from the pH measurement uncertainty (Appendix M).

The pH data from the hydration phase for the Ca-Na-HCO_3-Cl solution (Figure 5) do not overlap with the measurements from the evaporation phase. This suggests that the composition of the Ca-Na-HCO_3-Cl solution has changed, which is expected due to the calcite formation. The geochemical calculation for the hydration of the Ca-Na-HCO_3-Cl solution, much like that for the Na-HCO_3 solution, indicates that the pH should have been higher. This is consistent with the results from the Na-HCO_3 solution, and the prediction for the evaporation phase for the Ca-Na-HCO_3-Cl solution. The alternative pH calculation with the P_{CO2} of $10^{-2.7}$ results is a pH that is still too high to match the hydration data.

The Na-HCO_3 solution (Figure 6) showed a steady increase in electrical conductivity over the course of evaporation, as the dissolved salts are concentrated in the solution. The Ca-Na-HCO_3-Cl solution (Figure 7) containing a greater quantity of dissolved salts, started with a higher electrical conductivity and then ended the evaporation phase with a higher value than the Na-HCO_3 solution. There was one small drop in conductivity between an $f = 0.9$ and $f = 0.85$ that coincided with the addition of the Percol flocculant. The flocculant most likely removed additional species from solution as well as the precipitate.

Theoretically, the electrical conductivity measurements for the hydration of the $Na\text{-}HCO_3$ solution should overlap with the evaporation measurements with small differences due to sampling. The data from the $Na\text{-}HCO_3$ solution (Figure 6) confirm this conceptual idea. Conversely, the $Ca\text{-}Na\text{-}HCO_3\text{-}Cl$ solution electrical conductivity measurements should not show a similar pattern. The evaporation and hydration measurements should show a change in composition due to the precipitation of calcite during the evaporation phase. The data confirm this (Figure 7).

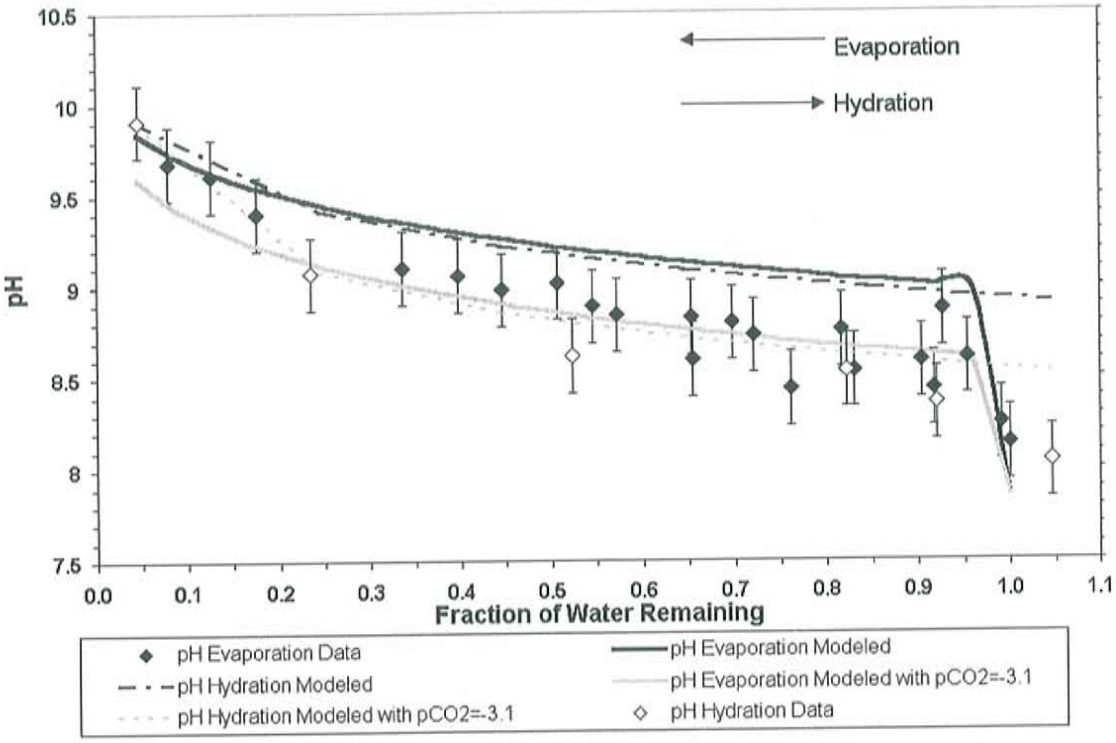

Figure 4 Measured pH in black diamonds with 0.2 pH units error bars for the evaporation of the $Na\text{-}HCO_3$ solution, with model calculation from PHREEQC as a solid black line. The open diamonds and black dashed line are measurement and model calculations for the hydration of the $Na\text{-}HCO_3$ solution. The solid gray line and gray dashed line are evaporation and hydration calculated with a P_{CO2} of $10^{-3.1}$.

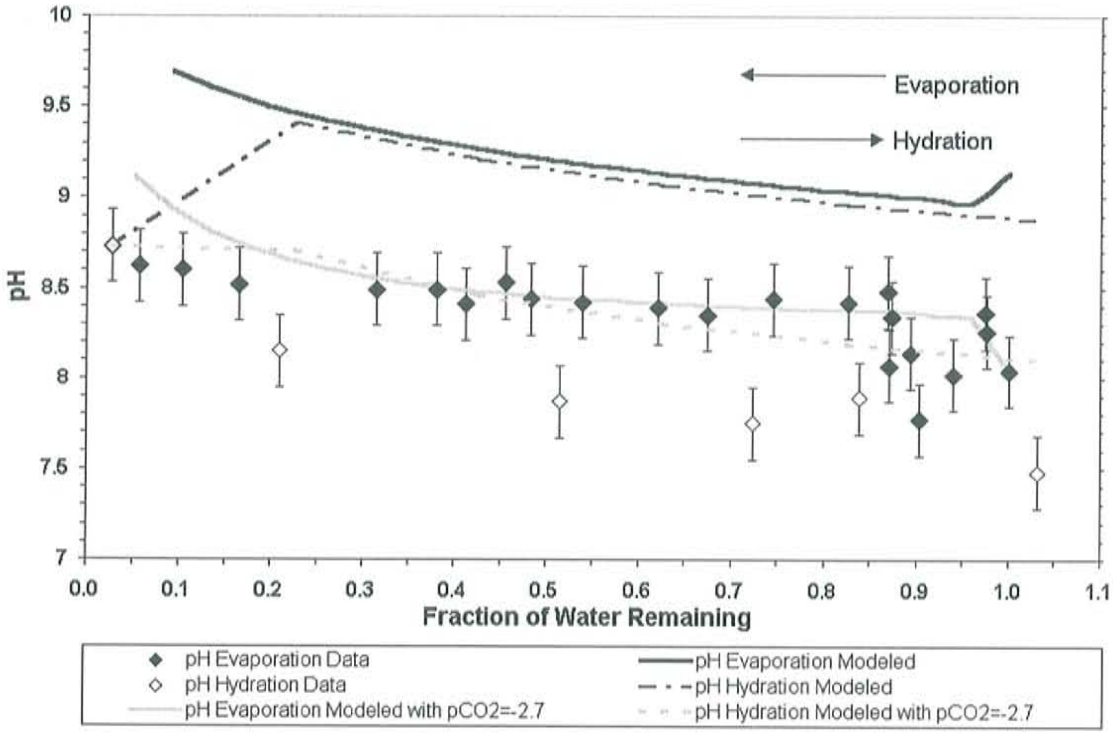

Figure 5 Measured pH in black diamonds with 0.2 pH units error bars for the evaporation of the Ca-Na-HCO_3-Cl solution, with model calculation from PHREEQC as a solid black line. The open diamonds and dashed black line are measurement and model calculations for the hydration of the Ca-Na-HCO_3-Cl solution. The solid gray line and gray dashed line are evaporation and hydration calculated with a P_{CO2} of $10^{-2.7}$.

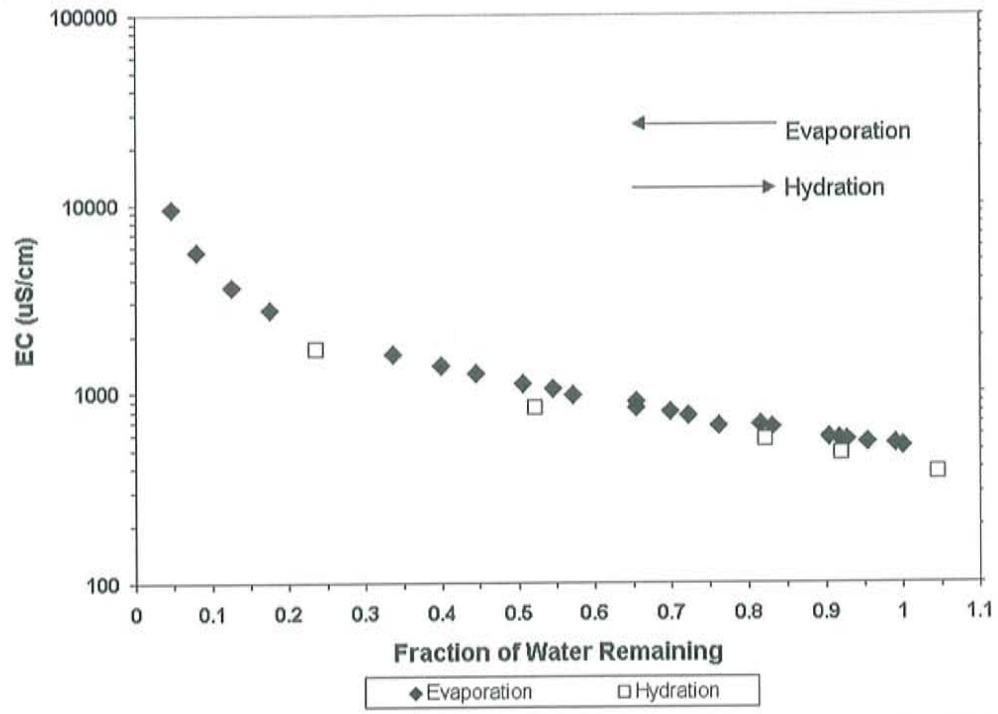

Figure 6 The electrical conductivity measurements from the evaporation and hydration of the Na-HCO_3 solution.

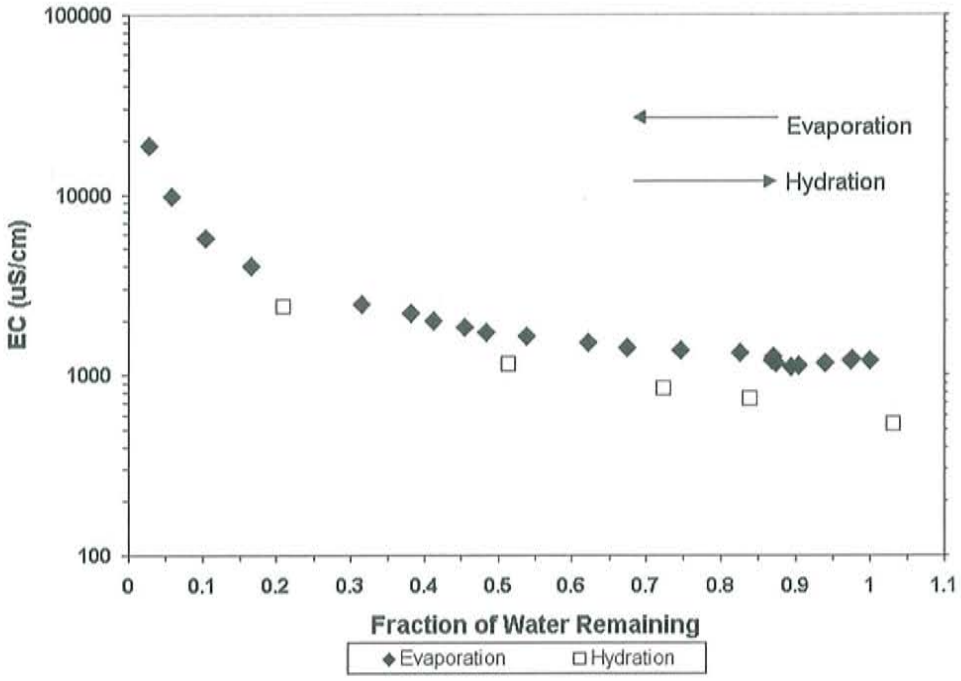

Figure 7 The electrical conductivity measurements from the evaporation and hydration of the Ca-Na-HCO_3-Cl solution.

4.1.3. Alkalinity Data

The measured alkalinity and the model calculation for the evaporation and hydration phases of the Na-HCO_3 solution are in Figure 8. The model, using a P_{CO2} of $10^{-3.5}$, matched the data well with the exception of small errors in the late stages of evaporation due to errors in measuring mass removed during sampling. There was a steady increase in alkalinity in the Na-HCO_3 solution as the water was evaporated. The alkalinity data from the Na-HCO_3 solution show the concentration of carbonate and bicarbonate with the removal of water.

The hydration data show a dilution of carbon species as the solution was returned to the original volume (Figure 8). The hydration data overlap with the evaporation data,

indicating that the change in alkalinity was reversible for the Na-HCO_3 solution. The geochemical calculations for the hydration phase were in good agreement with the measured alkalinity data. The overall trend was reproduced by the model but differences between f = 0.2 and f = 0.3 were most likely attributable to two types of errors. Either the error occurred in accounting for mass removed during sampling or the error in the total amount of deionized water added to the solution during the hydration phase.

The Ca-Na-HCO_3-Cl solution (Figure 9) had a different total alkalinity history than the Na-HCO_3 solution. The geochemical model was unable to match the Ca-Na-HCO_3-Cl solution because of the discrepancies in calcite formation in the model and the data. The model calculated that the calcium supply would be quickly exhausted. The data do not support this calculation. The early drop in the alkalinity data was associated with the beginning of calcite precipitation. The onset of calcite precipitation coincided with a decrease in alkalinity, as was also noted by Terranes et al (1991). The decrease in alkalinity was followed by stabilization, suggesting that a balance was achieved between evaporation and calcite precipitation. This balance was also apparent in the pH data (Section 4.1.2.). The alkalinity began to increase at $f < 0.2$. This also corresponds with the previously noted rise in pH at the end of the evaporation phase of the experiment.

The hydration and the evaporation alkalinity data for the Ca-Na-HCO_3-Cl solution (Figure 9) are not comparable patterns. The evaporation pattern shows a decrease in alkalinity associated with the onset of calcite precipitation. Then, a plateau period where evaporation and precipitation produced a steady alkalinity value. Followed by an increase in alkalinity when calcite precipitation decreases and the evaporation control becomes stronger. The carbonate alkalinity or phenothalein alkalinity was zero or slightly above

zero during most of the evaporation phase. The alkalinity during the hydration phase steadily decreased as the solution approached the original volume, but it did not overlap with evaporation phase pattern. The lack of overlap was due to the change in solution composition with calcite precipitation. The carbonate alkalinity returned to zero after the first hydration step. The geochemical model was unable to accurately calculate the alkalinity hydration data from the Ca-Na-HCO_3-Cl solution.

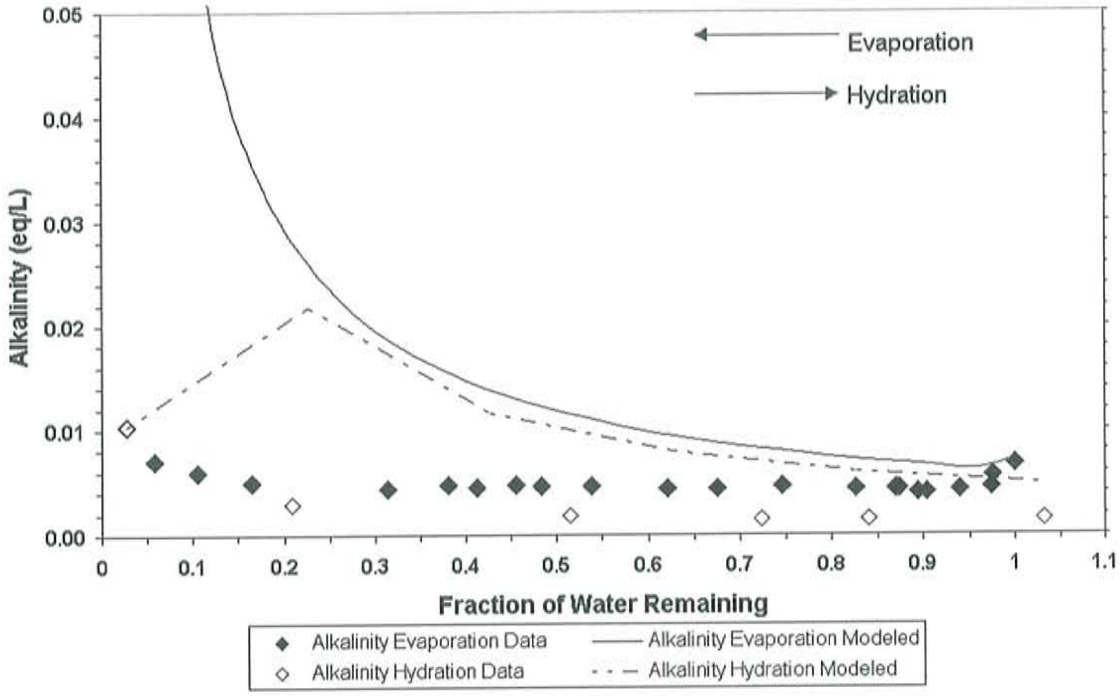

Figure 8 Alkalinity data measured in the Na-HCO_3 solution during the evaporation and hydration phase. The modeled values for both phases are shown as lines.

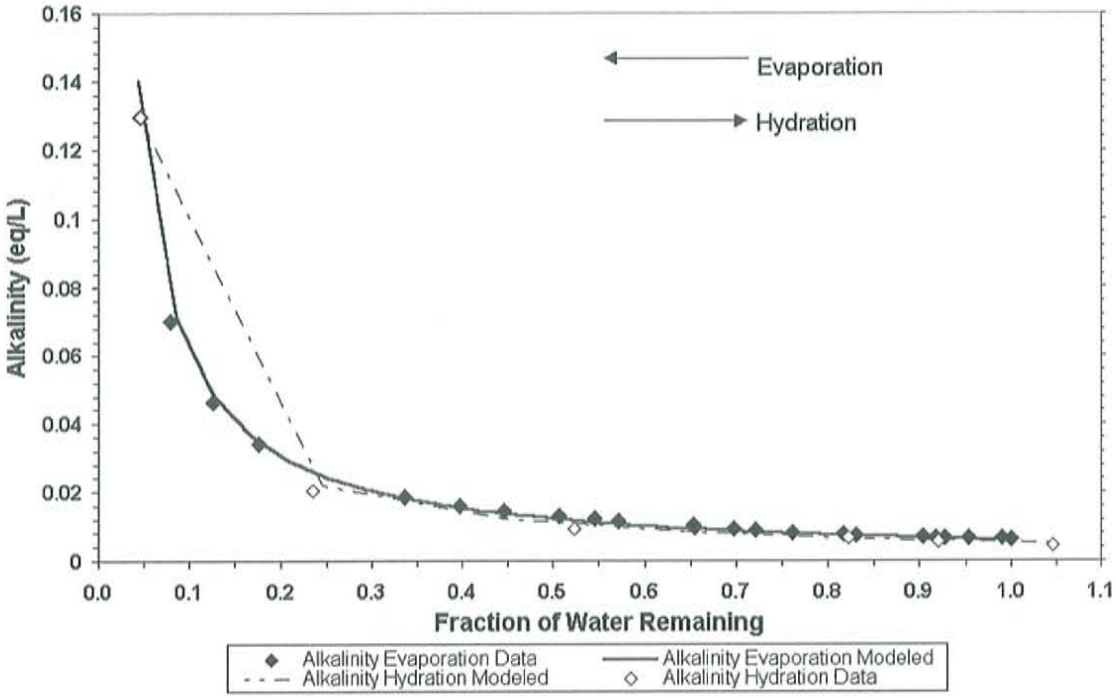

Figure 9 Alkalinity data measured in the Ca-Na-HCO_3-Cl solution during the evaporation and hydration phase. The modeled values for both phases are shown as lines.

4.2. Carbon-13 and Oxygen-18 Isotopic Evolution

Carbon-13 and oxygen-18 measurements were made on the dissolved inorganic carbon (DIC) for both the Na-HCO_3 and Ca-Na-HCO_3-Cl solutions. The $\delta^{13}C$ of the DIC in the Na-HCO_3 solution (Figure 10) rose smoothly from -19‰ to 1.2‰ as the fraction of water remaining dropped from 1.0 to 0.04. The final value of the carbon-13 of 1.2‰ is a good indication that biological activity was not an influence on the evaporative phase. As described by Li et al (1997), the influence of biological activity on carbon-13 would have resulted in a final value closer to 6‰. For the Ca-Na-HCO_3-Cl solution, the $\delta^{13}C$ of the DIC in the solution (Figure 11) rose smoothly from -19‰ to 0.4‰ as the fraction of

water remaining dropped from 1.0 to 0.02. This final value also suggests that biological activity also did not influence the Ca-Na-HCO_3-Cl solution. The two solutions have similar initial and final values but the two solutions did not follow the same path to the final values. An effective enrichment factor for $HCO_3 \rightarrow CO_2$ (g) was calculated using a mass balance approach (Appendix K) and determined to be -19.6‰, which is close to the kinetic enrichment observed by Stiller, et al. (1985). The Ca-Na-HCO_3-Cl solution was slightly more complicated because of the precipitation of calcite. The calculated effective enrichment factor for $HCO_3 \rightarrow CO_2$ (g), again using the mass balance approach, was -22.7‰. Neither of the carbon-13 data sets confirms a Rayleigh distillation process.

Examination of the delta carbon-13 data versus the fraction of total carbon indicates periods of degassing and exchange during the evaporation phase instead of the expected overall degassing. The exchange portions of the evaporation break up the expected Rayleigh distillation process. The Na-HCO_3 solution (Figure 12) has an initial period of degassing, then exchange followed by a final period of degassing. Overall, less that 50% of the total carbon initially present in the system was lost during the evaporation process. A degassing period is defined as a decrease in the fraction of total carbon with an increase in delta carbon-13. Exchange is the increase in delta carbon-13, without an overall decrease in the fraction of total carbon. The Ca-Na-HCO_3-Cl solution (Figure 13) has an initial exchange period followed by a period of degassing. The last segment of data from this solution has been labeled as final desiccation. These data represent the final stages of evaporation, with small fractions of water and carbon remaining and high

sodium and alkalinity concentrations. Their inclusion in the overall data set is questionable because of the influence of brine chemistry on the isotopic analysis.

Rayleigh distillation of carbonate oxygen-18 was observed in both the Na-HCO_3 and Ca-Na-HCO_3-Cl solutions (Figure 14 and Figure 15). . The Rayleigh equation has the following form

$$\delta_f = \delta_i + \varepsilon * \ln f \tag{35}$$

Where δ_f is the isotopic value at any fraction of water of fraction of carbon remaining, f , δ_i is the initial isotopic value and ε is the isotopic enrichment. Rayleigh curves can be fit to the data by varying the enrichment factors - best-fit values are -14.4‰ and -11.1‰ for the Na-HCO_3 and Ca-Na-HCO_3-Cl solutions, respectively. The difference in enrichment suggests different processes influencing oxygen isotope evolution for the two solutions. This was expected considering that the two solutions were chemically different and that one was designed to precipitate calcite. The changes in oxygen-18 during the evaporation phase were 45‰ and 40‰ for the Na-HCO_3 and Ca-Na-HCO_3-Cl solutions, respectively.

The oxygen-18 and carbon-13 measurements taken from the DIC of the Na-HCO_3 solution do show a covariant trend with an R-squared value of 0.75 (Figure 16). This value is greater than 0.7, which is the critical value suggested by Talbot (1990), as representative of a closed-basin lake. The Ca-Na-HCO_3-Cl solution does show a covariant trend for the calcite precipitate (Figure 17) (R^2=0.88) but not for the entire set of DIC solution measurements. The sampling interval for the calcite precipitate was longer than for the dissolved DIC because of the time required to collect enough calcite for analysis. The calcite values therefore represent composites of substantial periods of evaporation.

Examination of the carbon-13 DIC data for both the Na-HCO_3 and Ca-Na-HCO_3-Cl solutions show that there was a pattern in the data set that precludes fitting a straight line to the entire data set. Multiple subsets were chosen from each solution and straight lines were fitted to those portions only. The subsets were chosen based on the degassing and exchange. Figure 16 shows the trend lines for each subset of the evaporation data and the entire set of hydration data for the Na-HCO_3 solution. The subsets have much higher correlation coefficients ($R^2 > 0.85$ for all subsets and the hydration) than that for the entire evaporation data set ($R^2 = 0.75$).

The same types of subsets were chosen for the Ca-Na-HCO_3-Cl. The correlation coefficient for the trend line fit to the entire data set is 0.5. This is not a strong enough correlation to conclude that the experiment was conducted in a closed-basin system contrary to the design of the experiment. The Ca-Na-HCO_3-Cl solution showed R^2 values greater than 0.7 for the degassing and precipitation subsets of the experiment.

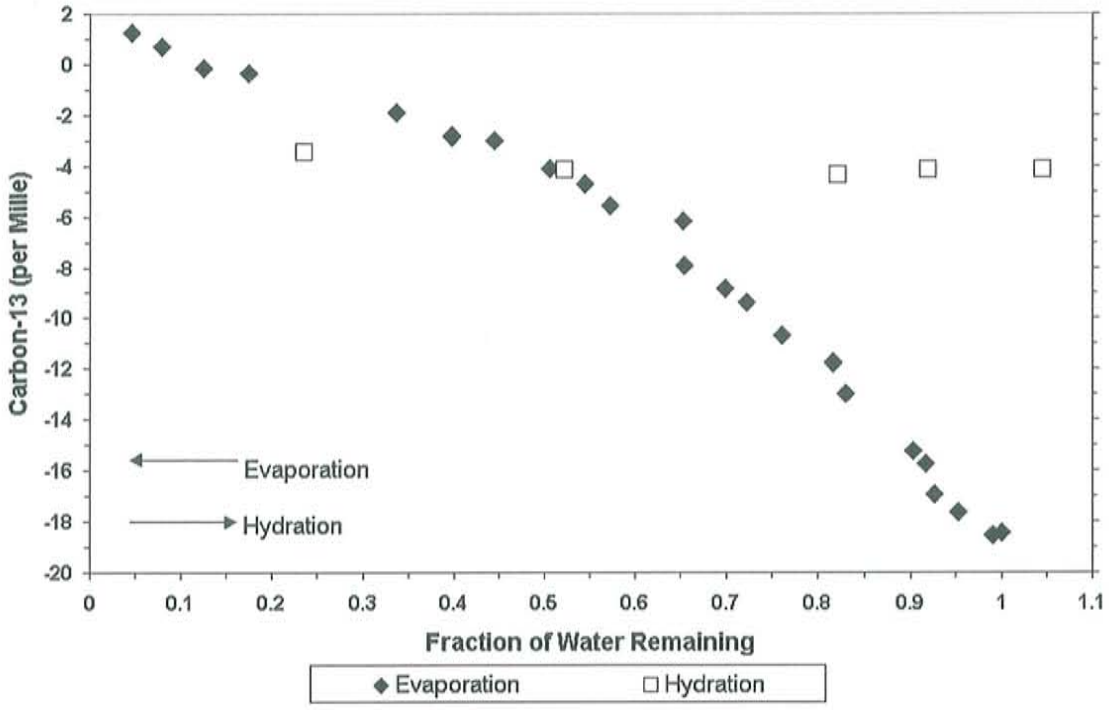

Figure 10 Carbon-13 data from DIC during the evaporation and hydration of the $NaHCO_3$ solution.

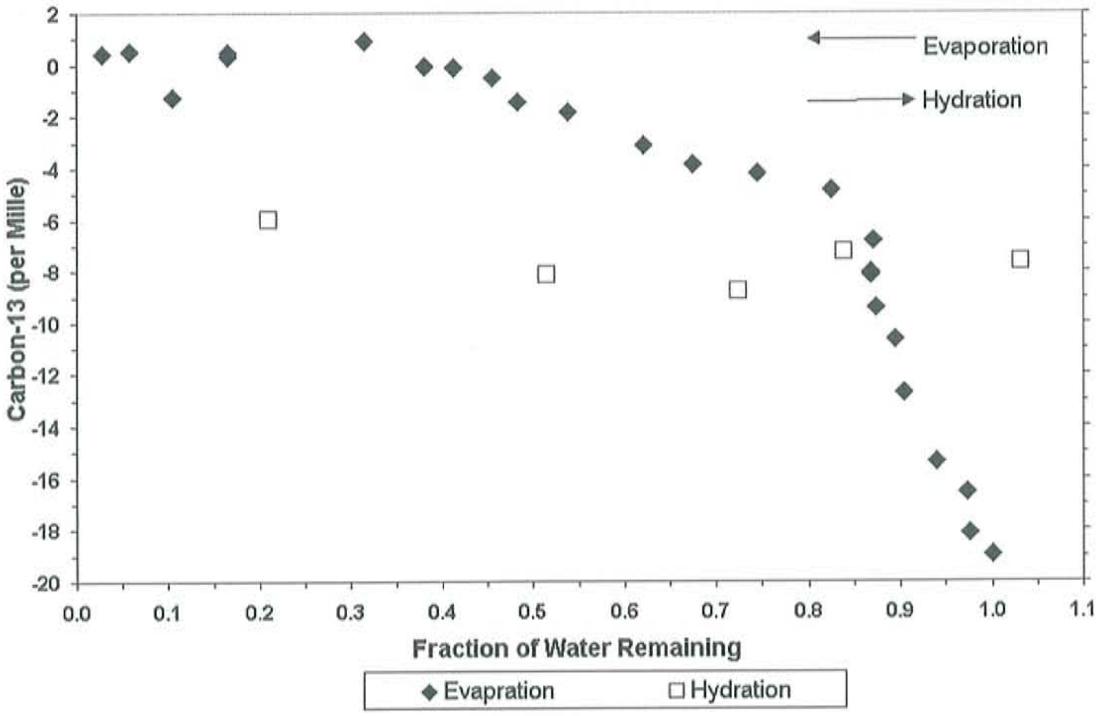

Figure 11 Carbon-13 data from DIC measured during the evaporation and hydration of the Ca-Na-HCO_3-Cl solution.

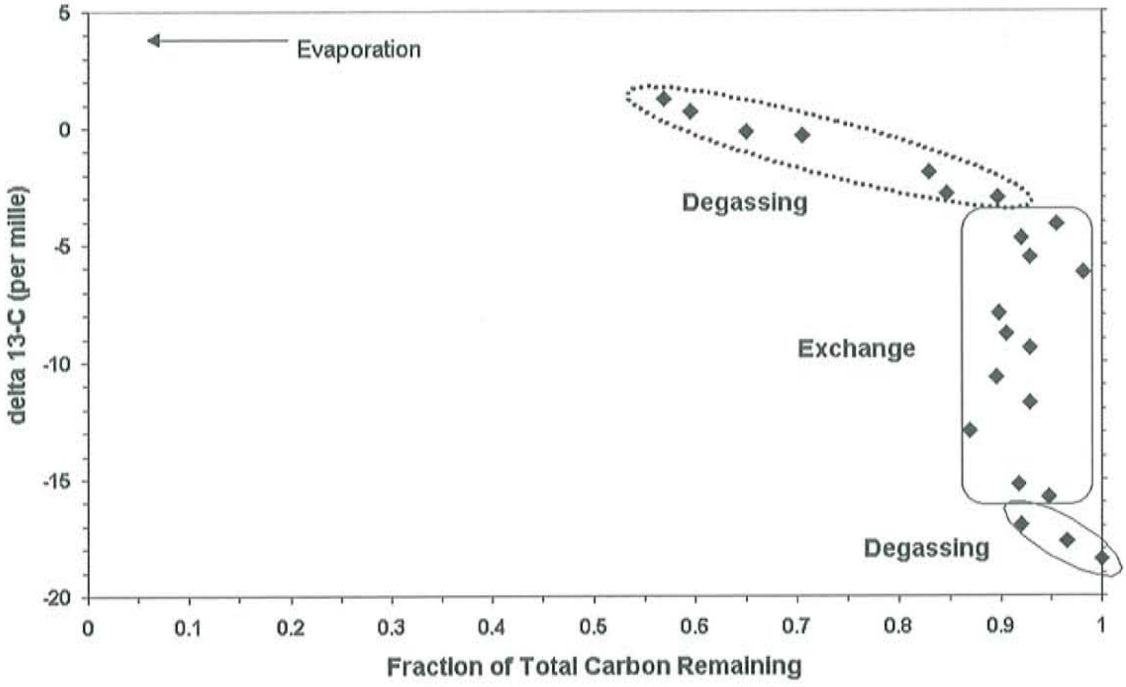

Figure 12 Delta carbon-13 measured in DIC versus fraction of total carbon during the $NaHCO_3$ solution evaporation. Data points are grouped into three subsets of degassing and exchange based on periods of loss of total carbon and delta carbon-13 enrichment.

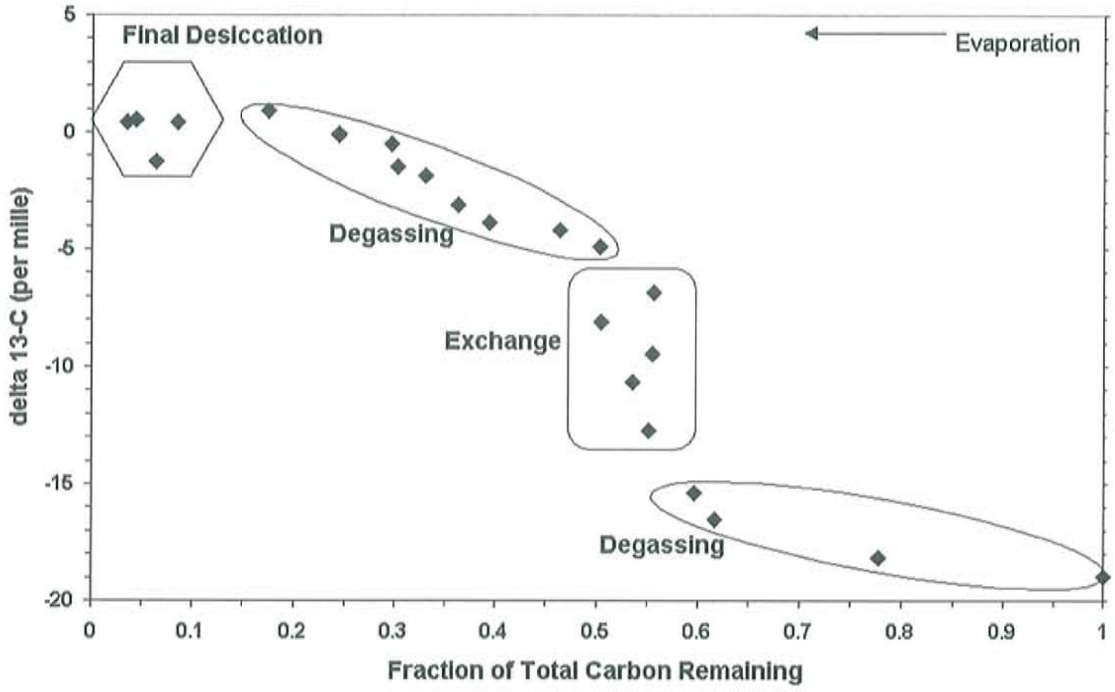

Figure 13 Delta carbon-13 measured in DIC versus fraction of total carbon during the Ca-Na-HCO_3-Cl solution evaporation. Data points are grouped into four subsets of degassing and exchange based on periods of loss of total carbon and enrichment of carbon-13.

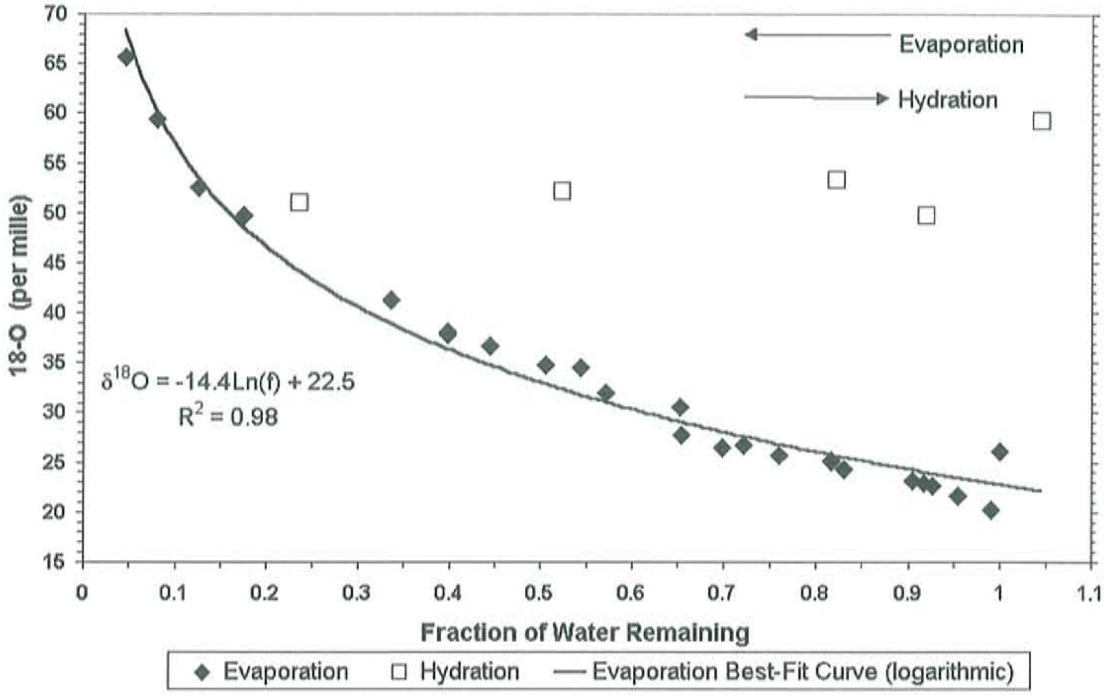

Figure 14 Oxygen-18 data from DIC during the evaporation and hydration of the $NaHCO_3$ solution. The best-fit Rayleigh curve to the evaporation data shows an average enrichment of -14.4‰.

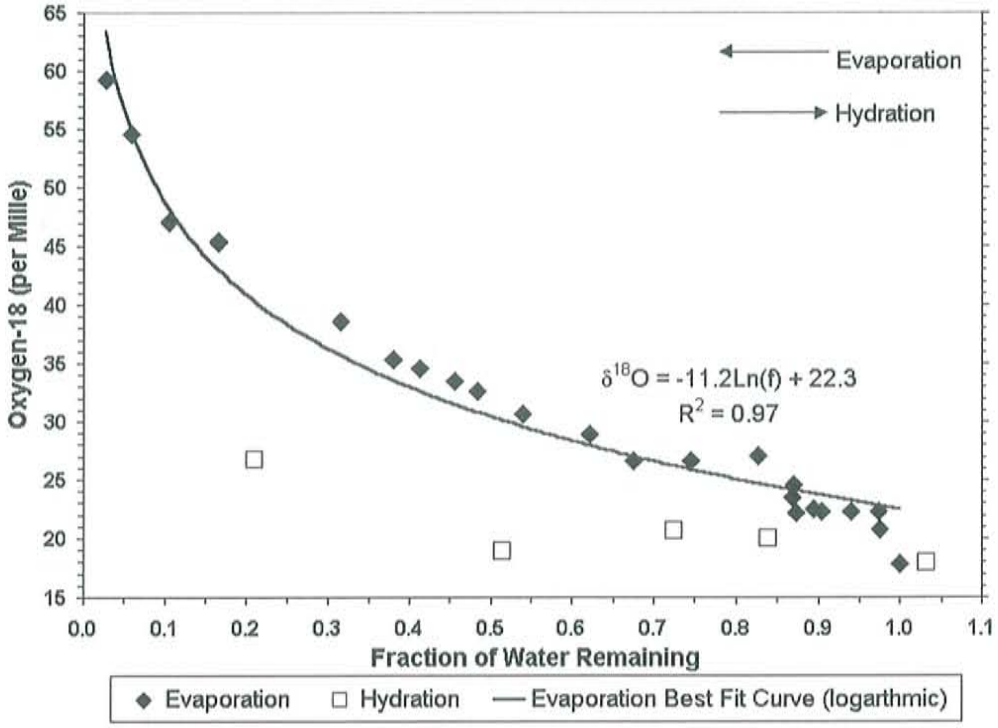

Figure 15 Oxygen-18 data from DIC measured during the evaporation and hydration of the Ca-Na-HCO_3-Cl solution.

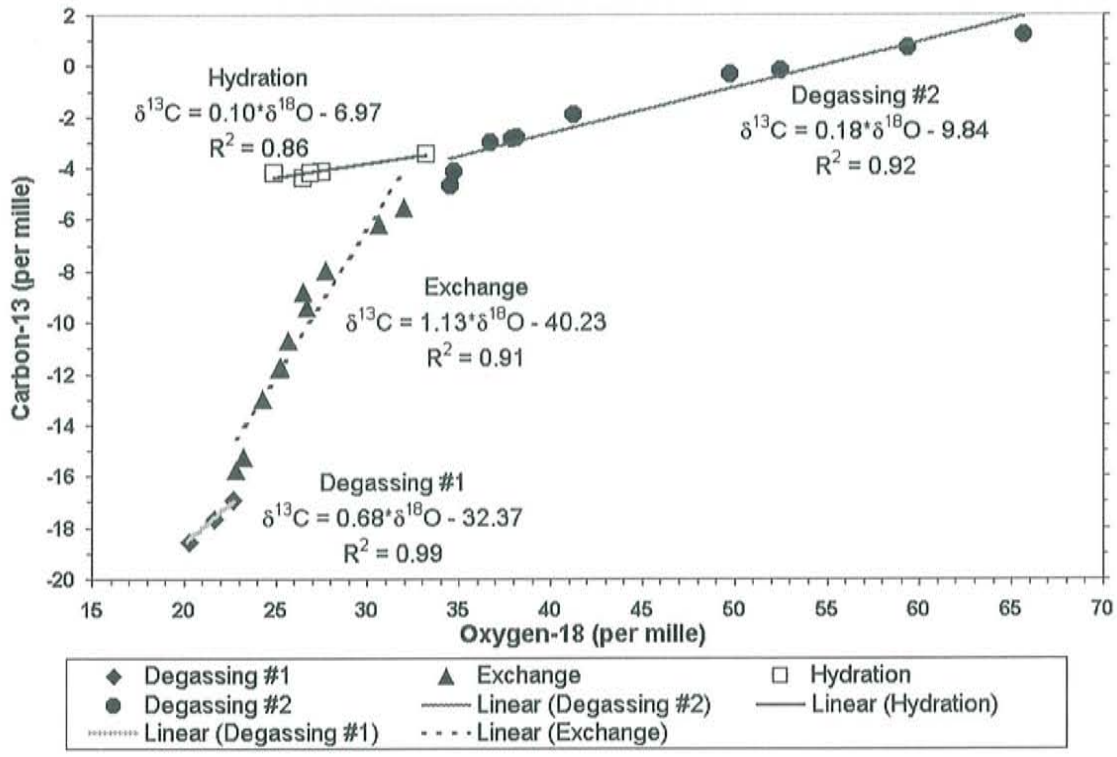

Figure 16 Carbon-13 versus Oxygen-18 data measured from DIC during the evaporation and hydration of the Na-HCO_3 solution. The data set has been subdivided into multiple subsets with linear lines fit to each. Each subset has an R^2 greater than 0.7. Subsets were defined in Figure 12 based on loss of carbon.

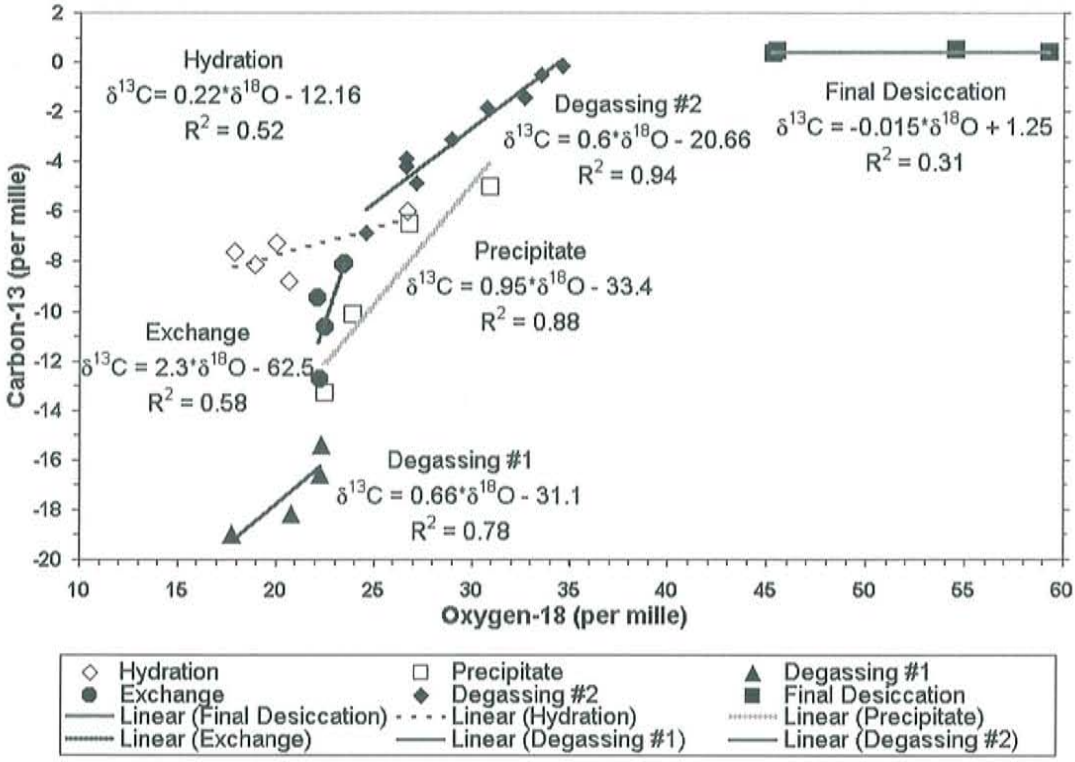

Figure 17 Carbon-13 versus oxygen-18 data measured from DIC during the evaporation and hydration of the Ca-Na-HCO_3-Cl solution. The carbon-13 and oxygen-18 from the collected precipitate has also been included. The data set has been subdivided into multiple subsets with linear lines fit to each. The subsets were defined in Figure 13 based on loss of carbon. The degassing subsets and the precipitate have R-squared values greater than 0.7.

4.3. Carbon Exchange and Degassing Model

The lack of Rayleigh-type evaporation in both of the experimental solutions prompted the development of a carbon model that would account for the exchange and degassing portions of the carbon evolution. The mass balance of dissolved inorganic carbon (DIC) in a water body open to the atmosphere as a function of time can be described by the following reactions:

$$-\frac{dN_{CO_2}}{dt} = k_1 Sp_{CO_2} - k_2 SK_{H,CO_2} m_{CO_2} - Q_{CaCO_3} \tag{36}$$

$$-\frac{dN_{^{13}CO_2}}{dt} = k_3 Sp_{^{13}CO_2} - k_4 SK_{H,^{13}CO_2} m_{^{13}CO_2} - Q_{Ca^{13}CO_3} \tag{37}$$

The parameters in the model are defined in Table 3. The model accounts for the gas, liquid and solid forms of carbon present in the system. Equations (36) and (37) can be converted into discrete forms for each measurement step of the evaporation experiments:

$$-\Delta N_{CO_2} = (k_1 Sp_{CO_2} - k_2 SK_{H,CO_2} m_{CO_2} - Q_{CaCO_3})\Delta t \tag{38}$$

$$-\Delta N_{^{13}CO_2} = (k_3 Sp_{^{13}CO_2} - k_4 SK_{H,^{13}CO_2} m_{^{13}CO_2} - Q_{Ca^{13}CO_3})\Delta t \tag{39}$$

Equation (38) is constrained by a mass-balance inventory of the carbon-12 present in the evaporating system. The parameters for equation (39) can then be calculated using the relationships described in equations (40) through (43).

Parameter	Definition	Value and/or Units
N	moles of Carbon in System	moles
S	Water surface area	0.4793 m^2
P	Partial pressure of atmospheric CO_2	3.30E-04 atm
K_H	Henry's Law Constant	32.2 (atm-L (mol H_2CO_3)$^{-1}$)
m	Aqueous phase concentration of carbon	moles
Q	Rate of calcite precipitated or dissolved	moles/day
t	Time	day
k_1	In Mixing Constant of CO_2	(moles m^{-2} atm^{-1} day^{-1})
k_2	Loss Constant of CO_2 to Atmosphere	(moles m^{-2} atm^{-1} day^{-1})
k_3	In Mixing Constant of $^{13}CO_2$	(moles m^{-2} atm^{-1} day^{-1})
k_4	Loss Constant of $^{13}CO_2$ to Atmosphere	(moles m^{-2} atm^{-1} day^{-1})
R_{atm}	Absolute isotopic abundance ratio for atmospheric CO_2	0.01115854
R_{sol}	Absolute isotopic abundance ratio for DIC in the solution	-
R_{pdb}	Absolute isotopic abundance ratio for PDB carbon reference standard	0.0112372
$\alpha_{13,sol-gas}$	Isotopic fractionation factor for the dissolved phase- gas transition	1.0085

Table 3 Definitions, units and constant values for parameters used in the carbon exchange and degassing model.

$$m_{CO_2} = \frac{\frac{\Delta N_{CO_2}}{\Delta t} + k_1 S p_{CO_2} - Q_{CaCO_3}}{k_2 S K_{H,CO_2}} \tag{40}$$

$$p_{^{13}CO_2} = R_{atm} p_{CO_2} \tag{41}$$

$$K_{H,^{13}CO_2} = \frac{K_{H,CO_2}}{\alpha_{13,sol-gas}} \tag{42}$$

$$m_{^{13}CO_2} = R_{sol} m_{CO_2} \tag{43}$$

After equation (39) has been solved for each time step, $R_{sol,\,new}$ can be calculated from equation (44).

$$R_{sol,new} = \frac{N^{\circ}_{^{13}CO_2} - \Delta N_{^{13}CO_2}}{N^{\circ}_{CO_2} - \Delta N_{CO_2}} \tag{44}$$

Using the $R_{sol,new}$, the new $\delta^{13}C$ can be calculated according to equation (45).

$$\delta^{13}C_{new} = \left(\frac{R_{sol,new}}{R_{pdb}} - 1 \right) * 10^3 \qquad (45)$$

Using this model, the known mass-balance relationships, and the constants defined in Table 3, the exchange constants k_1, k_2, k_3, and k_4 were adjusted yielding values for $R_{sol,\,new}$ and $\delta^{13}C_{new}$. The exchange constants were adjusted to give a best fit to the $\delta^{13}C$ data collected during the experiment.

The gas exchange constants represent the rate at which carbon dioxide moves into and out of a water body. In the case of natural lakes, this parameter has been difficult to quantify experimentally because of the large numbers of potentially contributing variables such as wind velocity, surface films, air-water temperatures and humidity. In most cases, the gas exchange constants have been inferred through long term monitoring of ^{14}C:^{12}C ratios (Peng and Broecker, 1980), mass balance accounting of carbon sources and sinks (Barkan, et al., 2000) and tracer injection (Wanninkhof, et al. 1987). However, the results are often suspect and investigations on the same lake with differing methods have not yielded comparable results (Peng and Broecker and Wanninkhof). These studies are not directly comparable to this experiment because of differences in model formulation and definitions of the exchange constant.

The exchange constants, k_1, k_2, k_3, and k_4, in the case of this experiment are a gross or unidirectional exchange constant and all assumed to equal a single value, k. This assumption is made based on the relatively short (121 days) duration of the experiment, the lack of direct wind and constant surface area. In the case of the Na-HCO_3 solution,

the best fit of the model to the experimental data occurred when k was equal to 26 moles*m^{-2}*atm^{-1}*day^{-1}. Figure 18 shows the excellent overall fit of the model to the experimental data when plotted against the running time of the experiment. The model also captures the erratic behavior of the carbon-13 enrichment when compared to the loss of carbon during the evaporation (Figure 19). The Ca-Na-HCO_3 solution had the best fit when k was equal to 22 moles*m^{-2}*atm^{-1}*day^{-1} (Figure 20). The comparison of experimental data and the model when plotted against the running time of the experiment shows a good fit overall with the exception of the last several data points. These data did not show a correlation as discussed in the previous section and were labeled as a period of final desiccation. Figure 21 plots the carbon-13 data and model results versus the residual fraction of carbon. This also indicates that the model was also able to capture the erratic behavior of the slightly more complicated solution with a calcite precipitate. The lack of a fit to the final few data points may suggest that k was not constant during the experiment or that the surface to volume ratio of the solution, which is not accounted for in this model, is an important factor. Overall, the model fit to both solutions is quite good.

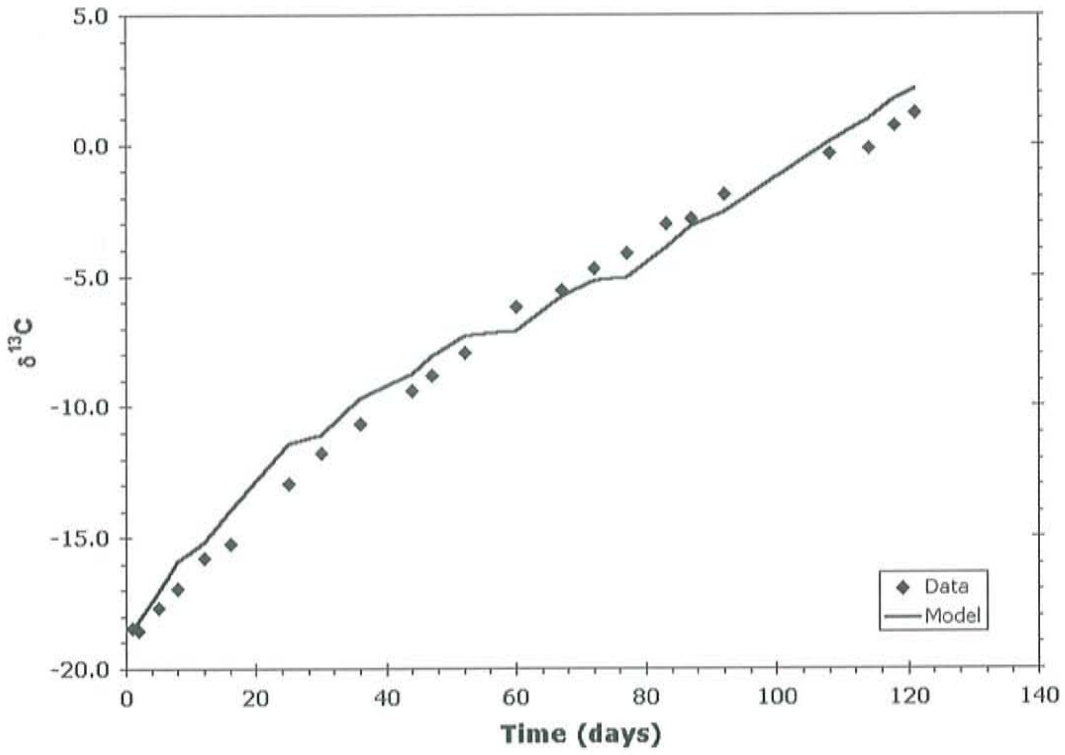

Figure 18 Experimental Carbon-13 data from the evaporation of the Na-HCO_3 solution plotted versus the running time of the experiment in days. The solid line indicates the model result with in mixing and loss parameters equal to 26 moles*m^{-2}*atm^{-1}*day^{-1}.

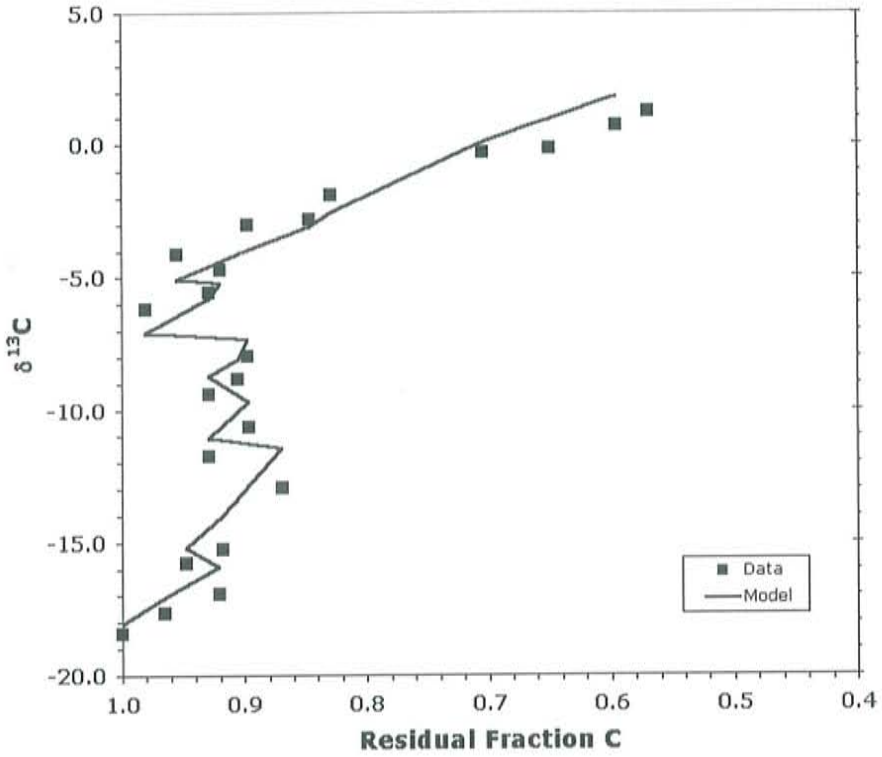

Figure 19 Experimental Carbon-13 data from the evaporation of the Na-HCO_3 solution plotted versus the residual fraction of carbon. The solid line indicates the model result with in mixing and loss parameters equal to 26 moles*m^{-2}*atm^{-1}*day^{-1}. The model captures of seemingly erratic behavior of the cabon-13 enrichment during the evaporation.

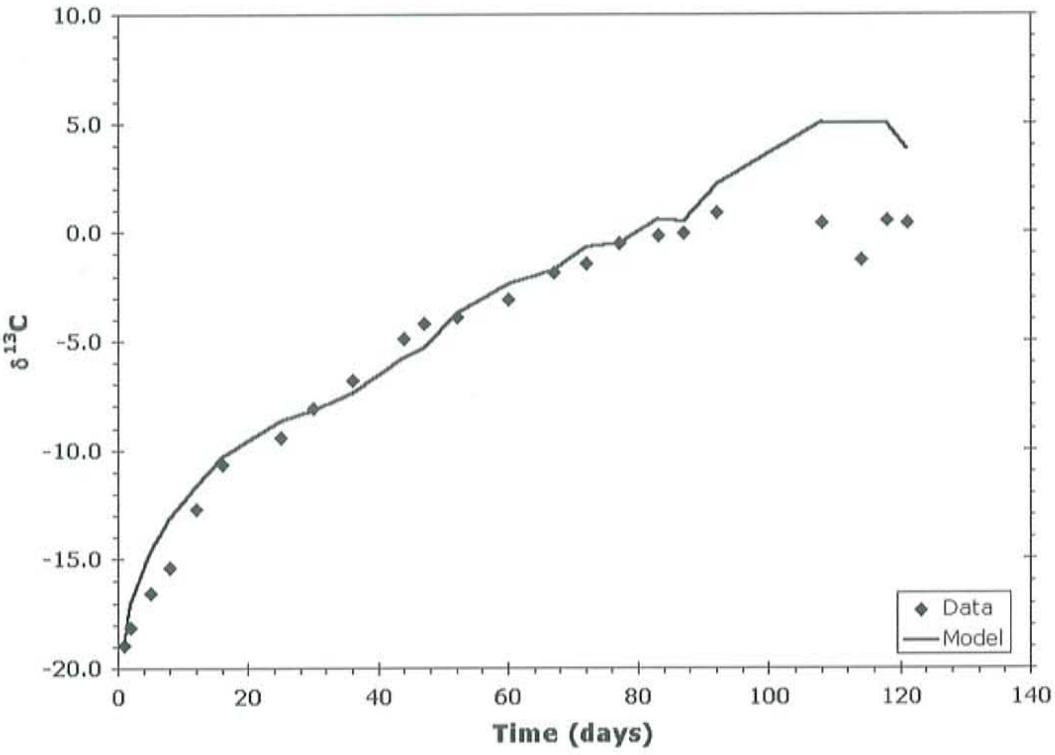

Figure 20 Experimental Carbon-13 data from the evaporation of the Ca-Na-HCO_3-Cl solution plotted versus the running time of the experiment in days. The solid line indicates the model result with in mixing and loss parameters equal to 22 moles*m^{-2}*atm^{-1}*day^{-1}. The model fits the data well with the exception of the last few data points which were labeled as final desiccation in the previous sections.

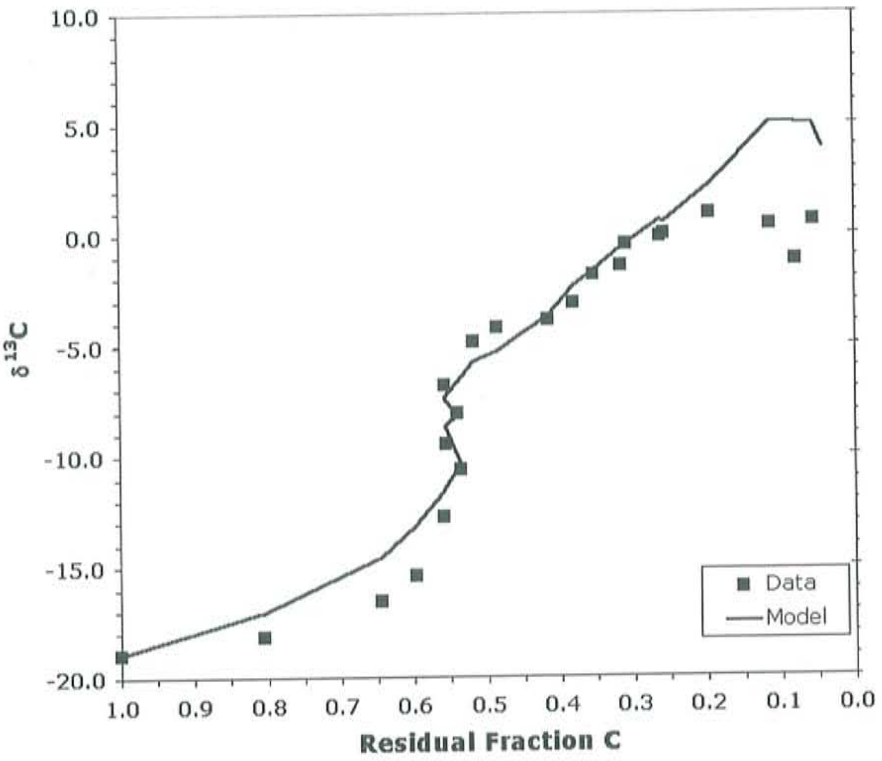

Figure 21 Experimental Carbon-13 data from the evaporation of the Ca-Na-HCO_3-Cl; solution plotted versus the residual fraction of carbon. The solid line indicates the model result with in mixing and loss parameters equal to 22 moles*m^{-2}*atm^{-1}*day^{-1}. The model captures the behavior of the cabon-13 enrichment during the evaporation and precipitation of calcite, with the exception of the last data points.

4.4. Additional Isotopic Enrichments and Results

The analysis of the water oxygen-18 and deuterium data (Appendix L) suggests that the wind velocities above the solution were higher than in a controlled laboratory but less than above a lake or ocean (Appendix L). The oxygen and deuterium measurement pairs deviated from the meteoric water line (Appendix L) with a slope of ~4, as expected for an evaporative trend with humidities less than 85% (Clark and Fritz, 1997). The oxygen-18 and deuterium data indicate Rayleigh distillation, which was the expected pattern for this type of experiment. The oxygen-18 data follow the expected mixing

changes during the hydration (Appendix L) of both solutions, yet the deuterium data show significant deviation from the calculations.

The oxygen-18 isotopic difference between the water ions and the carbonate ions (Appendix K) in the Na-HCO_3 solution averaged -30.9‰ with a standard deviation of 1.8‰. The Ca-Na-HCO_3-Cl solution had an isotopic difference of -28.0‰ with a standard deviation of 3.8‰. The isotopic differences tended toward smaller values at the latter stages of evaporation. The calculated values were similar to the experimental values of Usdowski et al. (1991). The reduction in isotopic differences was most likely due to the inclusion of carbonate in the isotopic measurement. The reduction in values at the end of the evaporation phase occurred at the peak of carbonate concentration. However, even using the bulk carbonate values, and recalling the temperature differences between this work and that of Usdowski et al. (1991), the similarity of the isotopic differences suggest equilibrium and rapid isotopic exchange between the water and carbonate reservoirs. The hydration calculations of isotopic difference in the Na-HCO_3 solution (-30.2‰, standard deviation of 1.1‰) are similar to the evaporation calculation (-30.9‰ standard deviation of 1.8‰) again consistent with the dilution effect during the hydration phase. During the hydration of the Ca-Na-HCO_3-Cl solution, the isotopic difference was -23.6‰ with a standard deviation of 1.5‰. The reduction from the evaporation value (-28.0‰, standard deviation of 3.8‰) was most likely due to changes in solution composition, but the bulk measurement do not allow for further analysis.

Calculated enrichment factors for the carbon-13 during evaporation were not similar to the published equilibrium values, but were similar to the published values during the hydration (Appendix K). The enrichment factors for the movement of carbon-

13 from bicarbonate to degassed carbon dioxide were calculated using a mass balance approach because direct measurements of the carbon dioxide reservoir above the solutions were not made. The expected equilibrium value was ±7.9‰ for both solutions. The calculated average enrichment factor for the Na-HCO_3 solution is –19.4‰. The calculated average enrichment factor between each sampling for the Ca-Na-HCO_3-Cl solution was –7.3‰, the cumulative average was -22.7‰. The values for the same carbon species during the hydration phase were 8.14‰ in the Na-HCO_3 solution and 11.1‰ in the Ca-Na-HCO_3-Cl solution. The enrichment factors for the hydration phase were most likely representative of equilibrium enrichment.

5. CONCLUSIONS: IMPLICATIONS FOR LACUSTRINE SYSTEMS

This work contributes to paleoclimate studies, which currently explore the possibility of obtaining a continental climate record from lake cores. The covariant trend between oxygen-18 and carbon-13 is considered diagnostic of a closed-basin lake condition, but little experimental work has been done to identify geochemical mechanisms that could lead to the covariant trend. This study demonstrates that covariation can be produced between oxygen-18 and carbon-13 in solution and calcite precipitate without the influence of biological processes on the carbon isotopes.

In addition to the demonstration of a geochemically produced covariant trend, the carbon-13 data was found to exhibit both degassing and exchange- type enrichment. A model accounting for the carbon mass balance in gas, liquid and solid phases and exchange between the gas and liquid phases was able to capture both behaviors. The data and the model were in good agreement when the exchange constants were equal to 26 and 22 $mol*m^{-2}*d^{-1}*atm^{-1}$ for the Na-HCO_3 and Ca-Na-HCO_3-Cl solutions respectively.

There were differences between this experiment and a natural lake worth noting. Most important were the reduced wind velocities in our experimental setting, and the comparatively short residence time of the solutions. In addition, the initial condition was generally not comparable to a dilute fresh water lake, in terms of chemistry or isotopic

composition. In this case, chemical and isotopic equilibration with the atmosphere normally occurring in the turbulent mixing environment of a river occurred in the still evaporating environment of the experimental lake. The experiments also had a much smaller volume to surface area ratio than a natural lake introducing a much larger exchange component to the isotopic enrichment of carbon.

There were other experimental difficulties, referred to in the appendices. Difficulties such as the apparent supersaturation of carbon dioxide, resulting in elevated pH and the dominance of exchange rather than degassing for most of the experimental evaporation. Experimental difficulties at the laboratory and field scales are expected and do not detract from the overall study. On the contrary, the presence of anomalous results that do not destroy the covariant relationship reinforce the ability of a geochemical mechanism to generate a covariant trend.

6. REFERENCES

Asher, W. and R. Wannikhof (1998). "Transient tracers and air-sea gas transfer." Journal of Geophysical Research **103**(c8): 15939-15958.

Benson, L., and Z. Peterman (1995). "Carbonate deposition, Pyramid Lake subbasin, Nevada: 3. The use of 87-Sr values in carbonate deposits (tufas) to determine the hydrologic state of paleolake systems." Palaeogeography, Palaeoclimatology, Palaeoecology **119**: 201-213.

Bevington, P.R. and D. K. Robinson (1992) *Data Reduction and Error Analysis for the Physical Sciences,* WCB McGraw-Hill, Boston.

Campbell, A.R. and P.B. Larson (1998). "Introduction to Stable Isotope Applications in Hydrothermal Systems." [Title Unknown] Richardson and Larson, Society of Economic Geologist, Volume 10.

Clark, I.D. and P. Fritz (1997) *Environmental Isotopes in Hydrogeology,* Lewis Publishers, Boca Raton.

Clark, I. D., J-C. Fontes and P. Fritz (1992). "Stable isotope disequilibria in travertine from high pH waters: Laboratory investigations and field observations from Oman." Geochimica et Cosomochimica Acta **56**: 2041-2050.

Cohn, M., and H.C. Urey (1938). "Oxygen Exchange Reactions of Organic Compounds and Water." J. Amer. Chem. Soc. **60**: 679-687.

Coleman, M.C., T.J. Shepherd, J.J. Durham, J.D. Rouse and G.R. Moore (1982) "Reduction of water with zinc for hydrogen isotope analysis." Analytical Chemistry. **54**: 993-995.

Conway, T.J., P.P. Tans, and L.S. Waterman (1994). "Atmospheric CO2 records from sites in the NOAA/CMDL air sampling network. In T.A. Boden, D.P. Kaiser, R.J. Sepanski, and F.W. Stoss (eds.), Trends '93: A Compendium of Data on Global Change. ORNL/CDIAC-65. Carbon Dioxide Information Analysis Center, Oak Ridge National Laboratory, U.S. Department of Energy, Oak Ridge, Tenn. U.S.A.

Craig, H. (1957). "Isotopic standard for carbon and oxygen and correction factors for mass-spectrometric analysis of carbon dioxide." Geochimica et Cosmochimica Acta **12**: 133-149.

Drummond, C. N., W.P. Patterson, and J.C.G. Walker (1995). "Climatic forcing of carbon-oxygen isotopic covariance in temperate-region marl lakes." Geology **23**(11): 1031-1034.

Friedman, I., and J.R. O'Neil (1977). Data of Geochemistry (Sixth Edition), U.S. Geological Survey Professional Paper 440-KK, USGS, Washington, D.C.

Fritz, P., T.W. Anderson, and C.F.M. Lewis (1975). "Late-Quaternary climatic trends and history of Lake Erie from stable isotope studies." Science **190**: 267-269.

Fritz, P. (1980). Tools to complement the classical techniques of physical hydrology and geochemistry. Environmetal Isotope Hydrology. Waterloo Ontario, University of Waterloo**:** 26-33.

Gasse, F. and J.C. Fontes, (1989). "Paleoenvironments and Paleohydrology of a tropical closed lake (Lake Asal, Djibouti) since 10,000yr B.P." Palaeogeography, Palaeoclimatology, Palaeoecology. **69**: 67-102.

Gasse, F., J.C. Fontes, J.C. Plaziat, P. Carbonel, I. Kacsmarska, P. De Deckker, I. Soulie-Marsche, Y. Callot, and P. Dupeuble (1987). "Biological remains, geochemistry ad stable isotopes for the reconstruction of environmental and hydrological changes in the Holocene lakes from North Sahara." Palaeogeography, Palaeoclimatology, Palaeoecology. **60**: 1-46.

Gat, G.R. (1981) Lakes. In *Stable Isotope Hydrology*: *Deuterium and Oxygen-18 in the Water Cycle*, Tech. Rept. Ser. No. 210 pp. 203-221. IAEA, Vienna.

Gilath, C., and R. Gonfiantini (1983). Lake Dynamics. Guidebook on Nuclear Techniques in Hydrology. Vienna, International Atomic Energy Agency**:** 129-161.

Gonfiantini, R. (1986). Environmental isotopes in lakes studies. Handbook of Environmental Isotope Geochemistry. P. Fritz, and J. Ch. Fontes, Elsevier Scientific. **2:** 113-168.

Hahn, B.D. (1996) Fortan 90 For Scientists and Engineers. Arnold.

Johnson, T. C., J.D. Halfman and W.J. Showers (1991). "Paleoclimate of the past 4000 years at Lake Turkana, Kenya, based on the isotopic composition of authigenic calcite." Palaeography, Palaeoclimatology, Palaeoecology **85**: 189-198.

Kim, S. E., and J.R. O'Neil (1997). "Equilibrium and nonequilibrium oxygen isotope effects in synthetic carbonates." Geochimica et Cosomochimca Acta **61**(16): 3461-3475.

Li, H.-C., and T. L. Ku (1997). "13-C - 18O covariance as a paleohydrological indicator for closed-basin lakes." Palaeogeography, Palaeoclimatology, Palaeoecology **133**: 69-80.

Majzoub, M. (1971). "Fractionation en oxygen-18 et en deuterium entre l'eau et sa vapeur." Jour. Chim. Phys. **68**: 1423-1436.

McKenzie, J.A. (1985). Carbon isotopes and productivity in the lacustrine and marine environment. Chemical Processes in Lakes. W. Strumm, Wiley, New York. 99-118.

Merlivat, L. and J. Jouzel (1979)."Global Climatic Interpretation of the Deuterium-Oxygen-18 Relationship for Precipitation." Jounal of Geophysical Reearch. **84**:5029-5033.

Mook, W. G., J.C. Boomerson, and W.H. Staverman (1974). "Carbon isotope fractionation between dissolved bicarbonate and gaseous carbon dioxide." Earth and Planetary Science Letters **22**: 169-176.

Parkhurst, D. L. and C.A.J. Appelo (1999). "User's guide to PHREEQC (Version 2)- A computer program for speciation, reaction-path, advective-transport, and inverse geochemical calculations." USGS Water-Resources Investigation Report 99-4259.

Smith, G. I. (1997). Stratigraphy, lithologies, and sedimentary structures of Owens Lake core OL-92. An 800,000-year Paleoclimatic record from Core OL-92, Owens Lake, Southeast California. G. I. Smith, and J.L. Bischoff, Geological Society of America. **Special Paper 317:** 9-23.

Socki, R. A., H.R. Karlsson, and E.K. Gibson Jr. (1992). "Extraction technique for the determination of Oxygen-18 in water using preevacuated glass vials." Anal. Chem. **64**: 829-831.

Spencer, R.J., M.J. Baedecker, H.P. Eugster, R.M. Forester, M.B. Goldhaber, B.F. Jones, K. Kelts, J. McKenzie, D.B. Madsen, S.L, Rettig, M. Rubin, and C.J. Bowser (1984). "Great Salt Lake, and precursors, Utah: the last 30,000 years." Contrib. Mineral. Petrol. **86**: 321-334.

Stiller, M., J.S. Rounick, and S. Shasha (1985). "Extreme carbon-isotope enrichments in evaporating brines." Nature **316**: 434-435.

Stuiver, M. (1970). "Oxygen and carbon isotope ratios of fresh-water carbonates as climatic indicators." Jounal of Geophysical Research **75**(27): 5247-5257.

Talbot, M.R. (1994). "Palehydrology of the late Miocene Ridge basin lake, California." Geological Society of America Bulletin. **106**: 1121-1129.

Talbot, M. R. (1990). "A review of the palaeohydrological interpretation of carbon and oxygen isotopic ratios in primary lacustrine carbonates." Chemical Geology **80**: 261-279.

Teranes, J. L., J.A. McKenzie, S.M. Bernasconi, A.F. Lotter, and M. Sturm (1999). "A study of oxygen isotopic fractionation during bio-induced calcite precipitation in eutropic Baldeggersee, Switzerland." Geochimica et Cosmochimica Acta **63**(13/14): 1981-1989.

Usdowski, E., J. Michaelis, M.E. Bottcher and J. Hoefs (1991). "Factor for the Oxygen Isotope Equilibrium Fractionation between Aqueous and Gaseous CO_2, Carbonic Acid, Bicarbonate, Carbonate, and Water (19°C)." Zeitschrift fur Physikalische Chemie, Bd **170**: 237-249.

APPENDICES

A. Stable Isotope Notation

$$R = \frac{\#\text{ of atoms of rare isotope}}{\#\text{ of atoms of common isotope}} \tag{46}$$

$$\delta_a = (\frac{R_a}{R_{std}} - 1) * 10^3 \tag{47}$$

$$\varepsilon_{ab} = (\frac{R_a}{R_b} - 1) * 10^3 \tag{48}$$

$$\varepsilon_{ab} \cong \delta_a - \delta_b \tag{49}$$

$$\varepsilon_{ab} \cong -\varepsilon_{ba} \tag{50}$$

$$\alpha_{ab} = \frac{R_a}{R_b} \tag{51}$$

$$10^3 * \ln \alpha_{ab} \cong \varepsilon_{ab} \tag{52}$$

$$\Delta_{ab} = \delta_a - \delta_b \tag{53}$$

$$\Delta_{ab} \cong \varepsilon_{ab} \tag{54}$$

B. Data from Sample Preservation

B.1. Precipitate yields

Sample	Weight of Precipitate (g)	Sample	Weight of Precipitate (g)
1 $Na\text{-}HCO_3$	0.1	1 $Ca\text{-}Na\text{-}HCO_3\text{-}Cl$	0.1
2 $Na\text{-}HCO_3$	0.1289	2 $Ca\text{-}Na\text{-}HCO_3\text{-}Cl$	0.1204
3 $Na\text{-}HCO_3$	0.1345	3 $Ca\text{-}Na\text{-}HCO_3\text{-}Cl$	0.1156
4 $Na\text{-}HCO_3$	0.1337	4 $Ca\text{-}Na\text{-}HCO_3\text{-}Cl$	0.1034
5 $Na\text{-}HCO_3$	0.1344	5 $Ca\text{-}Na\text{-}HCO_3\text{-}Cl$	0.0829
6 $Na\text{-}HCO_3$	0.1334	6 $Ca\text{-}Na\text{-}HCO_3\text{-}Cl$	0.0791
7 $Na\text{-}HCO_3$	0.1418	7 $Ca\text{-}Na\text{-}HCO_3\text{-}Cl$	0.0986
8 $Na\text{-}HCO_3$	0.1447	8 $Ca\text{-}Na\text{-}HCO_3\text{-}Cl$	0.1015
9 $Na\text{-}HCO_3$	0.1575	9 $Ca\text{-}Na\text{-}HCO_3\text{-}Cl$	0.0980
10 $Na\text{-}HCO_3$	0.1586	10 $Ca\text{-}Na\text{-}HCO_3\text{-}Cl$	0.0577
11 $Na\text{-}HCO_3$	0.1701	11 $Ca\text{-}Na\text{-}HCO_3\text{-}Cl$	0.0857
12 $Na\text{-}HCO_3$	0.1831	12 $Ca\text{-}Na\text{-}HCO_3\text{-}Cl$	0.0911
13 $Na\text{-}HCO_3$	0.1954	13 $Ca\text{-}Na\text{-}HCO_3\text{-}Cl$	0.0774
14 $Na\text{-}HCO_3$	0.2079	14 $Ca\text{-}Na\text{-}HCO_3\text{-}Cl$	0.0573
15 $Na\text{-}HCO_3$	0.2257	15 $Ca\text{-}Na\text{-}HCO_3\text{-}Cl$	0.0852
16 $Na\text{-}HCO_3$	0.2488	16 $Ca\text{-}Na\text{-}HCO_3\text{-}Cl$	0.0811
17 $Na\text{-}HCO_3$	0.2698	17 $Ca\text{-}Na\text{-}HCO_3\text{-}Cl$	0.1102
18 $Na\text{-}HCO_3$	0.2916	18 $Ca\text{-}Na\text{-}HCO_3\text{-}Cl$	0.0778
19 $Na\text{-}HCO_3$	0.3383	19 $Ca\text{-}Na\text{-}HCO_3\text{-}Cl$	0.0978
20 $Na\text{-}HCO_3$	0.5515	20 $Ca\text{-}Na\text{-}HCO_3\text{-}Cl$	0.1458
21 $Na\text{-}HCO_3$	0.7548	21 $Ca\text{-}Na\text{-}HCO_3\text{-}Cl$	0.0115
22 $Na\text{-}HCO_3$	1.1046	22 $Ca\text{-}Na\text{-}HCO_3\text{-}Cl$	0.1195
23 $Na\text{-}HCO_3$	1.8310	23 $Ca\text{-}Na\text{-}HCO_3\text{-}Cl$	0.2008
1 $Na\text{-}HCO_3$ Hydration	0.3599	1 $Ca\text{-}Na\text{-}HCO_3\text{-}Cl$ Hydration	0.0406
2 $Na\text{-}HCO_3$ Hydration	0.1837	2 $Ca\text{-}Na\text{-}HCO_3\text{-}Cl$ Hydration	0.0138
3 $Na\text{-}HCO_3$ Hydration	0.1379	3 $Ca\text{-}Na\text{-}HCO_3\text{-}Cl$ Hydration	0.0328
4 $Na\text{-}HCO_3$ Hydration	0.1145	4 $Ca\text{-}Na\text{-}HCO_3\text{-}Cl$ Hydration	0.0232
5 $Na\text{-}HCO_3$ Hydration	0.0894	5 $Ca\text{-}Na\text{-}HCO_3\text{-}Cl$ Hydration	0.0122
--	--	7 Precipitate	0.1309
--	--	13 Precipitate	0.0314
--	--	16 Precipitate	0.0045
--	--	17 Precipitate	0.0339
--	--	20 Precipitate	0.0025
--	--	23 Precipitate	0.3600

Table 4 Precipitate yields from $BaCl_2$ procedure and direct precipitation yields from the $Ca\text{-}Na\text{-}HCO_3\text{-}Cl$ solution.

C. Isotopic Data

C.1. Processing Data for CO_2 Analyses

Sample ID	mg CO_3	Δ Hg	μMoles CO_2	% Yield
7 Precipitate	11.8	7.3	85.55	72.5
13 Precipitate	10.9	6.7	78.32	71.85
17 Precipitate	10.8	6.5	75.92	70.3
23 Precipitate	12.5	8.1	95.24	76.19

Table 5 Isotopic processing data for the carbonate precipitate from the Ca-Na-HCO_3-Cl solution.

Sample ID	mg CO_3	Δ Hg	µMoles CO_2	% Yield
1 Na-HCO_3	10	3.5	40.37	40.37
2 Na-HCO_3	10.8	3.3	38.03	35.21
3 Na-HCO_3	10.8	4.1	47.41	43.9
4 Na-HCO_3	10.4	4	46.24	44.46
5 Na-HCO_3	20.4	7.1	83.14	40.75
6 Na-HCO_3	10.2	3.2	36.87	36.15
7 Na-HCO_3	20.7	7.4	86.76	41.91
8 Na-HCO_3	20.4	7	81.93	40.16
9 Na-HCO_3	20.5	7	81.93	39.97
10 Na-HCO_3	19.6	6.8	79.53	40.58
11 Na-HCO_3	19.4	5.6	65.17	33.59
12 Na-HCO_3	10.5	3.7	45.72	43.54
13 Na-HCO_3	21.2	7.2	84.34	39.78
14 Na-HCO_3	20.7	7.4	86.76	41.91
15 Na-HCO3	20.8	7.4	86.76	41.71
16 Na-HCO3	20.9	7.6	89.19	42.67
17 Na-HCO_3	20.9	7.5	87.97	42.09
18 Na-HCO_3	10.4	3.9	45.06	43.33
18 Na-HCO_3 Duplicate	10.7	4.1	47.41	44.31
19 Na-HCO_3	21.1	7.8	91.6	43.41
20 Na-HCO_3	21	7.5	87.97	41.89
20 Na-HCO_3 Duplicate	22.8	8.5	100.11	43.91
21 Na-HCO_3	10.6	4.1	47.41	44.73
22 Na-HCO_3	22.1	8.3	97.67	44.19
23 Na-HCO_3	20.2	8.1	95.24	47.15
24 Na-HCO_3	12.3	4.4	50.95	41.42
25 Na-HCO_3	11.3	4.5	52.13	46.13
26 Na-HCO_3	12.2	4.6	53.31	43.7
27 Na-HCO_3	113	4.5	52.13	46.13
28 Na-HCO_3	12.7	5.1	59.23	46.64

Table 6 Isotopic processing data for the $BaCl_2$ precipitated carbonates from the Na-HCO_3 solutions.

Sample ID	mg CO_3	Δ Hg	μMoles CO_2	% Yield
1 Ca-Na-HCO_3-Cl	10.8	4	46.24	42.81
2 Ca-Na-HCO_3-Cl	10.4	4.1	47.41	45.59
3 Ca-Na-HCO_3-Cl	20.3	8.2	96.46	47.52
4 Ca-Na-HCO_3-Cl	10.8	3.6	41.54	38.46
5 Ca-Na-HCO_3-Cl	20.2	7.6	89.18	44.15
6 Ca-Na-HCO_3-Cl	10.3	3.9	45.06	43.75
7 Ca-Na-HCO_3-Cl	20.5	6.1	71.13	34.7
8 Ca-Na-HCO_3-Cl	20.8	7.1	83.14	39.97
8 Ca-Na-HCO_3-Cl Duplicate	20.4	6.4	74.72	36.63
9 Ca-Na-HCO_3-Cl	22	3.9	45.06	20.48
10 Ca-Na-HCO_3-Cl	20.1	6.2	72.33	35.99
11 Ca-Na-HCO_3-Cl	20.3	5.	58.04	28.59
12 Ca-Na-HCO_3-Cl	10.5	3.5	40.37	38.45
13 Ca-Na-HCO_3-Cl	19.9	5.8	67.55	33.94
14 Ca-Na-HCO_3-Cl	20	5.9	68.74	34.37
15 Ca-Na-HCO_3-Cl	19.8	4.7	54.49	27.52
16 Ca-Na-HCO_3-Cl	20.6	5.1	59.23	28.75
17 Ca-Na-HCO_3-Cl	20.7	6.4	74.72	36.1
18 Ca-Na-HCO_3-Cl	10.5	3.3	38.03	36.22
19 Ca-Na-HCO_3-Cl	19.9	60	69.94	35.15
20 Ca-Na-HCO_3-Cl	20.8	2.5	28.72	13.81
20 Ca-Na-HCO_3-Cl Duplicate	20.1	3.9	45.06	22.42
21 Ca-Na-HCO_3-Cl	10.8	2.2	25.24	23.37
22 Ca-Na-HCO_3-Cl	22.3	1.6	18.31	8.21
23 Ca-Na-HCO_3-Cl	20.1	2.1	24.08	11.98
24 Ca-Na-HCO_3-Cl	12.2	1.7	19.46	15.95
25 Ca-Na-HCO_3-Cl	10.2	2.1	24.08	23.61
26 Ca-Na-HCO_3-Cl	12.8	3.4	39.2	30.63
27 Ca-Na-HCO_3-Cl	10.	2.2	25.24	25.24
28 Ca-Na-HCO_3-Cl	9.9	3.1	35.7	36.06

Table 7 Isotopic processing data for the $BaCl_2$ precipitated carbonates from the Ca-Na-HCO_3-Cl solution.

C.2. Processing Data for Oxygen-18 Analyses

Sample ID	Δ Hg in	Δ Hg out	μMoles CO_2 in	μMoles CO_2 out	T (°C)	% Yield
1 DI	31.4	16.1	404.61	195.54	26	48.33
2 DI	30.4	15.3	390.26	185.23	26	47.46
3 DI	31.6	15.9	407.5	192.96	24.7	47.35
3 DI Duplicate	31	16	398.86	194.25	24.7	48.7
4 DI	31.1	15.6	400.3	189.09	24.7	47.24
5 DI	30.8	15.3	359.99	185.23	26	46.78
5 DI Duplicate	30.6	15.5	393.12	187.8	24.7	47.77
6 DI	30.6	15.3	393.12	185.23	26	47.12
7 DI	30.6	15.4	393.12	186.51	24.7	47.44
8 DI	31	15.8	398.86	191.67	24.7	48.05
8 DI Duplicate	31.4	15.9	404.61	192.96	26	47.69
9 DI	31.6	16.4	407.5	199.42	24.7	48.94
10 DI	30.6	12.5	393.12	149.64	26	38.06
10 DI Duplicate	30.8	15.5	395.99	187.8	26	47.43
11 DI	31.4	15.7	404.61	190.38	29	47.05
11 DI Duplicate	30.9	0.6	397.42	6.84	27	1.72
12 DI	31.6	15.8	407.5	191.67	26	47.03
13 DI	31.6	15.8	407.5	191.67	26	47.03
14 DI	30.1	15.9	385.97	192.96	26	49.99
14 DI Duplicate	30.9	16.2	397.42	196.83	27	49.53
15 DI	31.6	16	407.5	194.25	24.7	47.67
16 DI	31.2	16.2	401.73	196.83	29	49
16 DI Duplicate	31.6	16.5	407.5	200.72	27	49.26
17 DI	30.8	15.9	395.99	192.96	29	48.73
18 DI	30.8	15.7	395.99	190.38	29	48.08
19 DI	31.2	14.7	401.73	177.54	29	44.19
19 DI Duplicate	31.2	15.7	401.73	190.38	29	47.39
20 DI	30.8	15.7	395.99	190.38	29	48.08
21 DI	30.6	15.3	393.12	185.23	26	47.12
22 DI	30.8	15.5	395.99	187.8	29	47.43
23 DI	30.9	15.7	397.42	190.38	26	47.9
24 DI	31.4	16	404.61	194.25	27	48.01
25 DI	31.4	15.7	404.61	190.38	27	47.05
26 DI	30.6	15.6	393.12	189.09	26	48.1
27 DI	30.9	15	397.42	181.38	26	45.64
28 DI	30.9	15.3	397.42	185.23	26	46.61

Table 8 Isotopic processing data for the analysis of Oxygen-18 samples for the deionized water solution.

Sample ID	Δ Hg in	Δ Hg out	μMoles CO_2 in	μMoles CO_2 out	T (°C)	% Yield
1 Na-HCO_3	31.1	15	400.3	181.38	24.7	45.31
1 Na-HCO_3 Duplicate	31.7	16.3	408.94	198.13	27	48.45
2 Na-HCO_3	30.4	15.1	390.26	182.66	26	46.81
2 Na-HCO_3 Duplicate	31.6	17.1	407.5	208.51	27	51.17
3 Na-HCO_3	31.6	15.6	407.5	189.09	27	46.4
4 Na-HCO_3	30.4	14.6	390.26	176.26	26	45.17
4 Na-HCO_3 Duplicate	31.4	16.1	404.61	195.54	29	48.33
5 Na-HCO_3	30.4	15.3	390.26	185.23	26	47.46
5 Na-HCO_3 Duplicate	31.6	16.6	407.5	202.01	27	49.57
6Na-HCO_3	31.1	15.6	400.3	189.09	24.7	47.24
6 Na-HCO_3 Duplicate	31.4	16	404.61	194.25	26	48.01
7 Na-HCO_3	30.6	15.4	393.12	186.51	26	47.44
8 Na-HCO_3	31.4	15.6	404.61	189.09	26	46.73
9 Na-HCO_3	30.6	6.2	393.12	72.33	26	18.4
9 Na-HCO_3 Duplicate	31.6	16.3	407.5	198.13	24.7	48.62
10 Na-HCO_3	31.4	16.4	404.61	199.42	26	49.29
11 Na-HCO_3	30.9	14.6	397.42	215.03	27	54.11
12 Na-HCO_3	31.4	15.7	404.61	190.38	26	47.05
13 Na-HCO_3	31	16	398.86	194.25	24.7	48.7
14 Na-HCO_3	30.8	15.6	395.99	189.09	29	47.75
15 Na-HCO_3	30.6	15.1	393.12	182.66	24.7	46.46
16 Na-HCO_3	31	15.4	398.86	186.51	26	46.76
17 Na-HCO_3	31.4	15.9	404.61	192.96	29	47.69
17 Na-HCO_3 Duplicate	31.6	16.8	407.5	204.61	24.7	50.21
18 Na-HCO_3	31.2	16.3	401.73	198.13	29	49.32
19 Na-HCO_3	31	15.4	398.86	186.51	26	46.76
20 Na-HCO_3	30.8	15.8	395.99	191.67	29	48.4
21 Na-HCO_3	30.6	15.3	393.12	185.23	26	47.12
21 Na-HCO_3 Duplicate	30.6	15	393.12	181.38	26	46.14
22 Na-HCO_3	31.4	15.4	404.61	186.51	29	46.1

23 $Na\text{-}HCO_3$	31.7	13.7	408.94	164.8	27	40.3
24 $Na\text{-}HCO_3$	30.6	15.8	393.12	191.67	26	48.76
25 $Na\text{-}HCO_3$	31.7	16.2	408.94	196.83	27	48.13
25 $Na\text{-}HCO_3$ Duplicate	31.7	16.2	408.94	196.83	27	48.13
26 $Na\text{-}HCO_3$	31	15.7	398.86	190.38	26	47.73
27 $Na\text{-}HCO_3$	30.1	16.3	385.97	198.13	26	51.33
28 $Na\text{-}HCO_3$	31.7	16.2	408.94	196.83	27	48.13
1 $Na\text{-}HCO_3$ Hydration	31.3	16.1	403.17	195.54	27	48.5
2 $Na\text{-}HCO_3$ Hydration	31.3	15.6	403.17	189.09	27	46.9
3 $Na\text{-}HCO_3$ Hydration	30.6	15.7	393.12	190.38	26	48.43
4 $Na\text{-}HCO_3$ Hydration	31.3	16.2	403.17	196.83	27	48.82
5 $Na\text{-}HCO_3$ Hydration	31.4	16.3	404.61	198.13	27	48.97

Table 9 Isotopic processing data for the analysis of Oxygen-18 samples taken from the $Na\text{-}HCO_3$ solution during both the evaporation and hydration phases.

Sample ID	Δ Hg in	Δ Hg out	µMoles CO_2 in	µMoles CO_2 out	T (°C)	% Yield
1 Ca-Na-HCO_3-Cl	31.1	15.7	400.3	190.38	24.7	47.56
2 Ca-Na-HCO_3-Cl	30.6	15.2	393.12	183.95	24.7	46.79
2 Ca-Na-HCO_3-Cl Duplicate	31	16.2	389.86	196.83	24.7	49.35
3 Ca-Na-HCO_3-Cl	30.4	15.3	390.26	185.23	26	47.46
3 Ca-Na-HCO_3-Cl Duplicate	30.6	15.4	393.12	186.51	24.7	47.44
4 Ca-Na-HCO_3-Cl	30.8	15.3	395.99	185.23	26	46.78
4 Ca-Na-HCO_3-Cl Duplicate	31.6	17.1	407.5	208.51	27	51.17
5 Ca-Na-HCO_3-Cl	31.6	16.3	407.5	198.13	24.7	48.62
6 Ca-Na-HCO_3-Cl	30.8	14.9	395.99	180.1	26	45.48
6 Ca-Na-HCO_3-Cl Duplicate	31.1	16.2	400.3	196.83	24.7	49.17
7 Ca-Na-HCO_3-Cl	31.4	5.6	404.61	65.17	26	16.11
8 Ca-Na-HCO_3-Cl	30.6	15	393.12	181.38	26	46.14
8 Ca-Na-HCO_3-Cl Duplicate	30.1	15.3	385.97	185.23	26	47.99
9 Ca-Na-HCO_3-Cl	30.6	15.5	393.12	187.8	26	47.77
10 Ca-Na-HCO_3-Cl	31.4	16	404.61	194.25	26	48.01
11 Ca-Na-HCO_3-Cl	31.4	15.4	404.61	186.51	26	46.1
12 Ca-Na-HCO_3-Cl	30.6	15.5	393.12	187.8	24.7	47.77
13 Ca-Na-HCO_3-Cl	31.4	15.5	404.61	187.8	26	46.42
13 Ca-Na-HCO_3-Cl Duplicate	31.4	15.3	404.61	185.23	26	45.78
14 Ca-Na-HCO_3-Cl	30.9	14.8	397.42	178.82	27	44.99
14 Ca-Na-HCO_3-Cl Duplicate	31.7	15.8	408.94	191.67	27	46.87
15 Ca-Na-HCO_3-Cl	31.6	16.1	407.5	195.54	27	47.99
16 Ca-Na-HCO_3-Cl	31.2	15.7	401.73	190.38	29	47.39
16 Ca-Na-HCO_3-Cl Duplicate	31.2	16.3	401.73	198.13	29	49.32
17 Ca-Na-HCO_3-Cl	30.9	15.3	397.42	185.23	26	46.61
17 Ca-Na-HCO_3-Cl Duplicate	30.9	15.9	397.42	192.96	26	48.55
18 Ca-Na-HCO_3-Cl	31.4	15.6	404.61	189.09	29	46.73
19 Ca-Na-HCO_3-Cl	30.6	15.2	393.12	183.95	26	46.79
20 Ca-Na-HCO_3-Cl	31.3	16.5	403.17	200.72	27	49.78
21 Ca-Na-HCO_3-Cl	30.6	15.8	393.12	191.67	26	48.76

22 Ca-Na-HCO_3-Cl	31.4	16.2	404.61	196.83	29	48.65
23 Ca-Na-HCO_3-Cl	31.7	16.5	408.94	200.72	27	49.08
24 Ca-Na-HCO_3-Cl	30.9	16.1	397.42	195.54	26	49.2
25 Ca-Na-HCO_3-Cl	31.3	16.7	403.17	203.31	27	50.43
26 Ca-Na-HCO_3-Cl	31.4	15.9	404.61	192.96	27	47.69
27 Ca-Na-HCO_3-Cl	31.4	15.9	404.61	192.96	27	47.69
27 Ca-Na-HCO_3-Cl Duplicate	31.4	15.8	404.61	191.67	27	47.37
28 Ca-Na-HCO_3-Cl	30.6	154	393.12	186.51	26	47.44
1 Ca-Na-HCO3-Cl Hydration	31.3	15.8	403.17	191.67	27	47.54
2 Ca-Na-HCO_3-Cl Hydration	30.6	15.8	393.12	191.67	26	48.76
3 Ca-Na-HCO_3-Cl Hydration	30.6	15.3	393.12	185.23	26	47.12
4 Ca-Na-HCO_3-Cl Hydration	31.7	15.9	408.94	192.96	27	47.18
5 Ca-Na-HCO_3-Cl Hydration	30.6	15.7	393.12	190.38	26	48.43

Table 10 Isotopic processing data for the analysis of Oxygen-18 samples from the Ca-Na-HCO_3-Cl solution for both the evaporation and hydration phases.

C.3. Deuterium Standard Curves

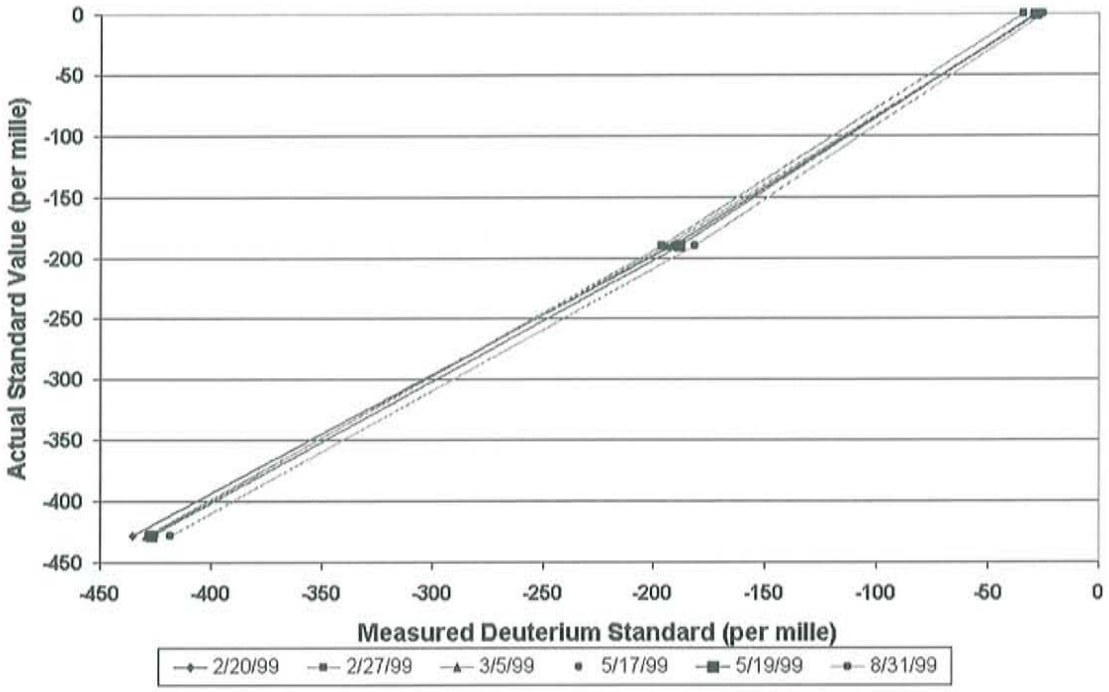

Figure 22 Standard curves for Deuterium analysis by date.

C.4. Final Isotopic Analyses

Sample ID	^{13}C ‰	^{18}O ‰
1 Na-HCO_3	-18.43	26.15
2 Na-HCO_3	-18.55	20.29
3 Na-HCO_3	-17.65	21.68
4 Na-HCO_3	-16.93	22.66
5 Na-HCO_3	-15.76	22.86
6 Na-HCO_3	-15.24	23.22
7 Na-HCO_3	-12.96	24.26
8 Na-HCO_3	-11.75	25.23
8 Na-HCO_3 Duplicate	-11.77	25.14
9 Na-HCO_3	-10.66	25.66
10 Na-HCO_3	-9.38	26.69
11 Na-HCO_3	-8.82	26.48
12 Na-HCO_3	-7.94	27.72
13 Na-HCO_3	-6.18	30.61
14 Na-HCO_3	-5.55	31.99
15 Na-HCO_3	-4.71	34.47
16 Na-HCO_3	-4.14	34.72
17 Na-HCO_3	-3.01	36.71
18 Na-HCO_3	-2.8	38.13
18 Na-HCO_3 Duplicate	-2.86	37.9
19 Na-HCO_3	-1.9	41.25
20 Na-HCO_3	-0.35	49.74
20 Na-HCO_3 Duplicate	-0.35	49.75
21 Na-HCO_3	-0.18	52.48
22 Na-HCO_3	0.7	59.37
23 Na-HCO_3	1.23	65.69
1 Na-HCO_3 Hydration	-3.45	33.22
2 Na-HCO_3 Hydration	-4.16	27.48
3 Na-HCO_3 Hydration	-4.38	26.45
4 Na-HCO_3 Hydration	-4.19	26.85
5 Na-HCO_3 Hydration	-4.18	24.88

Table 11 Carbonate isotope measurements from the Na-HCO_3 solution after precipitation with $BaCl_2$.

Sample ID	^{13}C ‰	^{18}O ‰
1 Ca-Na-HCO_3-Cl	-18.96	17.79
2 Ca-Na-HCO_3-Cl	-18.15	20.81
3 Ca-Na-HCO_3-Cl	-16.55	22.26
4 Ca-Na-HCO_3-Cl	-15.4	22.23
5 Ca-Na-HCO_3-Cl	-12.73	22.25
6 Ca-Na-HCO_3-Cl	-10.64	22.52
7 Ca-Na-HCO_3-Cl	-9.44	22.15
8 Ca-Na-HCO_3-Cl	-8.14	23.44
8 Ca-Na-HCO_3-Cl Duplicate	-8.06	23.46
9 Ca-Na-HCO_3-Cl	-6.83	24.54
10 Ca-Na-HCO_3-Cl	-4.87	27.12
11 Ca-Na-HCO_3-Cl	-4.2	266
12 Ca-Na-HCO_3-Cl	-3.88	26.63
13 Ca-Na-HCO_3-Cl	-3.1	28.91
14 Ca-Na-HCO_3-Cl	-1.86	30.71
15 Ca-Na-HCO_3-Cl	-1.45	32.64
16 Ca-Na-HCO_3-Cl	-0.5	33.51
17 Ca-Na-HCO_3-Cl	-0.13	34.59
18 Ca-Na-HCO_3-Cl	-0.05	35.28
19 Ca-Na-HCO_3-Cl	0.9	38.63
20 Ca-Na-HCO_3-Cl	0.34	45.33
20 Ca-Na-HCO_3-Cl Duplicate	0.49	45.46
21 Ca-Na-HCO_3-Cl	-1.24	47.08
22 Ca-Na-HCO_3-Cl	0.53	54.54
23 Ca-Na-HCO_3-Cl	0.44	59.26
1 Ca-Na-HCO_3-Cl Hydration	-5.99	26.69
2 Ca-Na-HCO_3-Cl Hydration	-8.12	18.94
3 Ca-Na-HCO_3-Cl Hydration	-8.8	20.68
4 Ca-Na-HCO_3-Cl Hydration	-7.26	20.04
5 Ca-Na-HCO_3-Cl Hydration	-7.63	17.88

Table 12 Carbonate isotope data from the Ca-Na-HCO_3-Cl solution after precipitation with $BaCl_2$ for both the evaporation and hydration phases.

Sample ID	^{13}C ‰	^{18}O ‰
7 Precipitate	-13.31	22.49
13 Precipitate	-10.15	23.92
17 Precipitate	-6.48	26.8
23 Precipitate	-5	30.91

Table 13 Carbonate isotope data of the direct precipitate from the Ca-Na-HCO_3-Cl solution.

Sample ID	^{13}C ‰	^{18}O ‰
1 DI	-4.02	-10.6
2 DI	-4.09	-11.92
3 DI	-4.16	-9.78
3 DI Duplicate	-4	-9.73
4 DI	-3.98	-10.8
5 DI	-4.17	-9.52
6 DI	-4.13	-10.54
7 DI	-4.1	-8.35
8 DI	-4.02	-7.95
8 DI Duplicate	-4.01	-7.82
9 DI	-4.22	-7.17
10 DI	-4.07	-7.85
11 DI	-4.04	-5.86
12 DI	-4.04	-5.88
13 DI	-4.06	-4.94
14 DI	-4.11	-4.28
15 DI	-4.3	-3.27
16 DI	-4.18	-2.69
16 DI Duplicate	-4.22	-2.39
17 DI	-4.0	-1.54
18 DI	-4.05	-0.78
19 DI	-4.14	0.5
19 DI Duplicate	-4.18	0.5
20 DI	-4	3.88
21 DI	-4.16	4.92
22 DI	-4.02	6.61
23 DI	-4.1	7.12
24 DI	-4	10.37
25 DI	-4	12.15
26 DI	-4.01	13.54
27 DI	-4.02	18.2
28 DI	-4.04	21.16

Table 14 Oxygen-18 data for the deionized water control solution.

Sample ID	^{13}C ‰	^{18}O ‰
1	-4.69	-10.51
2	-4.77	-10
3	-4.76	-9.46
4	-4.6	-8.77
5	-4.8	-8.82
6	-4.57	-8.24
7	-4.58	-8.37
8	-4.5	-6.27
9	-4.24	-7.1
9 Duplicate	-4.68	-5.33
10	-4.45	-4.2
11	-4.55	-3.4
12	-4.38	-2.75
13	-4.39	-0.61
14	-4.42	1.27
15	-4.55	2.3
16	-4.49	3.28
17	-4.41	6.17
18	-4.55	7.89
19	-4.49	10.44
20	-4.6	20.02
21	-4.87	23.31
21 Duplicate	-4.83	23.8
22	-5.06	31.46
23	-5.51	38.02
1 Hydration	-4.64	1.84
2 Hydration	-4.28	-3.2
2 Hydration Duplicate	-4.3	-3.17
3 Hydration	-4.33	-4.38
4 Hydration	-4.23	-2.78
5 Hydration	-4.07	-3.7

Table 15 Oxygen-18 data for the Na-HCO_3 solution.

Sample ID	^{13}C ‰	^{18}O ‰
1	-4.34	-11.73
2	-4.39	-9.99
2 Duplicate	-4.21	-10.07
3	-4.26	-9.31
4	-4.3	-8.95
5	-4.27	-8.46
6	-4.25	-9.12
7	-5.22	-9.21
8	-4.18	-6.2
9	-4.16	-6.15
10	-4.12	-3.75
11	-4.11	-2.71
12	-4.38	-2.75
12 Duplicate	-4.32	-1.41
13	-4.06	0.46
13 Duplicate	-4.07	0.39
14	-4.19	1.93
14 Duplicate	-4.16	1.75
15	-4.22	3.38
16	-4.15	5.26
16 Duplicate	-4.22	5.33
17	-4.09	7.13
17 Duplicate	-4.08	7.1
18	-4.06	9.53
19	-4.06	12.25
20	-4.15	21.78
21	-4.25	26.37
22	-4.03	34.33
23	-3.96	40.51
1 Hydration	4.13	1.38
2 Hydration	-4.15	-3.7
3 Hydration	-3.96	-4.57
4 Hydration	-3.96	-2.98
4 Hydration Duplicate	-3.98	-2.93
5 Hydration	-4.1	-4.11

Table 16 Oxygen-18 data for the Ca-Na-HCO_3-Cl solution during both evaporation and hydration phases.

Sample ID	Deuterium ‰	Sample ID	Deuterium ‰	Sample ID	Deuterium ‰
1 DI	-83.79	1 Na-HCO_3	-80.08	1 Ca-Na-HCO_3-Cl	-88.31
1 DI Duplicate	-82.91	2 Na-HCO_3	-75.93	2 Ca-Na-HCO_3-Cl	-85.5
3 DI	-81.48	3 Na-HCO_3 Duplicate	-72.18	3 Ca-Na-HCO_3-Cl	-88.16
4 DI	-81.08	4 Na-HCO_3	-68.16	4 Ca-Na-HCO_3-Cl	-84.09
5 DI	-78.51	5 Na-HCO_3	-70.42	4 Ca-Na-HCO_3-Cl Duplicate	-75.83
6 DI	-76.31	5 Na-HCO_3 Duplicate	-67.55	5 Ca-Na-HCO_3-Cl	-81.53
7 DI	-72.16	6Na-HCO_3	-76.15	6 Ca-Na-HCO_3-Cl	-80.86
8 DI	-72.64	7 Na-HCO_3	-68.3	6 Ca-Na-HCO_3-Cl Duplicate	-74.08
9 DI	-70.67	7 Na-HCO_3 Duplicate	-71.13	7 Ca-Na-HCO_3-Cl	-74.94
10 DI	-67.97	8 Na-HCO_3 Duplicate	-66.63	8 Ca-Na-HCO_3-Cl	-69.91
11 DI	-64.12	8 Na-HCO_3 Duplicate	-69.16	9 Ca-Na-HCO_3-Cl	-67.59
11 DI Duplicate	-69.73	9 Na-HCO_3	-63.39	10 Ca-Na-HCO_3-Cl	-57.91
12 DI	-63.89	10 Na-HCO_3	-61.88	11 Ca-Na-HCO_3-Cl	-53.66
13 DI	-62.18	11 Na-HCO_3	-50.31	12 Ca-Na-HCO_3-Cl	-60
14 DI	-59.3	11 Na-HCO_3 Duplicate	-58.25	12 Ca-Na-HCO_3-Cl Duplicate	-58.99
15 DI	-53.56	12 Na-HCO_3	-49.87	13 Ca-Na-HCO3-Cl	-44.2
17 DI	-52.52	13 Na-HCO_3	-45.84	14 Ca-Na-HCO_3-Cl	-38.32
18 DI	-44.73	14 Na-HCO_3	-33.94	15 Ca-Na-HCO_3-Cl	-34.63
19 DI	-45.42	14 Na-HCO_3 Duplicate	-33.18	16 Ca-Na-HCO_3-Cl	-28.58
20 DI	-28.3	15 Na-HCO_3	-29.74	17 Ca-Na-HCO3-Cl	-19.01
20 DI Duplicate	-29.47	16 Na-HCO_3	-21.7	17 Ca-Na-HCO_3-Cl Duplicate	-13.96
21 DI	-25.27	16 Na-HCO_3 Duplicate	-24.15	18 Ca-Na-HCO_3-Cl	-10.52
22 DI	-17.04	17 Na-HCO_3	-13.74	19 Ca-Na-HCO_3-Cl	2.86
23 DI	-13.77	18 Na-HCO_3	-10.62	20 Ca-Na-HCO_3-Cl	45.01
23 DI Duplicate	-16.03	18 Na-HCO_3 Duplicate	-9.53	21 Ca-Na-HCO_3-Cl	61.38
24 DI	-2.65	19 Na-HCO_3	7.38	21 Ca-Na-HCO_3-Cl	62.55

				Duplicate	
25 DI	6.39	**19 $Na\text{-}HCO_3$ Duplicate**	7.85	**22 $Ca\text{-}Na\text{-}HCO_3\text{-}Cl$**	100.11
26 DI	13.4	**20 $Na\text{-}HCO_3$**	40.84	**23 $Ca\text{-}Na\text{-}HCO_3\text{-}Cl$**	126.65
27 DI	35.44	**21 $Na\text{-}HCO_3$**	58.48	**1 $Ca\text{-}Na\text{-}HCO_3\text{-}Cl$ Hydration**	-37.69
28 DI	45.54	**22 $Na\text{-}HCO_3$**	88.8	**2 $Ca\text{-}Na\text{-}HCO_3\text{-}Cl$ Hydration**	-67.44
		22 $Na\text{-}HCO_3$ Duplicate	90.23	**3 $Ca\text{-}Na\text{-}HCO_3\text{-}Cl$ Hydration**	-68.22
		23 $Na\text{-}HCO_3$	126.51	**4 $Ca\text{-}Na\text{-}HCO_3\text{-}Cl$ Hydration**	-59.09
		1 $Na\text{-}HCO_3$ Hydration	-31.58	**4 $Ca\text{-}Na\text{-}HCO_3\text{-}Cl$ Hydration Duplicate**	-62.07
		2 $Na\text{-}HCO_3$ Hydration	-54.76	**5 $Ca\text{-}Na\text{-}HCO_3\text{-}Cl$ Hydration**	-63.62
		3 $Na\text{-}HCO_3$ Hydration	-55.47		
		4 $Na\text{-}HCO_3$ Hydration	-53.65		
		5 $Na\text{-}HCO_3$ Hydration	-55.32		

Table 17 Deuterium data for the Deionized water control, $Na\text{-}HCO_3$ and $Ca\text{-}Na\text{-}HCO_3\text{-}Cl$ solutions.

D. Chemical Data

D.1. Alkalinity Data

Sample	Initial pH	C. mL acid	C. pH	Alkalinity mL acid	Alkalinity pH	Alkalinity meq/L	C. Alkalinity meq/L
1	8.31	0	0	3.4	4.57	6.29	0
2	8.4	0.1	7.85	3.6	4.52	6.66	0.19
3	8.47	0.1	8.29	3.6	4.62	6.66	0.19
4	8.64	0.2	8.3	3.7	4.53	6.85	0.37
5	8.67	0.1	8.3	3.7	4.63	6.85	0.19
6	8.68	0.2	8.3	3.8	4.68	7.03	0.37
7	8.78	0.25	7.8	4	4.46	7.4	0.46
8	8.99	0.2	8.35	4.25	4.53	7.86	0.37
9	8.72	0.2	8.35	4.4	4.58	8.14	0.37
10	8.86	0.2	8.3	4.8	4.57	8.88	0.37
11	8.96	0.3	8.35	5	4.49	9.25	0.56
12	9.05	0.25	8.1	5.2	4.42	9.62	0.46
13	8.72	0.2	8.38	5.6	4.47	10.36	0.37
14	8.88	0.3	8.28	6.2	4.56	11.47	0.56
15	8.9	0.4	8.2	6.6	4.53	12.21	0.74
16	8.95	0.25	8.2	7.1	4.51	13.14	0.46
17	9.1	0.4	8.3	7.8	4.54	14.43	0.74
18	9.14	0.65	8.28	8.6	4.58	15.91	1.2
19	9.08	0.8	8.32	10.05	4.53	18.59	1.48
20	9.6	2.7	8.34	18.4	4.58	34.04	5
21	9.61	4.4	8.35	25.03	4.55	46.3	8.14
22	9.73	7.85	8.38	38	4.58	70.3	14.52
23	9.94	18.6	8.35	70.01	4.56	129.52	34.41
24	9.4	1.8	8	11	4.49	20.35	3.33
25	8.86	0.2	8.27	5	4.35	9.25	0.37
26	8.63	0.1	8.1	3.6	4.48	6.66	0.19
27	8.51	0.05	8.35	3	4.45	5.55	0.09
28	8.37	0	0	2.4	4.3	4.44	0

Table 18 Alkalinity data measured from the Na-HCO_3 solution. Carbonate has been abbreviated with a C.

Sample	Initial pH	C. mL acid	C. pH	Alkalinity mL acid	Alkalinity pH	Alkalinity meq/L	C Alkalinity meq/L
1	8.18	0	0	3.6	4.59	6.66	0
2	8.91	0	0	3	4.49	5.55	0
3	7.54	0	0	2.43	4.64	4.496	0
4	7.61	0	0	2.3	4.65	4.255	0
5	7.8	0	0	2.2	4.5	4.070	0
6	8.24	0.03	0	2.4	4.46	4.44	0
7	8.4	0.05	8.35	2.4	4.51	4.44	0.046
8	8.44	0.03	8.31	2.4	4.48	4.44	0.093
9	8.42	0.03	8.32	2.4	4.5	4.44	0.046
10	8.46	0.03	8.38	2.4	4.6	4.44	0.046
11	8.44	0.03	8.38	2.5	4.54	4.625	0.046
12	8.48	0.05	8.39	2.4	4.5	4.44	0.093
13	8.42	0.05	8.2	2.4	4.56	4.44	0.093
14	8.3	0	0	2.5	4.56	4.625	0
15	8.28	0	0	2.5	4.54	4.625	0
16	8.31	0	0	2.6	3.89	4.810	0
17	8.3	0	0	2.45	4.52	4.533	0
18	8.33	0	0	2.6	4.5	4.810	0
19	8.33	0	0	2.45	4.57	4.44	0
20	8.6	0.05	8.3	2.7	4.57	4.995	0.093
21	8.68	0.2	8.3	3.2	4.56	5.920	0.037
22	8.68	0.2	8.3	3.8	4.59	7.030	0.370
23	8.83	0.2	8.2	5.6	4.58	10.360	0.370
24	8.31	0	0	1.6	4.58	2.960	0
25	7.3	0	0	1	4.2	1.850	0
26	7	0	0	0.8	4.4	1.480	0
27	7	0	0	0.8	4.51	1.480	0
28	6.8	0	0	0.8	4.4	1.480	0

Table 19 Alkalinity data measured from the Ca-Na-HCO_3-Cl solution. Carbonate has been abbreviated with a C.

D.2. pH and Electrical Conductivity Data

Sample	pH	EC (µS/cm)	Sample	pH	EC (µS/cm)
1 Na-HCO_3	8.14	523	**1 Ca-Na-HCO_3-Cl**	8.04	1210
2 Na-HCO_3	8.25	541	**2 Ca-Na-HCO_3-Cl**	8.26	1219
3 Na-HCO_3	8.61	551	**3 Ca-Na-HCO_3-Cl**	8.36	1212
4 Na-HCO_3	8.87	566	**4 Ca-Na-HCO_3-Cl**	8.02	1170
5 Na-HCO_3	8.44	573	**5 Ca-Na-HCO_3-Cl**	7.77	1119
6 Na-HCO_3	8.59	586	**6 Ca-Na-HCO_3-Cl**	8.14	1106
7 Na-HCO_3	8.54	660	**7 Ca-Na-HCO_3-Cl**	8.34	1169
8 Na-HCO_3	8.76	682	**8 Ca-Na-HCO_3-Cl**	8.48	1202
9 Na-HCO_3	8.44	667	**9 Ca-Na-HCO_3-Cl**	8.35	1264
10 Na-HCO_3	8.73	762	**10 Ca-Na-HCO_3-Cl**	8.42	1320
11 Na-HCO_3	8.8	797	**11 Ca-Na-HCO_3-Cl**	8.44	1370
12 Na-HCO_3	8.6	838	**12 Ca-Na-HCO_3-Cl**	8.35	1424
13 Na-HCO_3	8.83	904	**13 Ca-Na-HCO_3-Cl**	8.35	1518
14 Na-HCO_3	8.84	981	**14 Ca-Na-HCO_3-Cl**	8.42	1633
15 Na-HCO_3	8.89	1053	**15 Ca-Na-HCO_3-Cl**	8.44	1733
16 Na-HCO_3	9.02	1123	**16 Ca-Na-HCO_3-Cl**	8.53	1823
17 Na-HCO_3	8.98	1260	**17 Ca-Na-HCO_3-Cl**	8.41	1995
18 Na-HCO_3	9.06	1394	**18 Ca-Na-HCO_3-Cl**	8.49	2182
19 Na-HCO_3	9.1	1594	**19 Ca-Na-HCO_3-Cl**	8.49	2447
20 Na-HCO_3	9.4	2733	**20 Ca-Na-HCO_3-Cl**	8.52	4033
21 Na-HCO_3	9.61	3654	**21 Ca-Na-HCO_3-Cl**	8.6	5700
22 Na-HCO_3	9.68	5640	**22 Ca-Na-HCO_3-Cl**	8.62	9730
23 Na-HCO_3	9.91	9500	**23 Ca-Na-HCO_3-Cl**	8.73	18690
24 Na-HCO_3	9.07	1689	**24 Ca-Na-HCO_3-Cl**	8.15	2394
25 Na-HCO_3	8.62	834	**25 Ca-Na-HCO_3-Cl**	7.87	1143
26 Na-HCO_3	8.54	568	**26 Ca-Na-HCO_3-Cl**	7.75	844
27 Na-HCO_3	8.36	481.6	**27 Ca-Na-HCO_3-Cl**	7.89	734
28 Na-HCO_3	8.04	376.2	**28 Ca-Na-HCO_3-Cl**	7.48	537

Table 20 pH and electrical conductivity measurements for both the Na-HCO_3 and Ca-Na-HCO_3-Cl solutions.

D.3. Sodium and Calcium Data

Sample	Concentration (mg/L)	Sample	Concentration (mg/L)
1 Na-HCO_3	140.4	1 Ca-Na-HCO_3-Cl	135.33
2 Na- HCO_3	141.8	2 Ca-Na-HCO_3-Cl	138.75
3 Na- HCO_3	147.2	3 Ca-Na-HCO_3-Cl	139
4 Na- HCO_3	150.8	4 Ca-Na-HCO_3-Cl	144
4 Na- HCO_3 Duplicate	151.5	5 Ca-Na-HCO_3-Cl	149.75
5 Na- HCO_3	152.5	6 Ca-Na-HCO_3-Cl	151.25
6 Na- HCO_3	154.6	7 Ca-Na-HCO_3-Cl	154.8
7 Na-HCO_3	168.4	8 Ca-Na-HCO_3-Cl	155.6
8 Na-HCO_3	171.1	9 Ca-Na-HCO_3-Cl	155.1
9 Na-HCO_3	183.4	10 Ca-Na-HCO_3-Cl	163.4
10 Na-HCO_3	193.2	11 Ca-Na-HCO_3-Cl	183
11 Na-HCO_3	199.4	11 Ca-Na-HCO_3-Cl Duplicate	179
12 Na-HCO_3	212.4	12 Ca-Na-HCO_3-Cl	198
13 Na-HCO_3	228.8	12 Ca-Na-HCO_3-Cl Duplicate	201
13 Na-HCO_3 Duplicate	209	13 Ca-Na-HCO_3-Cl	220
13 Na-HCO_3 Triplicate	202	13 Ca-Na-HCO_3-Cl Duplicate	213
14 Na-HCO_3	246	14 Ca-Na-HCO_3-Cl	249
14 Na-HCO_3 Duplicate	238	14 Ca-Na-HCO_3-Cl Duplicate	249
15 Na-HCO_3	258	15 Ca-Na-HCO_3-Cl	287
15 Na-HCO_3 Duplicate	249	15 Ca-Na-HCO_3-Cl Duplicate	267
16 Na-HCO_3	268	16 Ca-Na-HCO_3-Cl	292
16 Na-HCO_3 Duplicate	276	16 Ca-Na-HCO_3-Cl Duplicate	293
17 Na-HCO_3	313	17 Ca-Na-HCO_3-Cl	321
17 Na-HCO_3 Duplicate	303	17 Ca-Na-HCO_3-Cl Duplicate	322
18 Na-HCO_3	343	18 Ca-Na-HCO_3-Cl	353
18 Na-HCO_3 Duplicate	343	18 Ca-Na-HCO_3-Cl Duplicate	340
19 Na-HCO_3	403	19 Ca-Na-HCO_3-Cl	415
19 Na-HCO_3 Duplicate	403	19 Ca-Na-HCO_3-Cl Duplicate	418
20 Na-HCO_3	762	20 Ca-Na-HCO_3-Cl	786
20 Na-HCO_3 Duplicate	775	20 Ca-Na-HCO_3-Cl Duplicate	788
21 Na-HCO_3	1054	21 Ca-Na-HCO_3-Cl	1247
21 Na-HCO_3 Duplicate	1057	21 Ca-Na-HCO_3-Cl Duplicate	1194
22 Na-HCO_3	1612	22 Ca-Na-HCO_3-Cl	2120
22 Na-HCO_3 Duplicate	1626	22 Ca-Na-HCO_3-Cl Duplicate	2140
23 Na-HCO_3	2670	23 Ca-Na-HCO_3-Cl	4140
23 Na-HCO_3 Duplicate	2680	23 Ca-Na-HCO_3-Cl Duplicate	4200
24 Na-HCO_3	447	24 Ca-Na-HCO_3-Cl	453
24 Na-HCO_3 Duplicate	444	24 Ca-Na-HCO_3-Cl Duplicate	432

25 Na-HCO_3	193	**25 Ca-Na-HCO_3-Cl**	177
25 Na-HCO_3 Duplicate	203	**25 Ca-Na-HCO_3-Cl Duplicate**	178
26 Na-HCO_3	125	**26 Ca-Na-HCO_3-Cl Duplicate**	131
26 Na-HCO_3 Duplicate	126	**26 Ca-Na-HCO_3-Cl**	121
27 Na-HCO_3	112	**27 Ca-Na-HCO_3-Cl**	105
27 Na-HCO_3 Duplicate	122	**27 Ca-Na-HCO_3-Cl Duplicate**	112
28 Na-HCO_3	96.5	**28 Ca-Na-HCO_3-Cl**	88.1

Table 21 Sodium measurements for both the Na-HCO_3 and Ca-Na-HCO_3-Cl solution.

Sample	Calcium Concentration (mg/L)
1 Ca-Na-HCO_3-Cl	74
2 Ca-Na-HCO_3-Cl	68.25
3 Ca-Na-HCO_3-Cl	60.5
4 Ca-Na-HCO_3-Cl	66.5
5 Ca-Na-HCO_3-Cl	67
6 Ca-Na-HCO_3-Cl	76.25
7 Ca-Na-HCO_3-Cl	87.7
8 Ca-Na-HCO_3-Cl	77.2
9 Ca-Na-HCO_3-Cl	79.7
10 Ca-Na-HCO_3-Cl	79
11 Ca-Na-HCO_3-Cl	79.5
12 Ca-Na-HCO_3-Cl	78.7
13 Ca-Na-HCO_3-Cl	77.5
14 Ca-Na-HCO_3-Cl	76.8
15 Ca-Na-HCO_3-Cl	77.9
16 Ca-Na-HCO_3-Cl	75.8
17 Ca-Na-HCO_3-Cl	70.5
18 Ca-Na-HCO_3-Cl	67.5
19 Ca-Na-HCO_3-Cl	62.8
20 Ca-Na-HCO_3-Cl	69.4
21 Ca-Na-HCO_3-Cl	64.6
22 Ca-Na-HCO_3-Cl	59.2
23 Ca-Na-HCO_3-Cl	43.6
24 Ca-Na-HCO_3-Cl	36.2
25 Ca-Na-HCO_3-Cl	27.9
26 Ca-Na-HCO_3-Cl	25.6
27 Ca-Na-HCO_3-Cl	26.5
28 Ca-Na-HCO_3-Cl	22.2

Table 22 Calcium measurement for the Ca-Na-HCO_3-Cl solution.

D.4. Corrected Fraction of Water Remaining Values

Sample ID	Date	Original f $Na\text{-}HCO_3$ Solution	Corrected f $Na\text{-}HCO_3$ Solution	Original f $Ca\text{-}Na\text{-}HCO_3\text{-}Cl$ solution	Corrected f $Ca\text{-}Na\text{-}HCO_3\text{-}Cl$ solution
Evaporation					
1	12/5/98	1.0000	1.0000	1	1.0000
2	12/6/98	0.9803	0.9901	0.99	0.9754
3	12/9/98	0.9606	0.9538	0.9816	0.9735
4	12/12/98	0.8819	0.926931	0.9	0.9396
5	12/16/98	0.8622	0.916696	0.86	0.9034
6	12/20/98	0.8425	0.903952	0.85	0.8941
7	12/29/98	0.7835	0.82956	0.81	0.8732
8	1/3/99	0.7638	0.815867	0.738	0.8682
9	1/9/99	0.7244	0.760531	0.708	0.8706
10	1/17/99	0.6654	0.721132	0.648	0.8259
11	1/20/99	0.6378	0.69773	0.608	0.7451
12	1/25/99	0.6043	0.653992	0.588	0.6751
13	2/2/99	0.5650	0.653181	0.508	0.6211
14	2/9/99	0.5059	0.571916	0.448	0.5387
15	2/14/99	0.4528	0.544489	0.388	0.4834
16	2/19/99	0.4193	0.505836	0.368	0.4554
17	2/25/99	0.3661	0.445115	0.328	0.4124
18	3/1/99	0.3327	0.397735	0.288	0.3808
19	3/6/99	0.2736	0.336187	0.224	0.3148
20	3/22/99	0.0768	0.17522	0.084	0.1652
21	3/28/99	0.0630	0.125307	0.044	0.1046
22	4/1/99	0.0374	0.079541	0.04	0.0579
23	4/4/99	0.0315	0.046027	0.02	0.0278
Hydration					
1	4/17/99	0.1949	0.234899	0.298	0.2094
2	4/23/99	0.5059	0.522783	0.5137	0.5149
3	4/30/99	0.7244	0.821611	0.708	0.7241
4	5/13/99	0.872	0.91992	0.827	0.8393
5	5/19/99	1.0689	1.045598	1.0078	1.0318

Table 23 Corrected fraction of water remaining values for the simple and $Ca\text{-}Na\text{-}HCO_3\text{-}Cl$ solution. Original values are included for comparison.

D.5. Change in Fraction of Water with Time

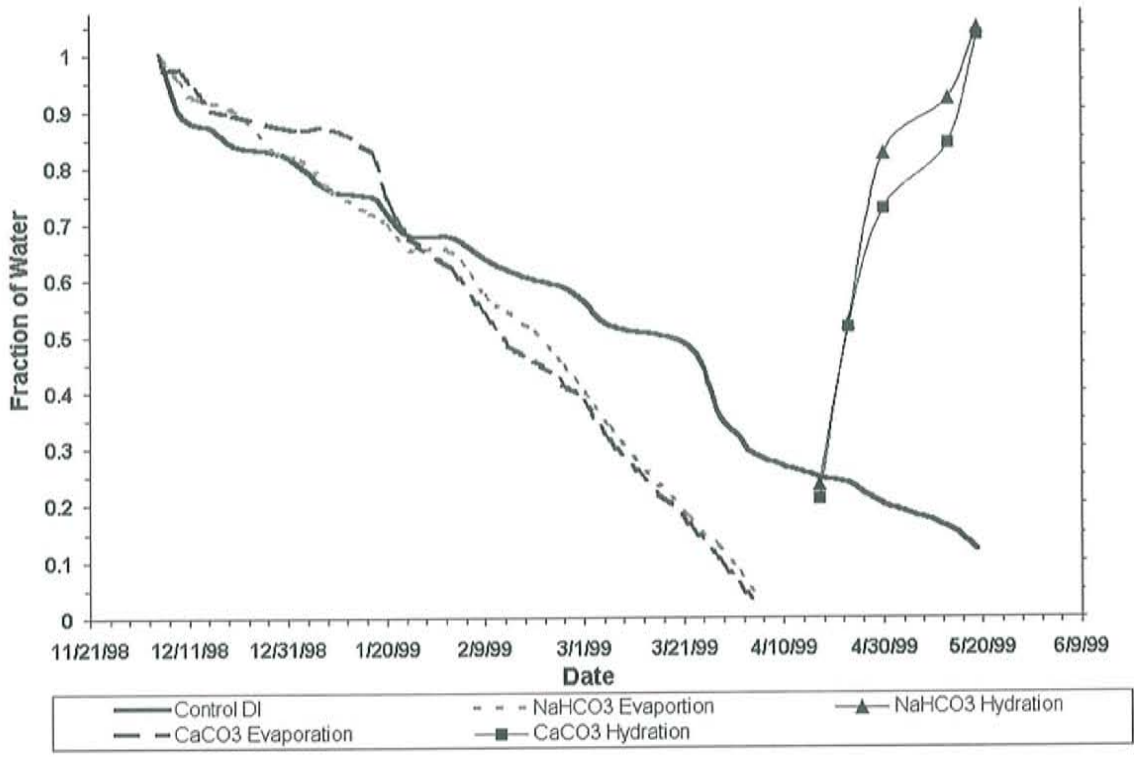

Figure 23 Change in fraction of water with time for all three solutions and the hydration.

E. Weather Data

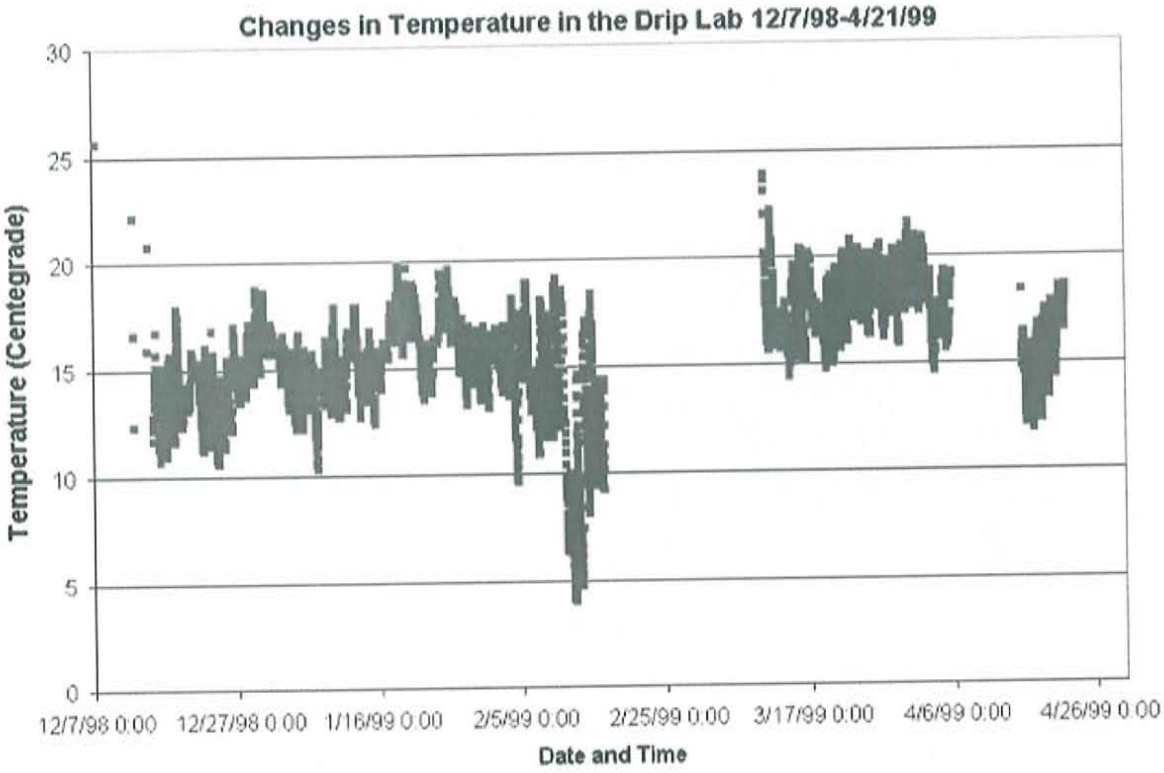

Figure 24 Temperature data collected during both phases of the experiment.

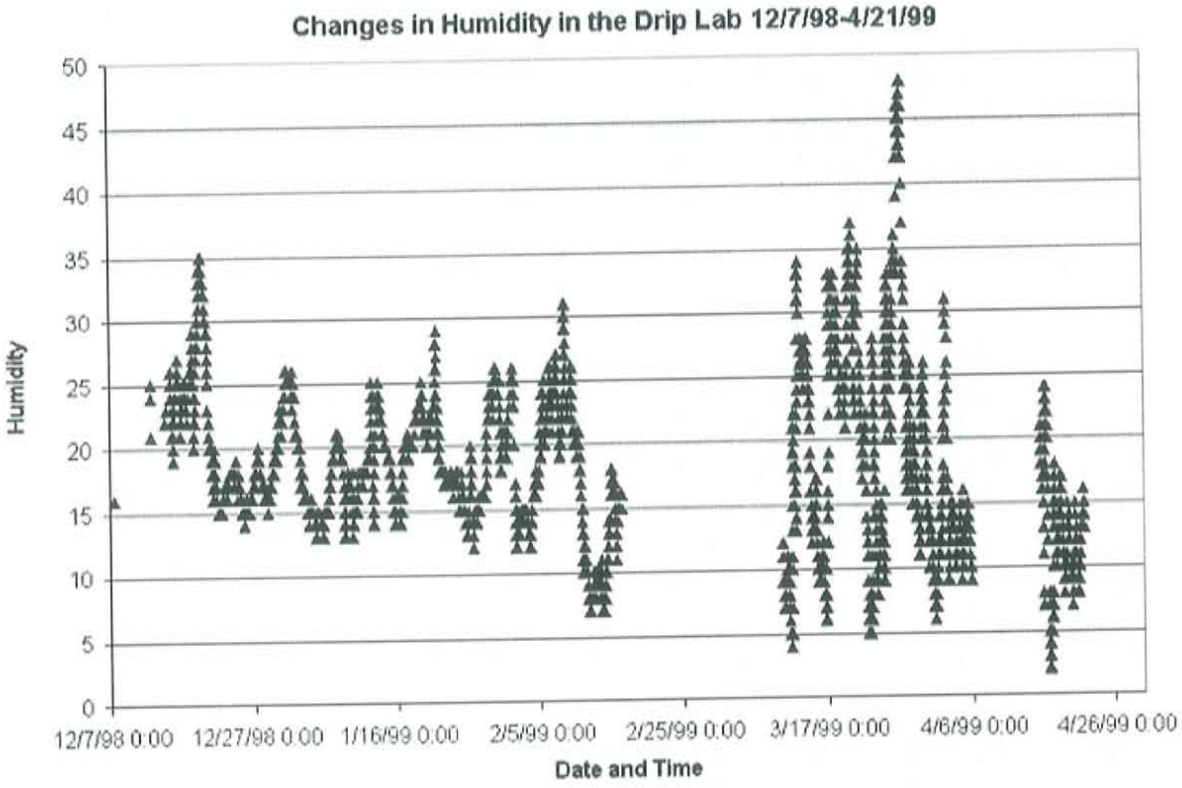

Figure 25 Humidity data collected during both phases of the experiment.

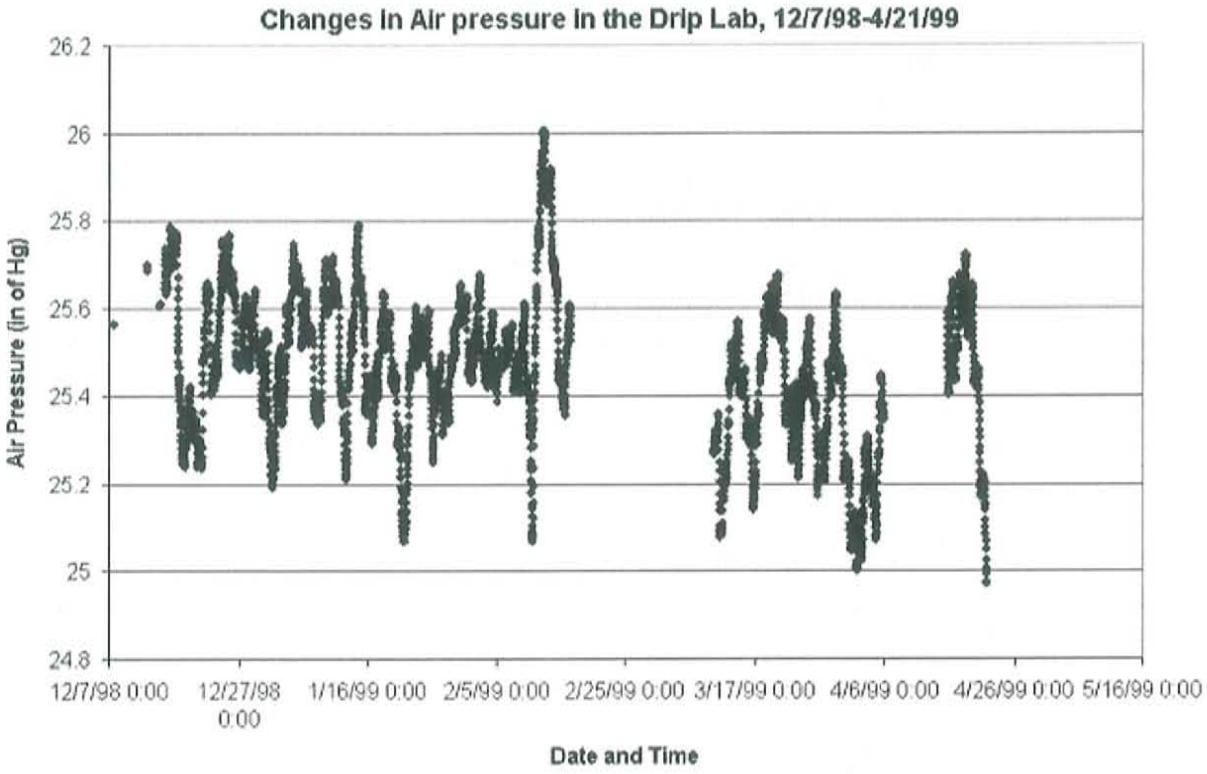

Figure 26 Barometric pressure data collected during both phases of the experiment.

F. FORTRAN Code

F.1. Solves system of Linear Equations for Carbon-13 distribution in Na-HCO_3 Solution

```
PROGRAM nahco3_evap
USE MatMult
IMPLICIT NONE

REAL, DIMENSION(:,:), ALLOCATABLE :: c, cInv, X(:), B(:)
real, allocatable :: h2co3(:),co3(:),hco3(:),co2(:),mass(:)
INTEGER I, J, N, k, number


open(8,file='input.dat')
open(10,file='solution.dat')
```

```
read(8,*)number !Number of Sets to solve
read(8,*) N   !Number of Equations


allocate(h2co3(number))
allocate(co2(number))
allocate(hco3(number))
allocate(co3(number))
allocate(mass(number))
write(*,*) "Done with space allocation"

do k=1,number
 read(8,*)co2(k),h2co3(k),hco3(k),co3(k),mass(k)
  !write(*,*)co2(k),h2co3(k),hco3(k),co3(k),mass(k)
enddo
write(*,*) "Done with coefficient reading"

do k=1,number
 open(11,file='temp.dat')
 rewind(11)
 write(11,15) H2CO3(k), 0, 0, -CO2(k)
 write(11,20) H2CO3(k),-HCO3(k), 0, 0
 write(11,25) 0, HCO3(k), -CO3(k), 0
 write(11,30) 1, 1, 1, 1
 write(11,35) -1.0, -9.0, 1.0, mass(k)
 rewind(11)
 close(11)
 write(*,*)'Done with write'

 15 format(F30.2,I3, I3, F30.2)
 20 format(F30.2, F30.1, I3, I3)
 25 format(I3, F30.2, F30.2, I2)
 30 format(4I3)
 35 format(F9.3, F9.3, F9.3, F15.10)

 !PRINT*, "Number of equations:"
 !READ*, N

 ALLOCATE( c(N, N), cInv(N, N), X(N), B(N) )
 !PRINT*, "Enter coefficient matrix A by rows:"
 open(11,file='temp.dat')
 READ(11,*) ((c(I,J), J = 1,N), I = 1,N)
 !PRINT*, "Enter RHS vector B:"
 READ(11,*) B
```

```
cInv=.INV. c
X = matmul(cinv , B)
write(*,*)
write(*,*) "Solution:"
write(*,"(4E20.8") X
write(10,"(4E20.8")X
deallocate(X,B,cInv,C)
enddo


END PROGRAM nahco3_evap
```

F.2. Solve system of Linear equations for Carbon-13 distribution in Ca-Na-HCO_3-Cl solution

```
PROGRAM caco3_evap
USE MatMult
IMPLICIT NONE

REAL, DIMENSION(:,:), ALLOCATABLE :: c, cInv, X(:), B(:)
real, allocatable :: h2co3(:),co3(:),hco3(:),co2(:),mass(:)
INTEGER I, J, N, k, number


open(8,file='input.dat')
open(10,file='solution.dat')
read(8,*)number !Number of Sets to solve
read(8,*) N   !Number of Equations


allocate(h2co3(number))
allocate(co2(number))
allocate(hco3(number))
allocate(co3(number))
allocate(mass(number))
write(*,*) "Done with space allocation"

do k=1,number
 read(8,*)co2(k),h2co3(k),hco3(k),co3(k),mass(k)
  !write(*,*)co2(k),h2co3(k),hco3(k),co3(k),mass(k)
enddo
write(*,*) "Done with coefficient reading"

do k=1,number
```

```
open(11,file='temp.dat')
rewind(11)
write(11,15) H2CO3(k), 0, 0, -CO2(k)
write(11,20) H2CO3(k),-HCO3(k), 0, 0
write(11,25) 0, HCO3(k), -CO3(k), 0
write(11,30) 1, 1, 1, 1
write(11,35) -1.0, -9.0, 1.0, mass(k)
rewind(11)
close(11)
write(*,*)'Done with write'

15 format(F20.2,I3, I3, F20.2, I3)
20 format(F20.2, F20.1, 3I3)
25 format(I3, F20.2, F30.2, 2I3)
30 format(5I3)
35 format(F9.3, F9.3, F9.3, F15.10, F9.3)


!PRINT*, "Number of equations:"
!READ*, N

ALLOCATE( c(N, N), cInv(N, N), X(N), B(N) )
!PRINT*, "Enter coefficient matrix A by rows:"
open(11,file='temp.dat')
READ(11,*) ((c(I,J), J = 1,N), I = 1,N)
!PRINT*, "Enter RHS vector B:"
READ(11,*) B

cInv=.INV. c
X = matmul(cinv , B)
write(*,*)
write(*,*) "Solution:"
write(*,"(4E15.8)") X
write(10,"(4E15.8)")X
deallocate(X,B,cInv,C)
enddo


END PROGRAM caco3_evap
```

F.3. Matmult Subprogram

```
MODULE MatMult
```

```
INTERFACE OPERATOR (.INV.)
 MODULE PROCEDURE Inv
END INTERFACE

CONTAINS

FUNCTION Inv( Mat )
 REAL, DIMENSION(:,:), Intent(in) :: Mat
 REAL, DIMENSION( SIZE(Mat,1), SIZE(Mat,1) ) :: Inv  ! must be
                  ! square
 REAL, DIMENSION( SIZE(Mat,1), 2 * SIZE(Mat,1) ) :: A ! augmented
 REAL, DIMENSION(:), ALLOCATABLE :: TempRow      ! spare row
 REAL PivElt, TarElt
 INTEGER :: N          ! number of equations
 INTEGER PivRow, TarRow

 N = SIZE( Mat, 1 )
 A = 0              ! initialize
 A( 1:N, 1:N ) = Mat       ! first N columns
 DO I = 1, N           ! identity in cols N+1 to 2N
  A( I, N+I ) = 1
 END DO

 DO PivRow = 1, N        ! process every row
  PivElt = A( PivRow, PivRow )  ! choose pivot element
  IF (PivElt == 0) THEN      ! check for zero pivot
   K = PivRow + 1   ! run down rows to find a non-zero pivot
   DO WHILE (PivElt == 0 .AND. K <= N)
    PivElt = A( K, PivRow )   ! try next row
    K = K + 1         ! K will be 1 too big
   END DO
   IF (PivElt == 0) THEN     ! it's still zero
    PRINT*, "Couldn't find a non-zero pivot: solution rubbish"
    RETURN
   ELSE
    ! non-zero pivot in row K, so swop rows PivRow and K:
    ALLOCATE( TempRow(2*N) )  ! dynamic store
    TempRow = A( PivRow, 1:2*N )
    K = K - 1         ! adjust for overcount
    A( PivRow, 1:2*N ) = A( K, 1:2*N )
    A( K, 1:2*N ) = TempRow
    DEALLOCATE( TempRow )    ! throw away
   END IF
  END IF
  A( PivRow, 1:2*N ) = A( PivRow, 1:2*N ) / PivElt ! divide
```

```
                ! whole row
  ! now replace all other rows by target row minus pivot row ...
 ! ... times element in target row and pivot column:

 DO TarRow = 1, N
  IF (TarRow /= PivRow) THEN
   TarElt = A( TarRow, PivRow )
   A( TarRow, 1:2*N ) = A( TarRow, 1:2*N ) &
         - A( PivRow, 1:2*N ) * TarElt
  END IF
 END DO
END DO

 ! finally extract the inverse from columns N+1 to 2N:
 Inv = A( 1:N, N+1:2*N )
END FUNCTION Inv
END MODULE MatMult
```

G. PHREEQCI Code for Geochemical Modeling

G.1. Input file for the Na-HCO_3 Solution Evaporation

```
SOLUTION 1 NaHCO3 Evaporation Calculation
    temp      15
    pH        8.14    charge
    pe        4
    units     mol/l
    redox     pe
    density   1
    Na        140.4   mg/l
    C         6.29    mMol/l
    -water    1       # kg
EQUILIBRIUM_PHASES 1 HOLD SYSTEM IN EQUILIBRIUM WITH
ATMOSPHERE
    CO2(g)    -3.5
REACTION 1 EVAPORATION STEP
    H2O        -1
    55.391 moles in 24 steps
SAVE solution 2
PRINT
     -reset true
     -surface false
     -selected_output true
SELECTED_OUTPUT
     -file NAHCO3_evapso_masscheck.out
```

```
      -reset true
     -totals   Na C
     -molalities    NaHCO3 CO3-2 HCO3- H+ Na+
     -saturation_indices CO2(g)
     -gases    CO2(g)
END
```

G.2. Input file for the Ca-Na-HCO_3-Cl solution Evaporation

```
SOLUTION 1 Mixed Solution Evaporation
    temp       15
    pH         8.04     charge
    pe         4
    units      mol/l
    redox      pe
    density    1
    Ca         74       mg/l        as CaCl2
    Na         135.3    mg/l
    C          6.66     mMol/l
    -water     1        # kg
EQUILIBRIUM_PHASES 1 Equilibrium with the atmosphere
    Calcite    0        0
    CO2(g)     -3.5
REACTION 1 Evaporate the Water
    H2O         -1
    54.9 moles in 24 steps

REACTION 2 Sample Na
    Na          -1
    .0538 moles in 24 steps
SAVE solution 2-2
PRINT
     -reset true
     -surface false
     -selected_output true
SELECTED_OUTPUT
     -file Caco3evapso.out
      -reset true
     -totals   Na C Ca
     -molalities     Ca+2 CO3-2 HCO3- H+ Na+
     -equilibrium_phases Calcite CO2(g)
     -saturation_indices Calcite CO2(g)
     -gases    CO2(g)
      -solid_solutions  Calcite
END
```

G.3. Input file for Hydration of the Na-HCO_3 Solution

```
SOLUTION 1 NaHCO3 Hydration Calculation
    temp      15
    pH        8.14    charge
    pe        4
    units     mol/l
    redox     pe
    density   1
    Na        140.4   mg/l
    C         6.29    mMol/l
    -water    1       # kg
EQUILIBRIUM_PHASES 1 HOLD SYSTEM IN EQUILIBRIUM WITH
ATMOSPHERE
    CO2(g)    -3.5
REACTION 1 Evaporate the Water
    H2O        -1
    54.1 moles in 24 steps
Save solution 2
PRINT
     -reset true
     -surface false
     -selected_output true
SELECTED_OUTPUT
     -file NAHCO3_hydration1.out
      -reset true
     -totals   Na C
     -molalities    NaHCO3 CO3-2 HCO3- H+ Na+
     -saturation_indices CO2(g)
     -gases    CO2(g)
END
SOLUTION 3 Deionized Water
    temp      15
    pH        7       charge
    pe        4
    units     mol/l
    redox     pe
    density   1
    -water    0.2     # kg
EQUILIBRIUM_PHASES 3 Equilibrate with the Atmosphere
    CO2(g)    -3.5
MIX 1 Add DI Water 1st Hydration Step
    2    1
    3    1
SAVE solution 4
PRINT
     -reset true
     -surface false
     -selected_output true
```

```
SELECTED_OUTPUT
      -file NAHCO3_hydration2.out
       -reset true
      -totals   Na C
      -molalities    NaHCO3 CO3-2 HCO3- H+ Na+
      -saturation_indices CO2(g)
      -gases    CO2(g)
end
SOLUTION 5 Deionized Water
     temp       15
     pH         7       charge
     pe         4
     units      mol/l
     redox      pe
     density    1
     -water     0.2      # kg
EQUILIBRIUM_PHASES 4 Equilibrate with the Atmosphere
     CO2(g)     -3.5
MIX 2 Add DI Water 2nd Hydration Step
     4     1
     5     1
Save Solution 6
PRINT
      -reset true
      -surface false
      -selected_output true
SELECTED_OUTPUT
      -file NAHCO3_hydration3.out
       -reset true
      -totals   Na C
      -molalities    NaHCO3 CO3-2 HCO3- H+ Na+
      -saturation_indices CO2(g)
      -gases    CO2(g)
end
SOLUTION 7 Deionized Water
     temp       15
     pH         7       charge
     pe         4
     units      mol/l
     redox      pe
     density    1
     -water     0.2      # kg
EQUILIBRIUM_PHASES 5 Equilibrate with the Atmosphere
     CO2(g)     -3.5
MIX 3 Add DI Water 3rd Hydration Step
     6     1
     7     1
Save Solution 8
PRINT
```

```
     -reset true
     -surface false
     -selected_output true
SELECTED_OUTPUT
     -file NAHCO3_hydration4.out
      -reset true
     -totals   Na C
     -molalities    NaHCO3 CO3-2 HCO3- H+ Na+
     -saturation_indices CO2(g)
     -gases    CO2(g)
end
SOLUTION 9 Deionized Water
    temp      15
    pH        7       charge
    pe        4
    units     mol/l
    redox     pe
    density   1
    -water    0.2     # kg
EQUILIBRIUM_PHASES 6 Equilibrate with the Atmosphere
    CO2(g)    -3.5
MIX 4 Add DI Water 4th Hydration Step
    8    1
    9    1
Save Solution 10
PRINT
     -reset true
     -surface false
     -selected_output true
SELECTED_OUTPUT
     -file NAHCO3_hydration5.out
      -reset true
     -totals   Na C
     -molalities    NaHCO3 CO3-2 HCO3- H+ Na+
     -saturation_indices CO2(g)
     -gases    CO2(g)
end
SOLUTION 11 Deionized Water
    temp      15
    pH        7       charge
    pe        4
    units     mol/l
    redox     pe
    density   1
    -water    0.2     # kg
EQUILIBRIUM_PHASES 7 Equilibrate with the Atmosphere
    CO2(g)    -3.5
MIX 5 Add DI Water 5th Hydration Step
    11    1
```

```
    10    1
Save Solution 12
PRINT
     -reset true
     -surface false
     -selected_output true
SELECTED_OUTPUT
     -file NAHCO3_hydration6.out
      -reset true
     -totals   Na C
     -molalities    NaHCO3 CO3-2 HCO3- H+ Na+
     -saturation_indices CO2(g)
     -gases    CO2(g)
END
```

G.4. Input files for Hydration of the Ca-Na-HCO_3-Cl solution

```
SOLUTION 1 CaCO3 Hydration Calculation
    temp       15
    pH         8.04     charge
    pe         4
    units      mol/l
    redox      pe
    density    1
    Ca         74       mg/l          as CaCl2
    Na         135.3    mg/l
    C          6.66     mMol/l
    -water     1        # kg
EQUILIBRIUM_PHASES 1 HOLD SYSTEM IN EQUILIBRIUM WITH
ATMOSPHERE
    Calcite    0      0
    CO2(g)     -3.5
REACTION 1 Evaporate the Water
    H2O         -1
    54.1 moles in 24 steps
Save solution 2
PRINT
     -reset true
     -surface false
     -selected_output true
SELECTED_OUTPUT
     -file CACO3_hydration1.out
      -reset true
     -totals   Na C Ca
     -molalities    NaHCO3 CO3-2 HCO3- H+ Na+ Ca-2
     -saturation_indices CO2(g)
     -gases    CO2(g)
```

```
END
SOLUTION 3 Deionized Water
    temp      15
    pH        7       charge
    pe        4
    units     mol/l
    redox     pe
    density   1
    -water    0.2     # kg
EQUILIBRIUM_PHASES 3 Equilibrate with the Atmosphere
    CO2(g)    -3.5
MIX 1 Add DI Water 1st Hydration Step
    2    1
    3    1
SAVE solution 4
PRINT
     -reset true
     -surface false
     -selected_output true
SELECTED_OUTPUT
     -file CACO3_hydration2.out
      -reset true
     -totals   Na C Ca
     -molalities    NaHCO3 CO3-2 HCO3- H+ Na+ Ca-2
     -saturation_indices CO2(g)
     -gases    CO2(g)
end
SOLUTION 5 Deionized Water
    temp      15
    pH        7       charge
    pe        4
    units     mol/l
    redox     pe
    density   1
    -water    0.2     # kg
EQUILIBRIUM_PHASES 4 Equilibrate with the Atmosphere
    CO2(g)    -3.5
MIX 2 Add DI Water 2nd Hydration Step
    4    1
    5    1
Save Solution 6
PRINT
     -reset true
     -surface false
     -selected_output true
SELECTED_OUTPUT
     -file CACO3_hydration3.out
      -reset true
     -totals   Na C Ca
```

```
     -molalities    NaHCO3 CO3-2 HCO3- H+ Na+ Ca-2
     -saturation_indices CO2(g)
     -gases    CO2(g)
end
SOLUTION 7 Deionized Water
    temp       15
    pH         7       charge
    pe         4
    units      mol/l
    redox      pe
    density    1
    -water     0.2      # kg
EQUILIBRIUM_PHASES 5 Equilibrate with the Atmosphere
    CO2(g)     -3.5
MIX 3 Add DI Water 3rd Hydration Step
    6    1
    7    1
Save Solution 8
PRINT
     -reset true
     -surface false
     -selected_output true
SELECTED_OUTPUT
     -file CACO3_hydration4.out
      -reset true
     -totals   Na C Ca
     -molalities    NaHCO3 CO3-2 HCO3- H+ Na+ Ca-2
     -saturation_indices CO2(g)
     -gases    CO2(g)
end
SOLUTION 9 Deionized Water
    temp       15
    pH         7       charge
    pe         4
    units      mol/l
    redox      pe
    density    1
    -water     0.2      # kg
EQUILIBRIUM_PHASES 6 Equilibrate with the Atmosphere
    CO2(g)     -3.5
MIX 4 Add DI Water 4th Hydration Step
    8    1
    9    1
Save Solution 10
PRINT
     -reset true
     -surface false
     -selected_output true
SELECTED_OUTPUT
```

```
     -file CACO3_hydration5.out
      -reset true
     -totals   Na C Ca
     -molalities    NaHCO3 CO3-2 HCO3- H+ Na+ Ca-2
     -saturation_indices CO2(g)
     -gases    CO2(g)
end
SOLUTION 11 Deionized Water
    temp      15
    pH        7       charge
    pe        4
    units     mol/l
    redox     pe
    density   1
    -water    0.2     # kg
EQUILIBRIUM_PHASES 7 Equilibrate with the Atmosphere
    CO2(g)    -3.5
MIX 5 Add DI Water 5th Hydration Step
    11    1
    10    1
Save Solution 12
PRINT
     -reset true
     -surface false
     -selected_output true
SELECTED_OUTPUT
     -file CACO3_hydration6.out
      -reset true
     -totals   Na C Ca
     -molalities    NaHCO3 CO3-2 HCO3- H+ Na+ Ca-2
     -saturation_indices CO2(g)
     -gases    CO2(g)
END
```

G.6. Geochemical Modeling with PHREEQC

The evolution of various chemical processes during the evaporation and hydration phases has been modeled with a geochemical modeling code, PHREEQC, version 2. This code is freeware distributed and maintained by the United States Geological Survey (USGS). The code has been designed to handle speciation, batch-reactions, one-dimensional transport, and inverse geochemical reactions. Specific test examples have

been developed by the USGS to test the stability of the code under a variety of situations; evaporation and mixing are problems included in the software package. Full documentation of the code can be found in Parkhurst and Appelo (1999). Input files used to model the evaporative phase of the experiment are listed in Appendix G.1-5.

H. Mass Balance Best-Fit Curves for Isotopic Enrichment

H.1. Carbon -12 and Carbon-13 Curves for the Evaporating Na-HCO_3 Solution

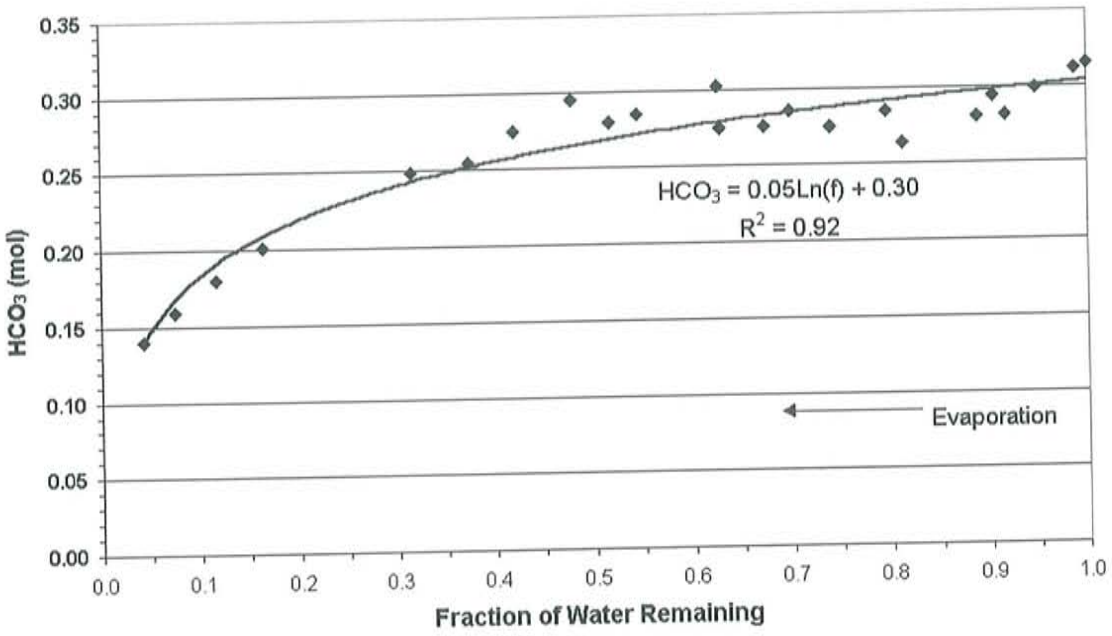

Figure 27 Calculations of bicarbonate for each sampling point for the Na-HCO_3 solution with trend line.

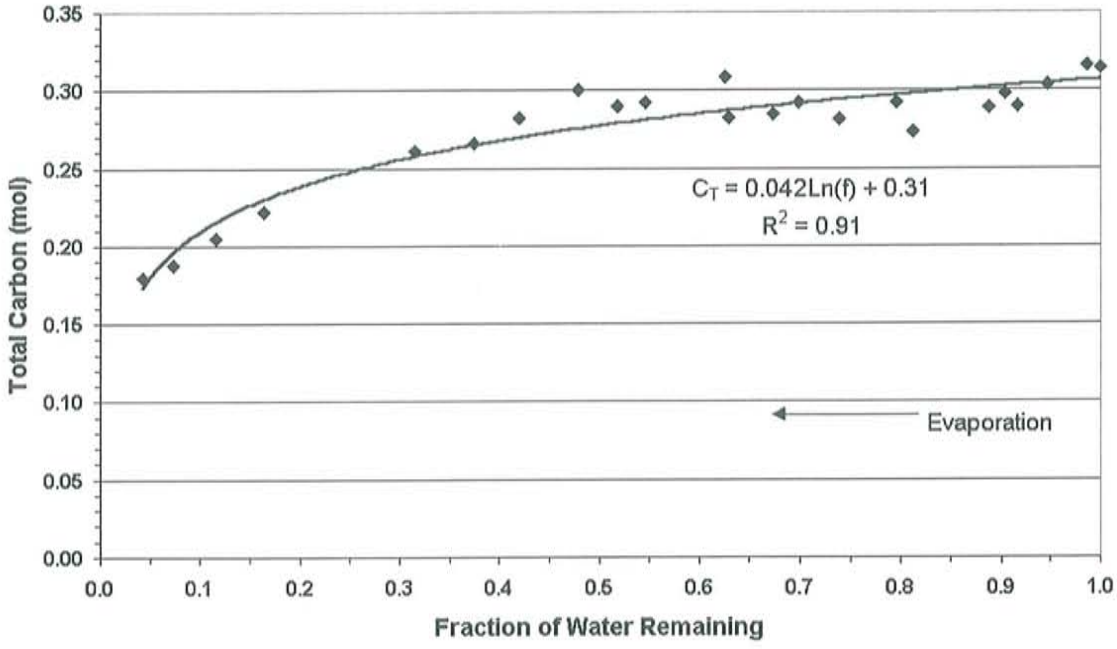

Figure 28 Calculations of total carbon for each sampling point for the Na-HCO_3 solution with trend line.

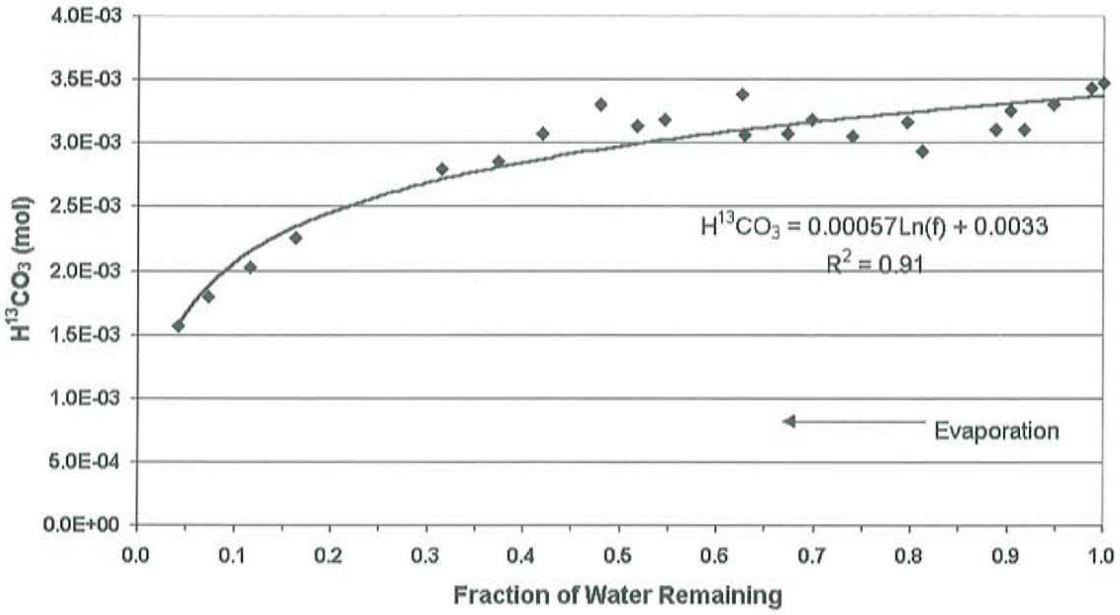

Figure 29 Carbon-13 calculations of bicarbonate for each sampling point for the Na-HCO_3 solution with trend line.

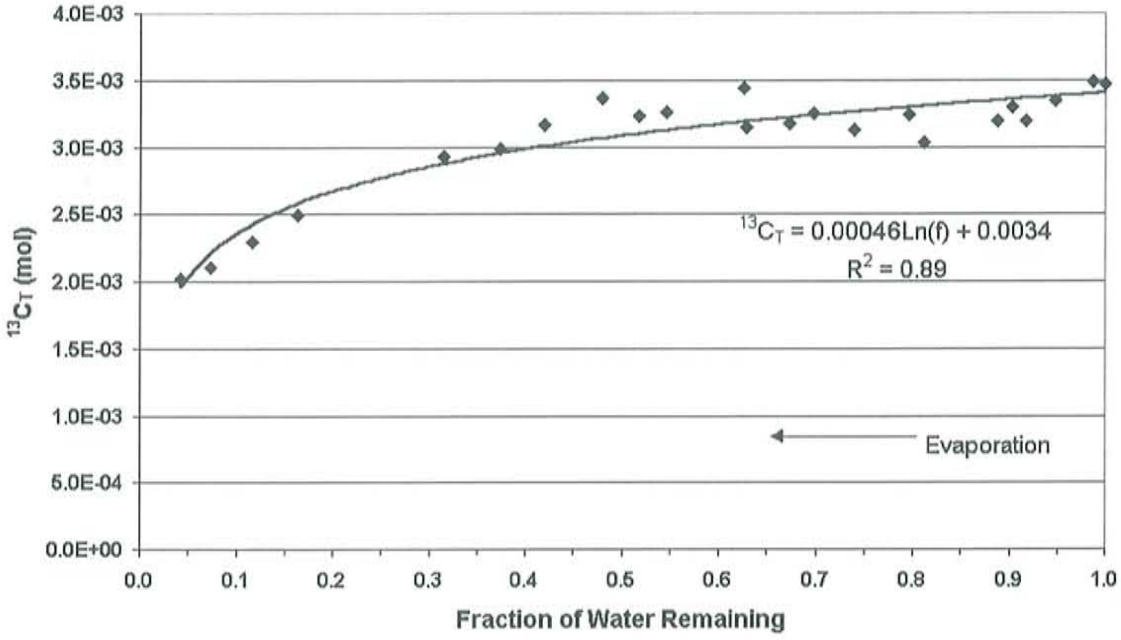

Figure 30 Calculations of total carbon-13 for each sampling point for the Na-HCO_3 solution with trend line.

H.2. Carbon -12 and Carbon-13 Curves for the Evaporating Ca-Na-HCO_3-Cl Solution

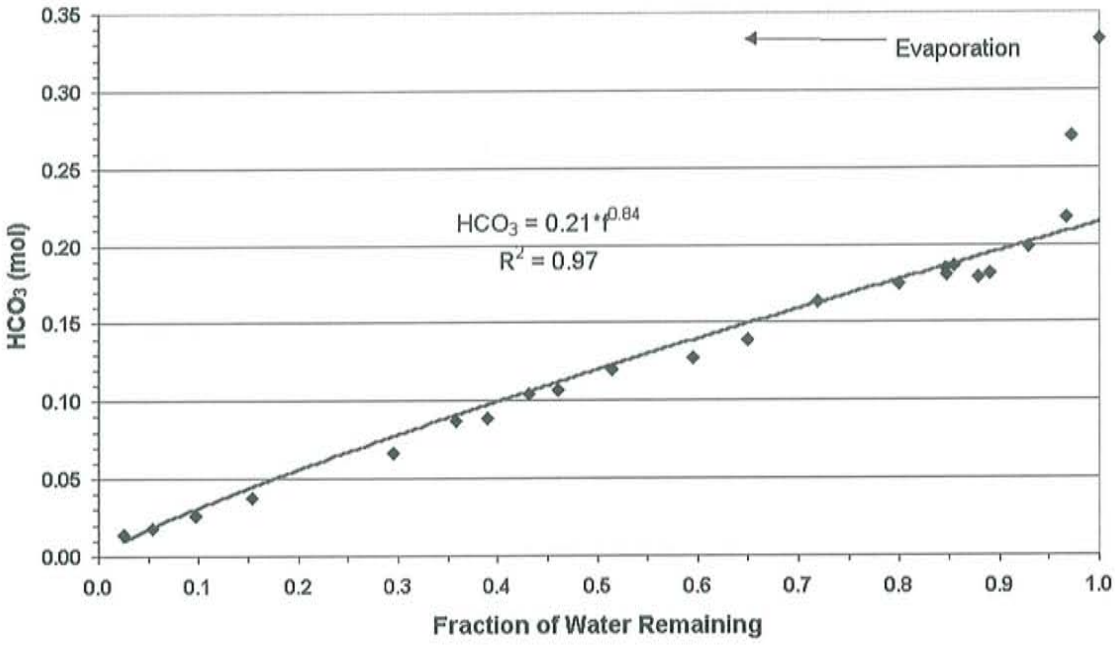

Figure 31 Calculations of bicarbonate for each sampling point for the Ca-Na-HCO_3-Cl solution with trend line.

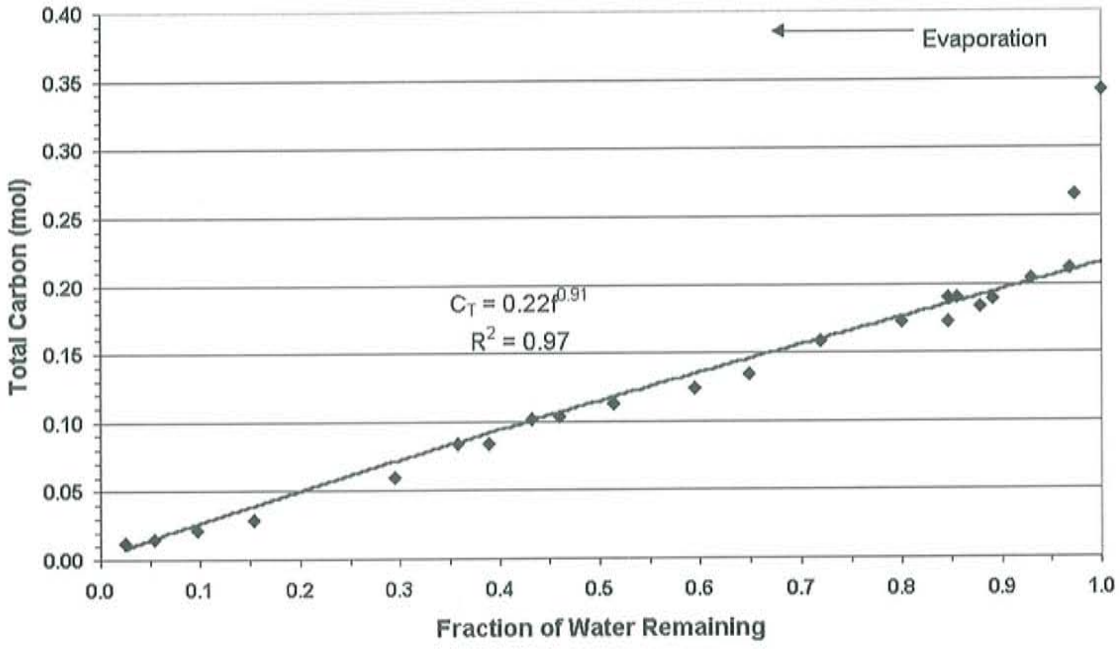

Figure 32 Calculated total carbon-12 data in the Ca-Na-HCO_3-Cl solution evaporation with trend line.

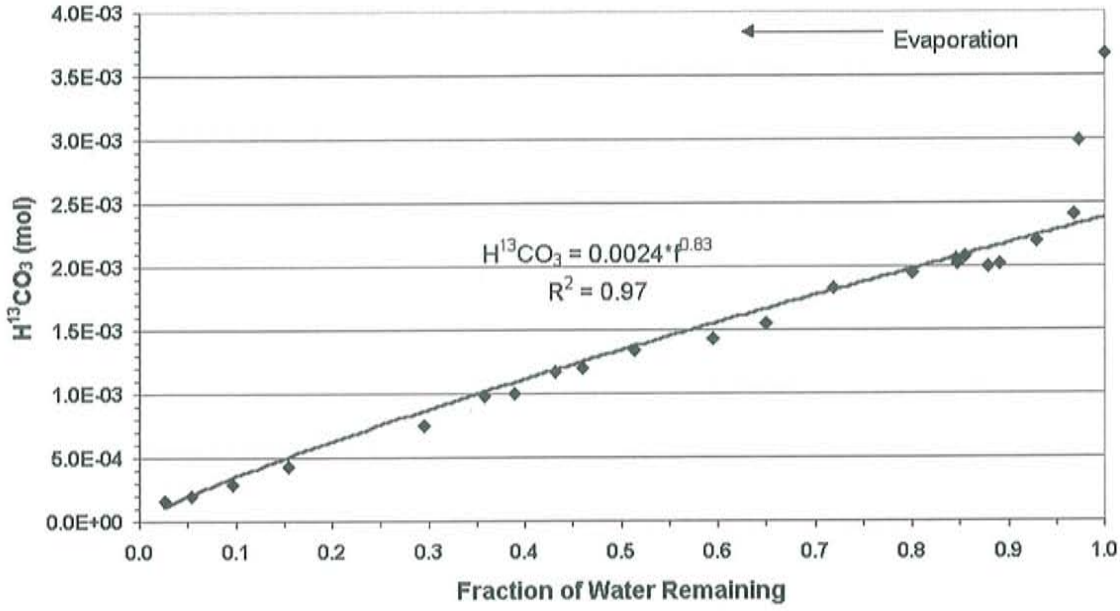

Figure 33 Calculations of carbon-13 bicarbonate for each sampling point for the Ca-Na-HCO_3-Cl solution with trend line.

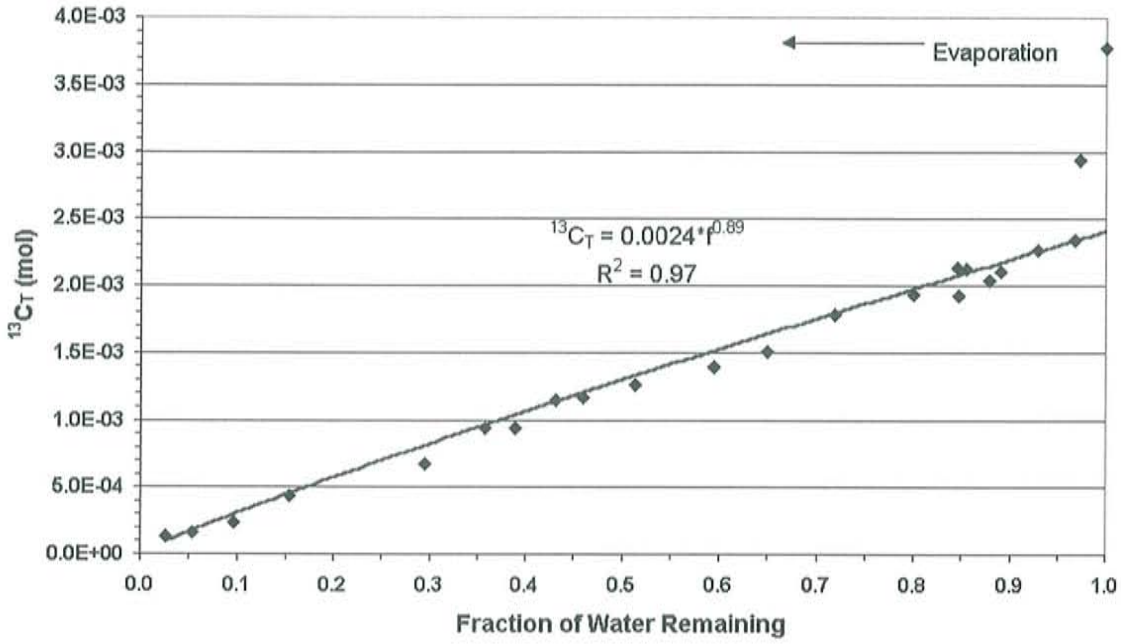

Figure 34 Calculated total carbon-13 data in the Ca-Na-HCO_3-Cl solution evaporation with trend line.

H.3. Mass Balance Data

Average f	HCO3 (mol)	CO_3 (mol)	H_2CO_3 (mol)	CO_2 aq (mol)	C_T (mol)
1.0000	0.3145	2.6E-09	7.205E-06	1.142E-08	0.3145
0.9901	0.3114	4.6E-03	5.538E-06	8.777E-09	0.3160
0.9538	0.3000	4.4E-03	2.321E-06	3.678E-09	0.3034
0.926931	0.2829	8.5E-03	1.199E-06	1.900E-09	0.2896
0.916696	0.2968	4.2E-03	3.373E-06	5.346E-09	0.2980
0.903952	0.2843	8.2E-03	2.279E-06	3.612E-09	0.2887
0.82956	0.2686	9.4E-03	2.408E-06	3.817E-09	0.2735
0.815867	0.2906	7.4E-03	1.564E-06	2.479E-09	0.2921
0.760531	0.2814	6.9E-03	3.155E-06	5.001E-09	0.2817
0.721132	0.2935	6.5E-03	1.682E-06	2.666E-09	0.2922
0.69773	0.2840	9.4E-03	1.381E-06	2.188E-09	0.2849
0.653992	0.2843	7.3E-03	2.184E-06	3.461E-09	0.2822
0.653181	0.3142	5.8E-03	1.416E-06	2.244E-09	0.3085

0.571916	0.2963	7.6E-03	1.301E-06	2.062E-09	0.2922
0.544489	0.2921	9.6E-03	1.139E-06	1.806E-09	0.2893
0.505836	0.3088	5.6E-03	8.901E-07	1.411E-09	0.3003
0.445115	0.2882	7.8E-03	9.084E-07	1.440E-09	0.2822
0.397735	0.2686	1.1E-02	7.022E-07	1.113E-09	0.2663
0.336187	0.2628	1.2E-02	6.253E-07	9.911E-10	0.2607
0.17522	0.2107	2.1E-02	2.529E-07	4.008E-10	0.2218
0.125307	0.1881	2.4E-02	1.398E-07	2.216E-10	0.2046
0.079541	0.1641	2.8E-02	1.052E-07	1.667E-10	0.1873
0.046027	0.1397	4.0E-02	5.429E-08	8.605E-11	0.1791
Hydration					
0.234077	0.160	0.0390	4.31E-04	6.83E-07	0.1996
0.519123	0.221	0.0096	1.68E-03	2.66E-06	0.2322
0.812984	0.256	0.0075	2.33E-03	3.70E-06	0.2655
0.907041	0.243	0.0042	3.36E-03	5.32E-06	0.2509
1.0273	0.228	0.0000	6.58E-03	1.04E-05	0.2346

Table 24 Carbonate species distributions in the Na-HCO_3 solution.

Average f	**HCO3 (mol)**	**CO_3 (mol)**	**H_2CO_3 (mol)**	**CO_2 aq (mol)**	**C_T (mol)**
1	0.333	0.0000	9.60E-03	1.52E-05	0.3426
0.975375	0.271	0.0000	4.70E-03	7.45E-06	0.2754
0.973534	0.218	0.0000	3.02E-03	4.79E-06	0.2211
0.939641	0.199	0.0000	6.04E-03	9.57E-06	0.2046
0.903355	0.182	0.0000	9.87E-03	1.56E-05	0.1919
0.894055	0.179	0.0000	4.17E-03	6.61E-06	0.1836
0.873182	0.187	0.0010	2.74E-03	4.35E-06	0.1903
0.86824	0.181	0.0020	1.93E-03	3.07E-06	0.1848
0.870563	0.185	0.0010	5.09E-03	8.07E-06	0.1908
0.825898	0.175	0.0009	2.16E-03	3.42E-06	0.1777
0.745111	0.164	0.0008	1.94E-03	3.07E-06	0.1665
0.675129	0.139	0.0015	2.03E-03	3.22E-06	0.1424
0.62115	0.127	0.0014	1.70E-03	2.70E-06	0.1304
0.538726	0.120	0.0000	1.50E-03	2.37E-06	0.1212
0.483374	0.107	0.0000	1.28E-03	2.03E-06	0.1084
0.455355	0.105	0.0000	1.02E-03	1.62E-06	0.1056
0.412443	0.089	0.0000	1.15E-03	1.82E-06	0.0902
0.38079	0.087	0.0000	9.37E-04	1.49E-06	0.0879
0.31476	0.066	0.0000	7.15E-04	1.13E-06	0.0670

0.165217	0.038	0.0004	3.79E-04	6.01E-07	0.0387
0.104558	0.026	0.0009	2.15E-04	3.41E-07	0.0272
0.057947	0.018	0.0005	1.38E-04	2.19E-07	0.0187
0.027775	0.014	0.0003	7.87E-05	1.25E-07	0.0144
Hydration					
0.209444	0.031	0.0000	6.94E-04	1.10E-06	0.0317
0.514898	0.048	0.0000	2.03E-03	3.22E-06	0.0497
0.724069	0.054	0.0000	3.01E-03	4.78E-06	0.0566
0.839262	0.062	0.0000	2.53E-03	4.01E-06	0.0646
1.031813	0.076	0.0000	8.00E-03	1.27E-05	0.0844

Table 25 Carbonate species distributions in the Ca-Na-HCO_3-Cl solution.

I. Diagram of Chemical Model

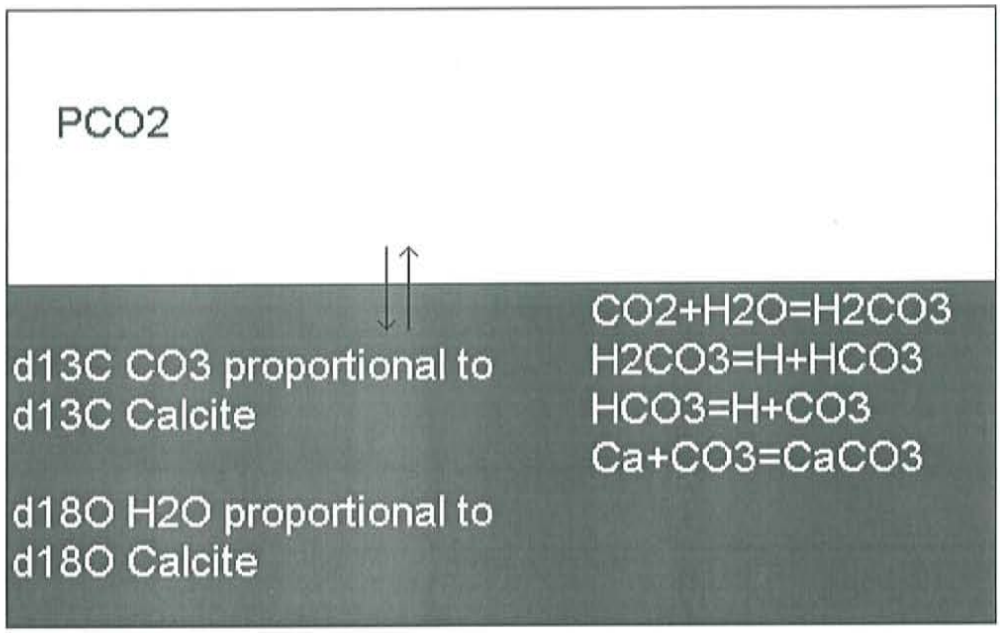

Figure 35 Model diagram of chemical and isotopic processes within a solution.

J. Correction of Water Volumes Using the Sodium Data

Sodium or chloride minerals were not detected from X-Ray Diffraction (XRD) analysis of the precipitate, confirming the conservative behavior of sodium during the experiment. Measured sodium values were used to adjust the fraction of water (f) for

both the evaporation and hydration phases of the experiment. The original observations were made using a plastic measuring tape and marks representing the 2 liter volume level on the sides of the tanks as described in Section 2.2. The correction using a conservative constituent such as sodium reduces of the uncertainty associated with the tape and volume marks.

The fractions were adjusted by multiplying the sampling volume of 0.175 L by the sodium concentration (mg/L) for each sample,

$$Na^{+}(mg\ /\ L) * 0.175(L) = \text{Mass Removed During Sampling (mg)} \qquad (55)$$

The mass removed during sampling is referred to as the sampling mass. The mass of the initial solution was known, therefore the mass of sodium in the solution at any sampling time was calculated by subtracting the sampling mass from the previous mass,

$$\text{Previous Mass in the Solution} - \text{Mass Removed} = \text{Current Mass in Solution} \qquad (56)$$

The volume was calculated by dividing the current mass in solution by the measured sodium concentration in the solution,

$$\text{Current Mass in Solution (mg)} \ /\ Na^{+}(mg\ /\ L) = \text{Volume of Solution (L)} \qquad (57)$$

The volume of solution was divided by the original volume of 50 liters corrected for the amount of water removed up to that point by sampling, providing a corrected fraction of water remaining. In many cases, the concentration of sodium was determined from duplicate measurements; the corrected fraction of water was an average of those calculations.

$$\frac{\text{Volume in Solution(L)}}{\text{Initial Volume (L)} - \text{Amount of Water Removed(L)}} = \text{Corrected f} \qquad (58)$$

The corrected mass fractions or the averaged mass fractions were used in all of the calculations, PHEEEQC calculations, tables and graphs presented. The original and corrected fractions of water are in Appendix D.4. The change of the water fraction with time is also shown in Appendix D.5.

K. Isotopic Enrichment Relationships

K.1. Calculation of HCO_3 to Gaseous Carbon Dioxide Enrichment Factors in the Evaporating Na-HCO_3 Solution

A detailed series of mass balance calculations was done using the approach described in section 3.2.5. The purpose of these calculations was to arrive at the enrichment factors for carbon dioxide being degassed from HCO_3 in the solution. The resulting calculated inventories of carbon species for both the carbon-12 and carbon-13 are shown in Figure 36 and Figure 37, respectively. The patterns of carbon-12 and carbon-13 change during the evaporation mimic each other and differ only by a couple orders of magnitude.

Figure 38 is an inventory of HCO_3 and CO_3 as the evaporation of the Na-HCO_3 solution progressed. The loss of carbon is assumed to be due to degassing of carbon dioxide to the atmosphere. The degassed carbon dioxide at each f is the total loss since the beginning of the evaporation but the HCO_3 and CO_3 inventories are not cumulative.

The enrichment factors for HCO_3-degassed CO_2 calculated between sampling points was highly variable. The cumulative enrichment factors, based changes from the initial conditions to the conditions at the sampling point, show even more variability.

The mass balance approach was particularly sensitive to this variability. To reduce the impact of the variability, trend lines were fit to the calculated data points for the total carbon-12, total carbon-13, the carbon-12 HCO_3 and the carbon-13 HCO_3. The corresponding plots are in appendix H. These trend lines were used to calculate the smoothed enrichment factors (Figure 39). The enrichment factor is calculated between each calculated concentration of HCO_3 and degassed carbon dioxide. The cumulative enrichment factor is calculated between the initial condition and each calculated concentration of HCO_3 and degassed carbon dioxide. The result is an averaged curve representing the HCO_3-degassed carbon dioxide enrichment factor during evaporation of the Na-HCO_3 solution. In this case, the enrichment and the cumulative are identical. The average enrichment factor calculated from the trend line fits was -19.6‰. The published equilibrium value is -7.9‰, (Mook et al, 1974) suggesting that the enrichment encountered during the evaporation was kinetic. Stiller et al. (1985) observed apparent enrichments of -19.4‰ during the evaporation of Dead Sea Brine, albeit at temperatures much higher than this experiment (45°C, versus 15°C).

In addition to calculating enrichment factors, the partial pressure of carbon dioxide, carbon-12 and carbon-13 can be calculated for the solution by the following equation

$$P_{x_{CO_2}} = \frac{H^x CO_3 * H^+}{10^{-1.47} * 10^{-6.35}} \qquad (59)$$

where x is the carbon isotope of interest (either 13 or 12). The P_{CO2} for carbon-12 can be compared to the known atmospheric value of $10^{-3.5}$. The same comparison can also be made for carbon-13 by assuming the value in the atmosphere was equal to -7‰ (Li,

1997). The resultant partial pressures (Figure 40) show that the Na-HCO_3 solution was not in equilibrium with atmospheric carbon dioxide. This elevated partial pressure coincides with the lowered pH measurements (Figure 4). This result suggests that the solution did not completely degas the excess carbon dioxide as would be expected of a solution in equilibrium with atmospheric carbon dioxide.

The equilibrium constants used to calculate the P_{co2} are for temperatures of 25°C, which is not consistent with the temperature data. Constants were calculated for the average temperature on the day of sampling, the minimum that day, and a constant temperature of 15°C (Figure 41). Adjusting the equilibrium constants according to temperature did not move the calculated P_{co2} significantly closer to the atmospheric value nor were there large differences in the calculated P_{co2} values.

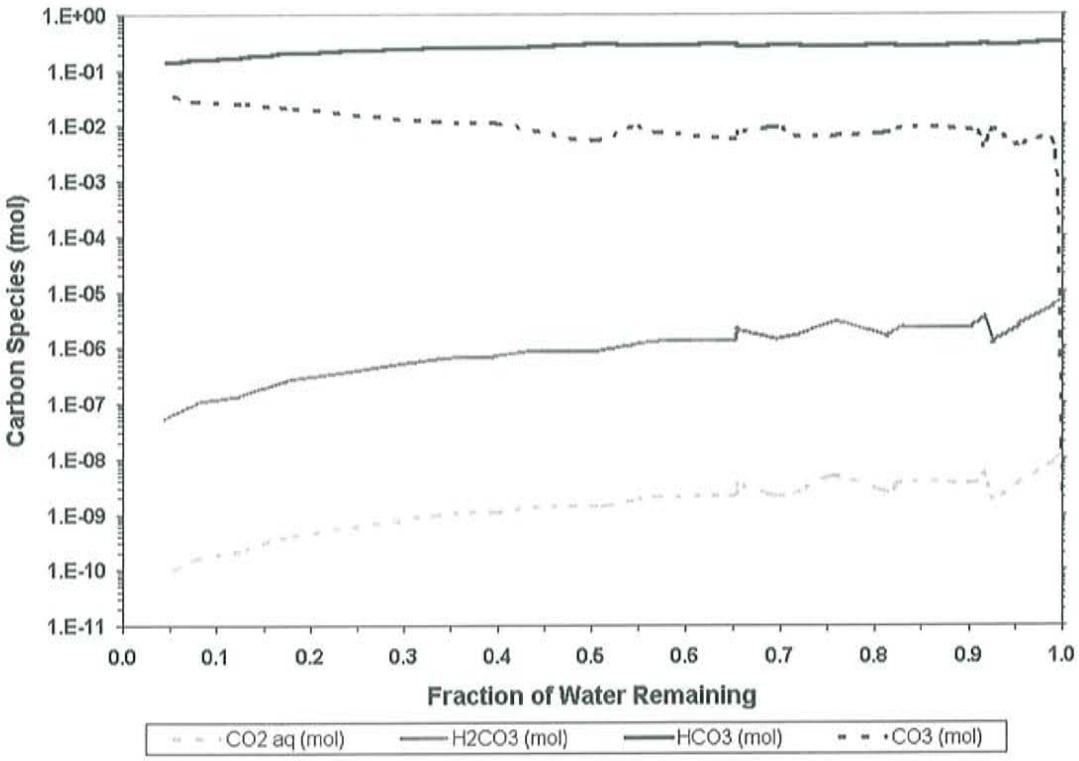

Figure 36 Calculations for each carbon-12 species at every sampling point during the evaporation of the Na-HCO_3 solution.

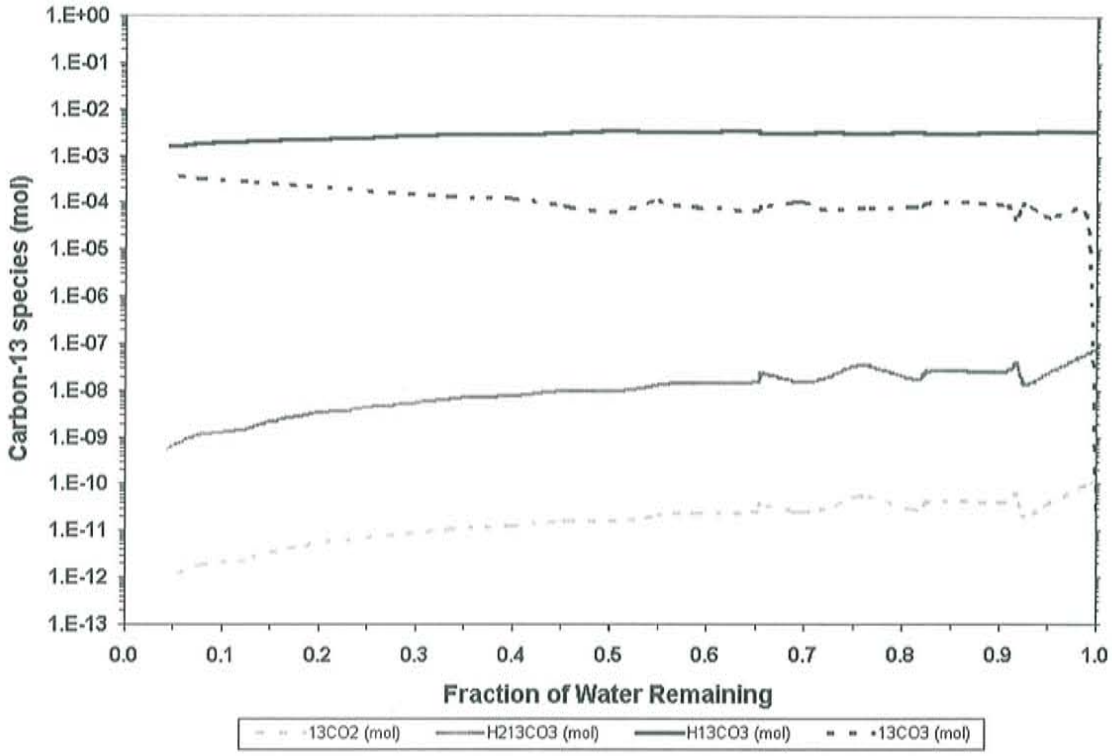

Figure 37 Calculations for each carbon-13 species at every sampling point during the evaporation of the Na-HCO_3 solution.

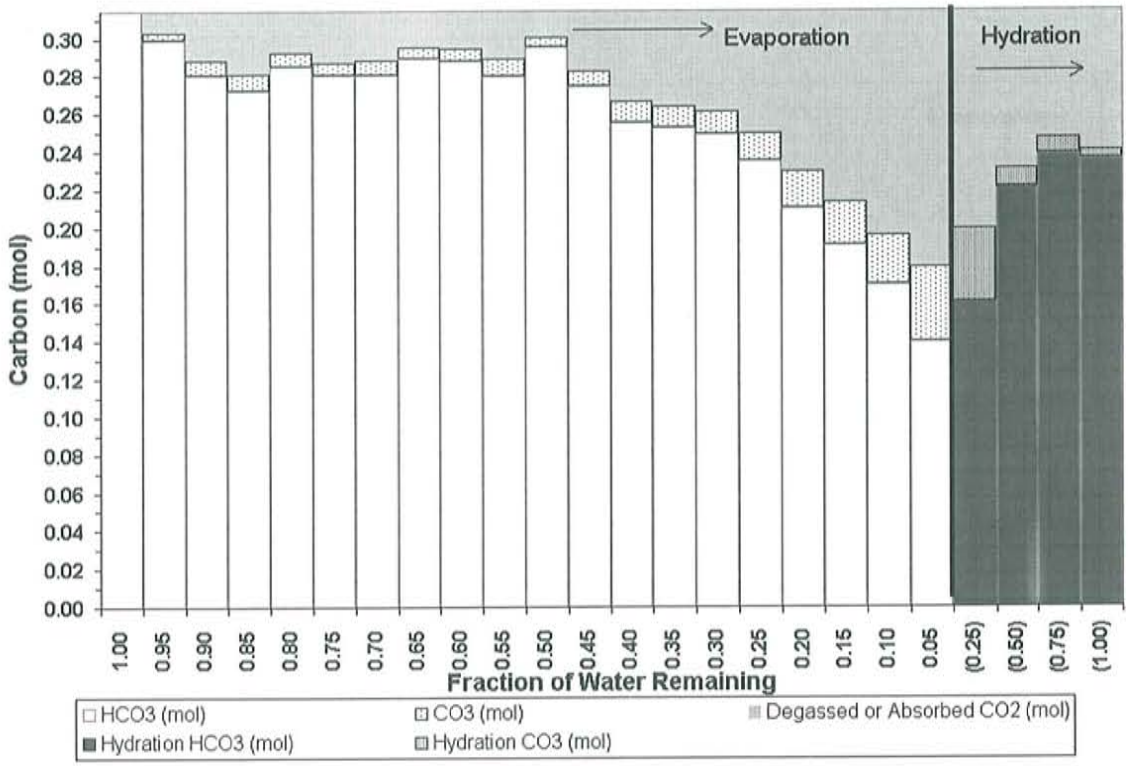

Figure 38 Average inventory of CO_3 and HCO_3 during the evaporation and hydration of the Na-HCO_3 solution. The overall decrease in carbon from the initial at each fraction of water remaining is labeled as degassed CO_2. In the hydration portion, which is included here for illustration, the increase in CO_3 and HCO_3 is due to absorbed CO_2.

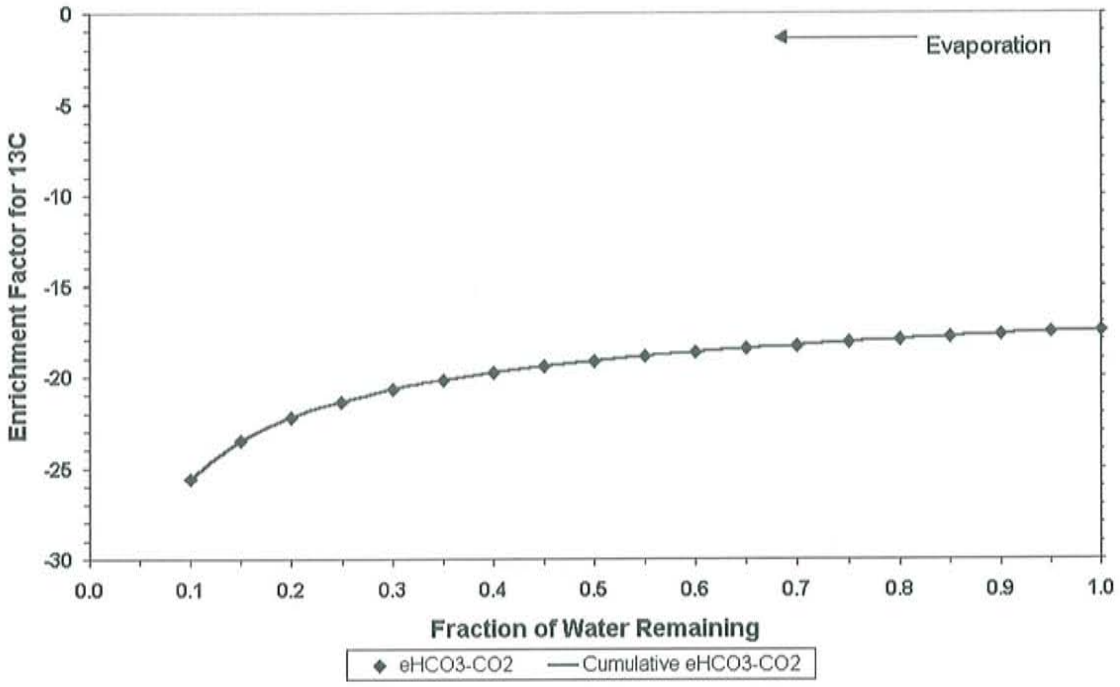

Figure 39 Smoothed enrichment factors for HCO_3 to degassed CO_2 during the evaporation of the Na-HCO_3 solution. The enrichment shown in black diamonds is calculated between sampling points and the cumulative shown as a blue line is calculated from the initial condition to each sampling point. The average enrichment factor is -19.63‰.

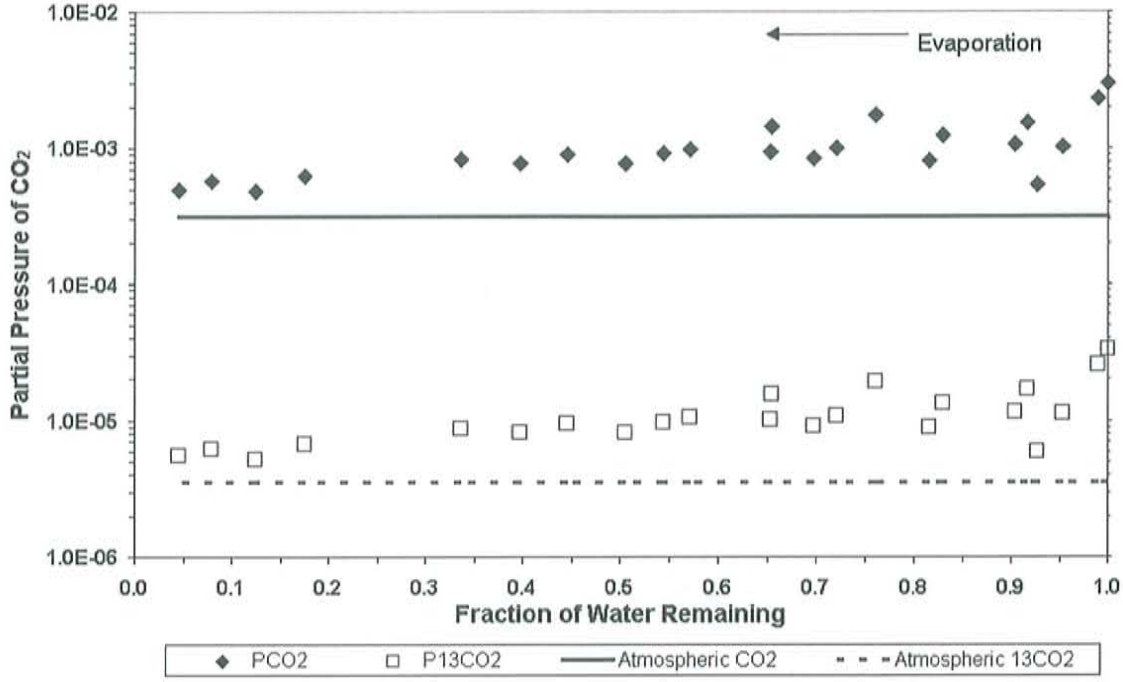

Figure 40 Calculation of the partial pressure of carbon dioxide in the Na-HCO_3 solution. Partial pressures for both $^{12}CO_2$ and $^{13}CO_2$ are shown as symbols with the atmospheric values shown as lines.

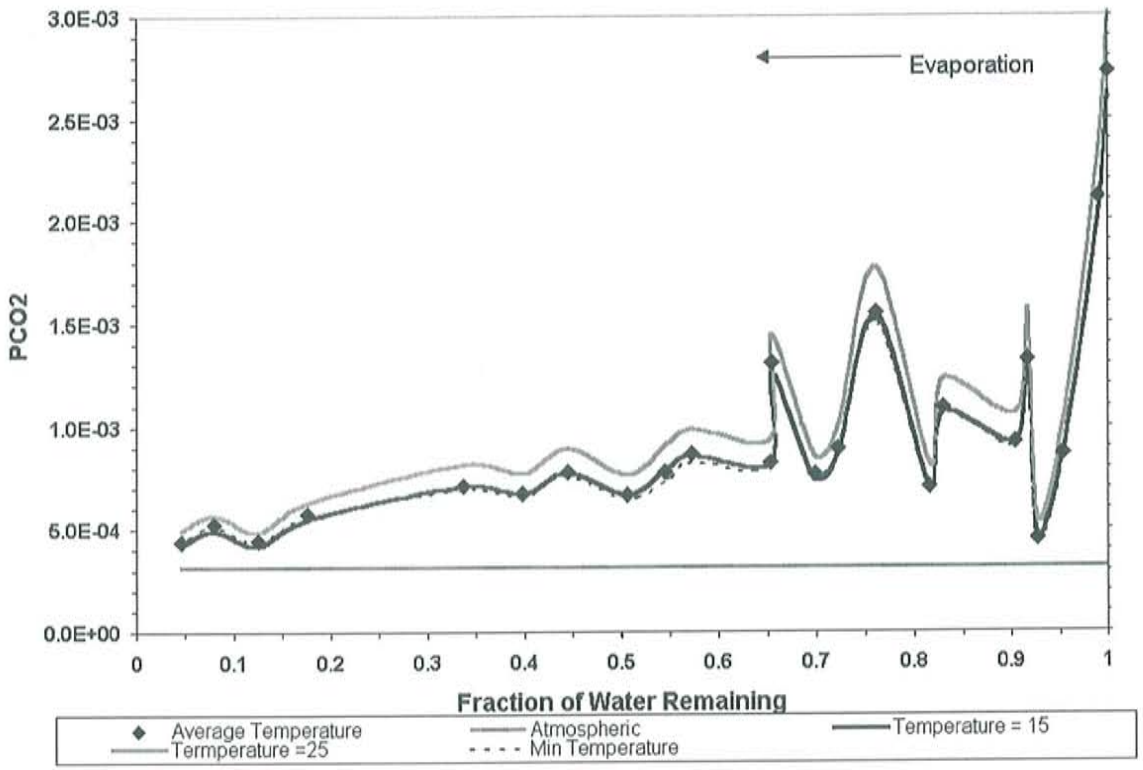

Figure 41 Comparison of calculated P_{CO2} using different temperatures to calculate the equilibrium constants. The changes in temperature do not bring the solution closer to equilibrium with the atmosphere.

K.2. Calculation of HCO_3 to Gaseous Carbon Dioxide Enrichment Factors in the Evaporating Ca-Na-HCO_3-Cl solution

As in appendix K.2, a detailed series of mass balance calculations was performed using the approach described in section 3.2.5. The purpose of these calculations was to arrive at the enrichment factors for carbon dioxide being degassed from HCO_3 in the solution. The resulting calculated inventories of carbon species for both the carbon-12 and carbon-13 are shown in Figure 42 and Figure 43, respectively. The intermittent CO_3

in the Ca-Na-HCO_3-Cl is due to calcite precipitation and the analytical limits of the alkalinity titration.

Figure 44 is an inventory of HCO_3, CO_3 and calcite as the evaporation of the Ca-Na-HCO_3-Cl solution progressed. The loss of carbon after the precipitation of calcite is assumed to be due to degassing of carbon dioxide to the atmosphere. The degassed carbon dioxide and calcite at each f are the total loss or gain since the beginning of the evaporation but the HCO_3 and CO_3 inventories are not cumulative.

The Ca-Na-HCO_3-Cl solution enrichment factors for HCO_3 and the calculated degassed carbon dioxide were highly variable. Enrichment factors were calculated based on curves fitted to the data in order to smooth the high degree of variability that analytical error produces when point-to-point calculations are employed. The total carbon-12, total carbon-13, the carbon-12 HCO_3, and the carbon-13 HCO_3 graphs with fitted curves are in appendix H. These trend lines were used to calculate the smoothed enrichment factors (Figure 45). The result is a smoother curve representing the HCO_3-degassed carbon dioxide enrichment factor for the evaporation phase of the Ca-Na-HCO_3-Cl solution. The average enrichment factor calculated between individual points of the trend line was -7.3‰. The average from the cumulative enrichment factors calculated from the initial condition and individual points on the trend line was -22.7‰. The published equilibrium value is -7.9‰ suggesting that the average enrichment encountered during the evaporation was similar to the expected equilibrium enrichment. The large kinetic enrichment of the cumulative curve is due to the very large fractionation during the initial degassing phase. The divergence of the two curves, the cumulative and the step

enrichment, suggests that the impact of calcite precipitation was much larger between sampling periods than over the entire experiment.

Using the same approach taken for the Na-HCO_3 solution, the partial pressures of $^{12}CO_2$ and $^{13}CO_2$ were calculated for the Ca-Na-HCO_3-Cl solution (Figure 46). The Ca-Na-HCO_3-Cl solution also exhibited elevated partial pressures relative to the bulk atmosphere. Unlike the Na-HCO_3 solution, which tended toward P_{CO2} (atm), the P_{CO2} in the Ca-Na-HCO_3-Cl solution seemed to stabilize at ~10^{-3} atm after reaching a mass fraction of 0.85. This steady state value was still considerably higher than the P_{CO2} (atm) = $10^{-3.5}$ expected for a solution in equilibrium with the atmosphere.

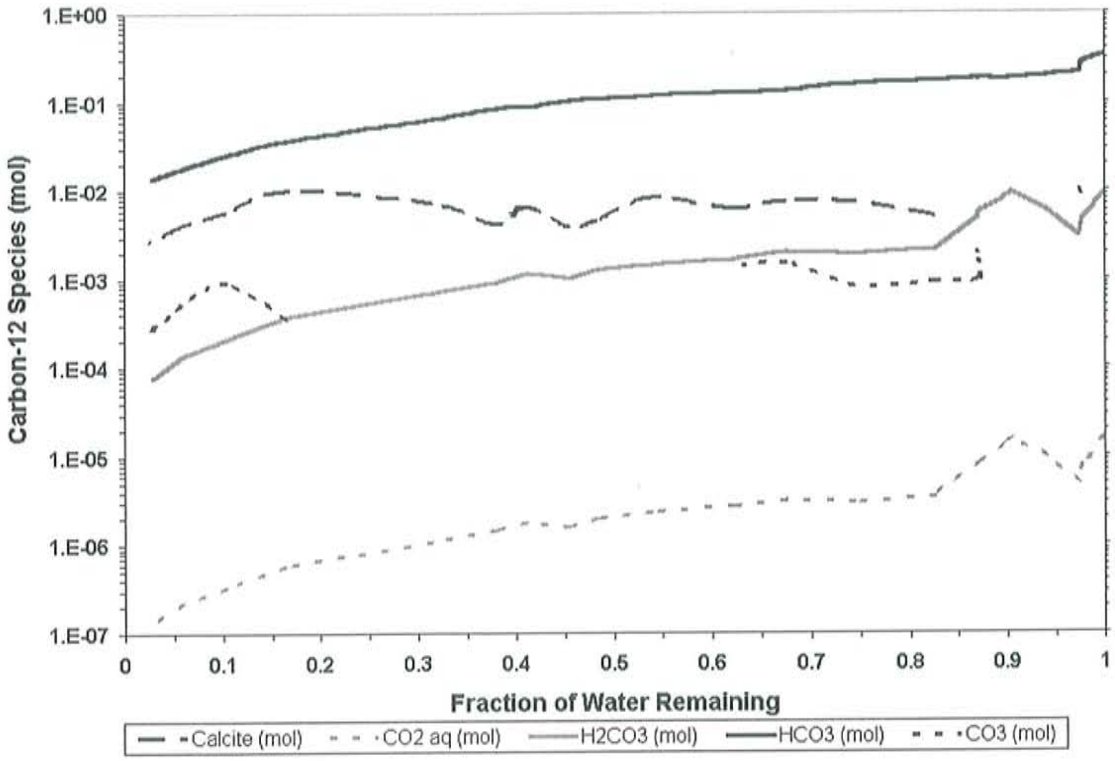

Figure 42 Calculations for each carbon-12 species (mols) at each sampling point during the evaporation of the Ca-Na-HCO_3-Cl solution.

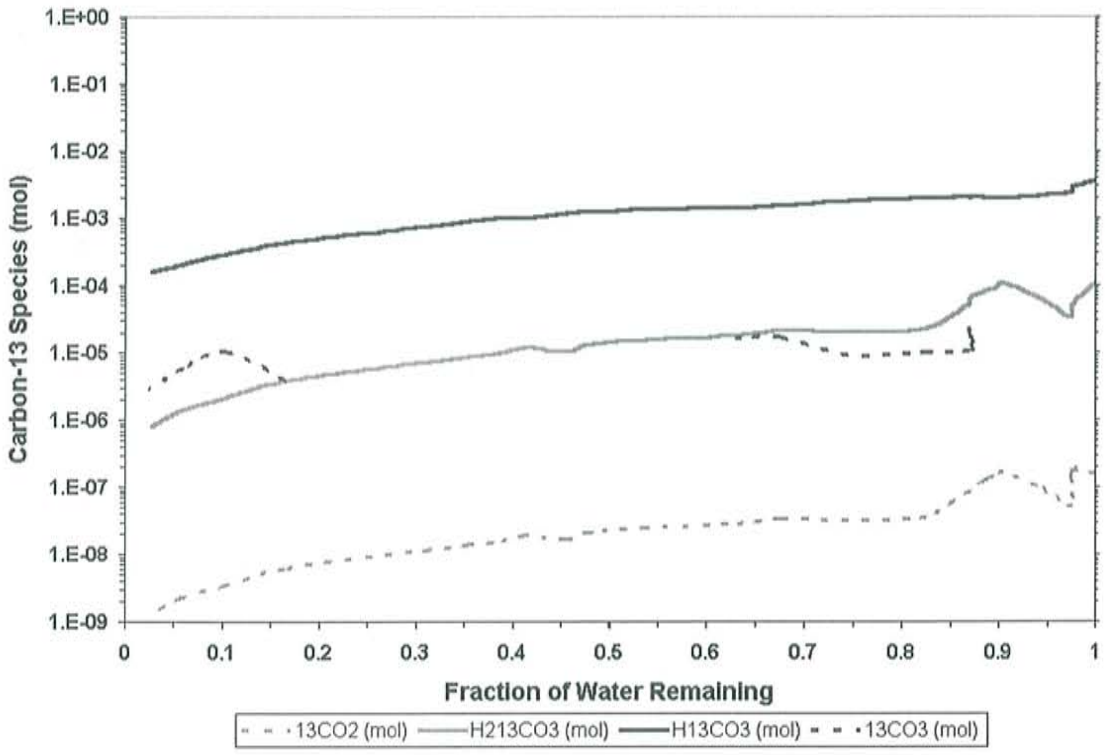

Figure 43 Calculations for each carbon-13 species at every sampling point during the evaporation of the Ca-Na-HCO_3-Cl solution.

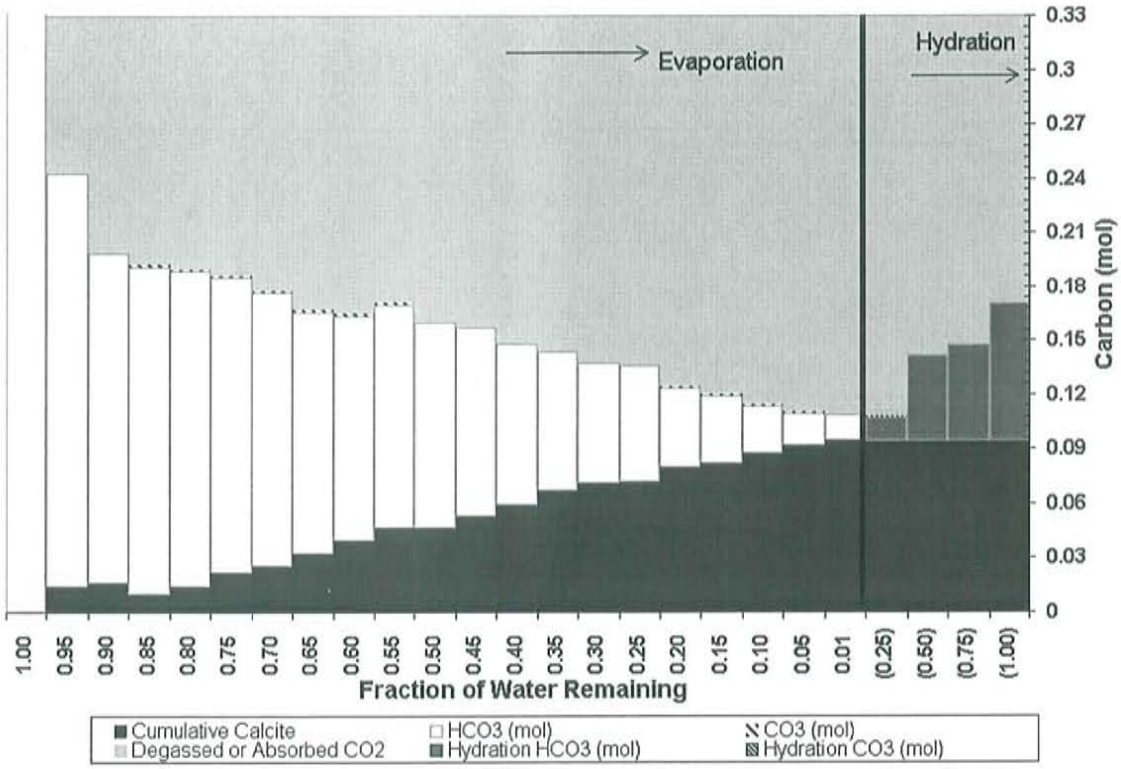

Figure 44 Inventory of CO_3, HCO_3 and calcite during the evaporation of the Na-HCO_3 solution. The overall decrease in carbon from the initial at each fraction of water remaining is labeled as degassed CO_2. In the hydration portion, which is included here for illustration, the increase in CO_3 and HCO_3 is due to absorbed CO_2.

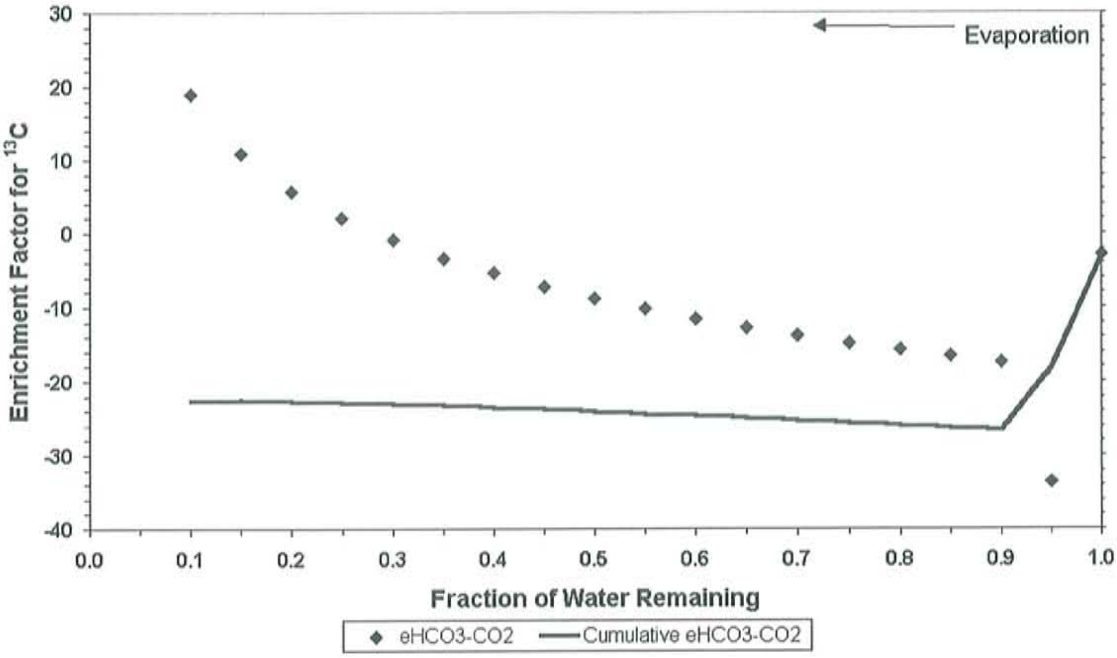

Figure 45 Smoothed enrichment factors for conversion of HCO_3 to CO_2 gas during the evaporation of the Ca-Na-HCO_3-Cl solution. The average enrichment factor is -7.26‰. The average cumulative enrichment factor is -22.69‰.

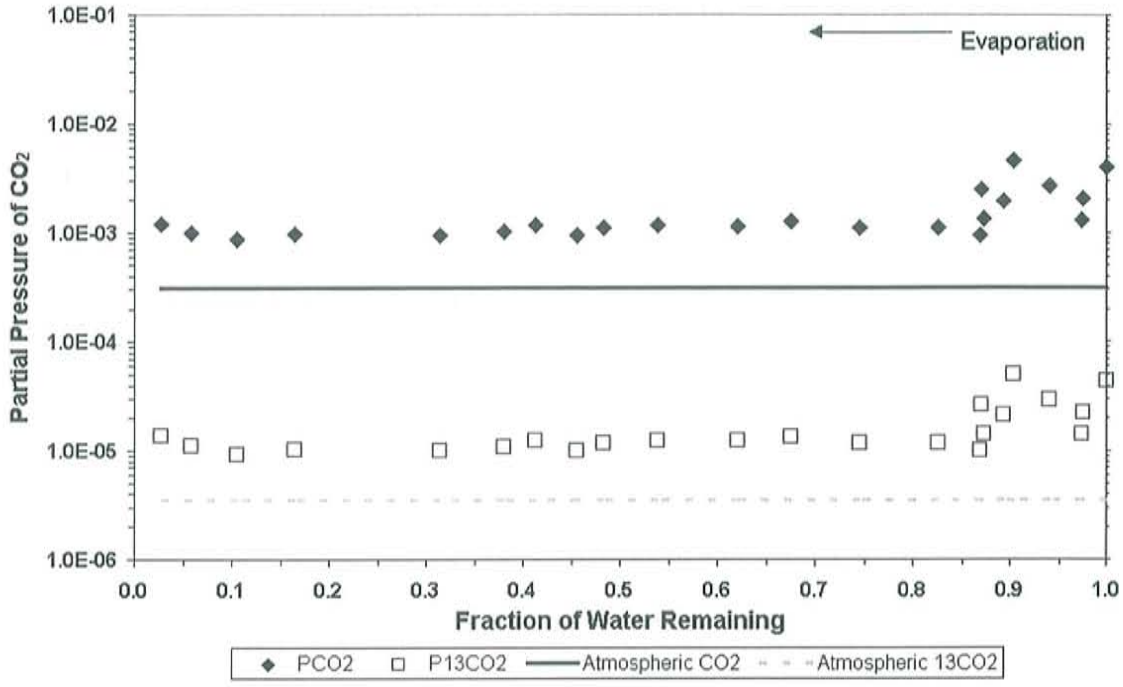

Figure 46 Calculation of the partial pressure of carbon dioxide in the Ca-Na-HCO_3-Cl solution. Partial pressures for both $^{12}CO_2$ and $^{13}CO_2$ are shown as symbols with the atmospheric values shown as lines.

K.3. Calculation of HCO_3 to Gaseous Carbon Dioxide Enrichment Factors in the Na-HCO_3 Solution during the Hydration Phase

The hydration of the remaining evaporation solution took place in 5 steps. The measurements were made after pH of the new solution had converged around a single value, approximately 5 days after the addition of deionized water. The distribution of carbon species for both carbon-12 and carbon-13 are shown in Figure 47 and Figure 48, respectively. With each addition of water, the pH decreases, the total carbon increases, as shown with the increase in HCO_3, carbonic acid and aqueous carbon dioxide. The CO_3 decreases below detection as the solution returns to the original volume. The fractional

increase in HCO_3 above the HCO_3 at the end of the hydration is shown in Figure 49. The fraction of HCO_3 increased by 0.8.

Unlike the evaporation phase of the experiment, the enrichment factors relating the isotopic composition of the absorbed carbon dioxide to that of the HCO_3 were not highly variable. The curve-fitting technique required during evaporation was not required for the hydration phase of the Na-HCO_3 solution. The average enrichment factor from the trend line fits was 8.17‰, with a standard deviation of 0.37 (Figure 50). The expected equilibrium value was 7.9‰ indicating that the enrichment encountered during the hydration was close to the published equilibrium value, unlike the evaporation phase.

In addition to the calculation of enrichment factors, the partial pressures of $^{12}CO_2$ and $^{13}CO_2$ were also calculated following the same method as for the evaporation phase. These calculations (Figure 51) show that the Na-HCO_3 solution during the hydration phase was not in equilibrium with the atmosphere with respect to carbon dioxide. The partial pressures of both $^{12}CO_2$ and $^{13}CO_2$ show an increase during the hydration above the standard assumed partial pressures.

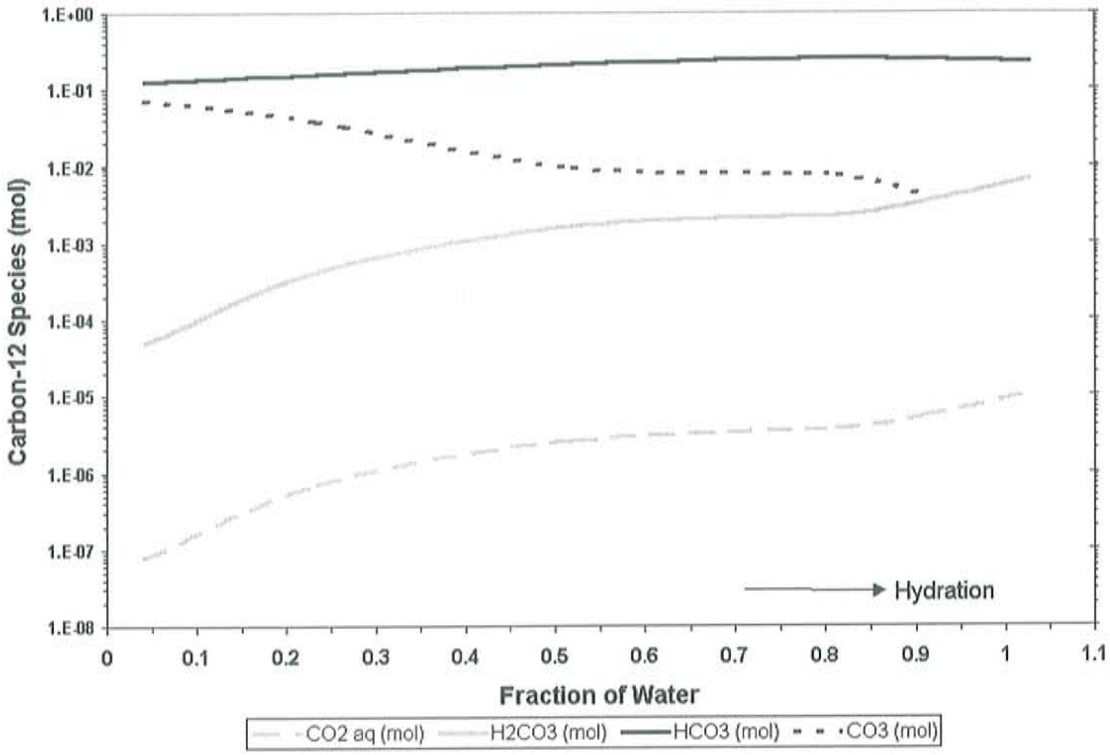

Figure 47 Calculations for each carbon-12 species at each sampling point during the hydration of the Na-HCO_3 solution.

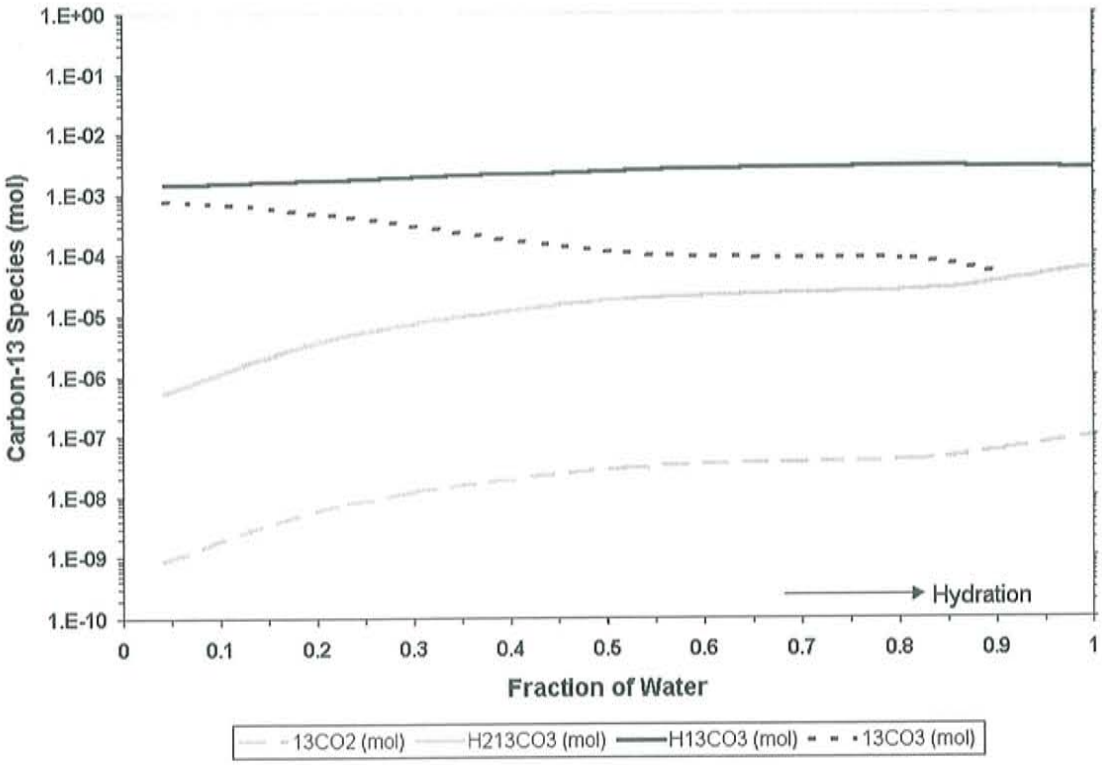

Figure 48 Calculations for each carbon-13 species at every sampling point during the hydration of the Na-HCO_3 solution.

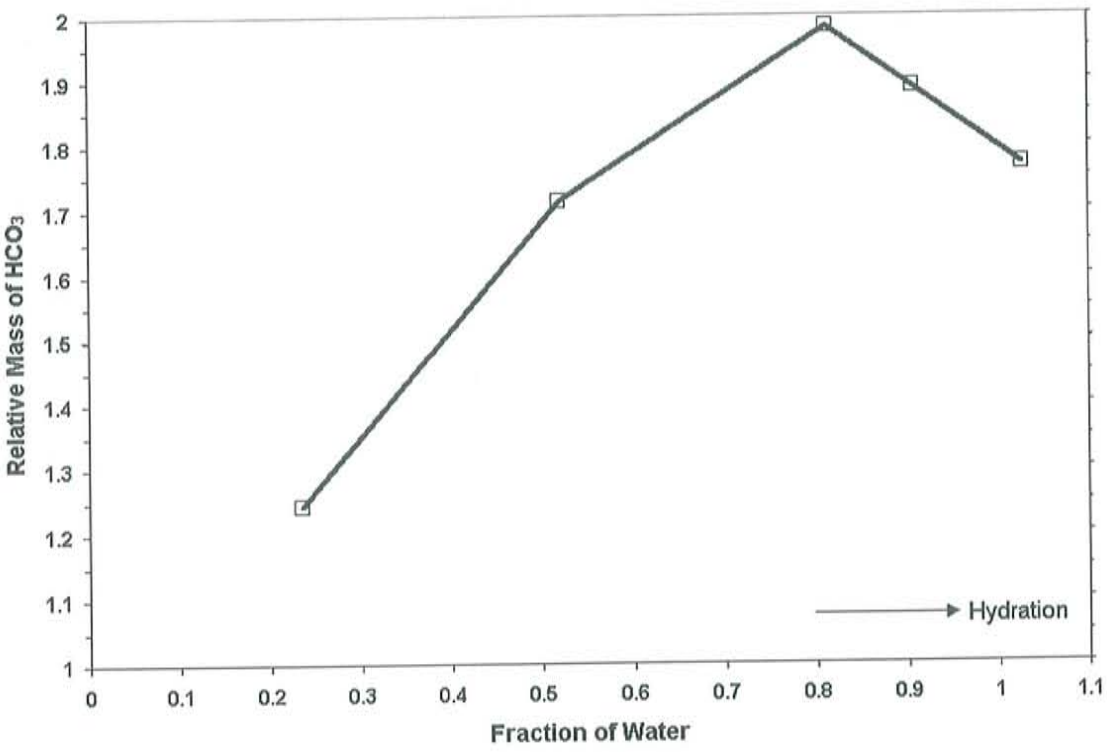

Figure 49 Relative mass of HCO_3 during the hydration of the Na-HCO_3 solution. At the end of the evaporation, the HCO_3 is counted as the initial condition for hydration, so that at the end of the hydration this solution has increased the HCO_3 in solution by a fraction of 0.8.

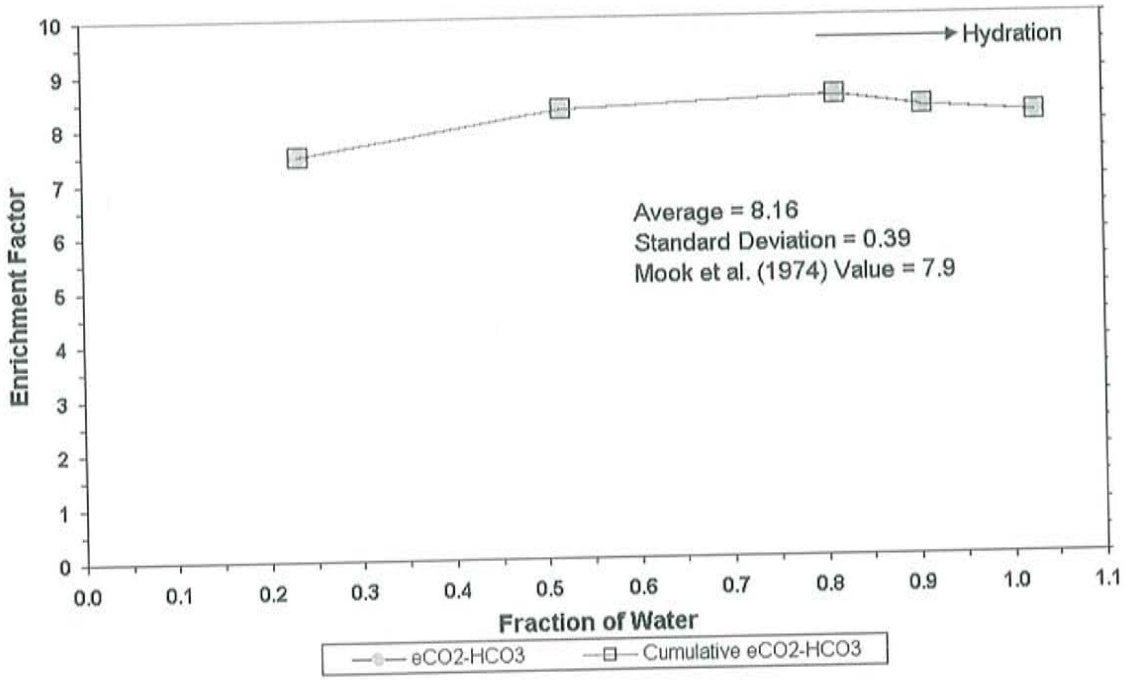

Figure 50 Enrichment factors from the hydration of the Na-HCO_3 solution. The average enrichment factor is 8.17‰. The published value is 7.9‰ from Mook et al. (1974).

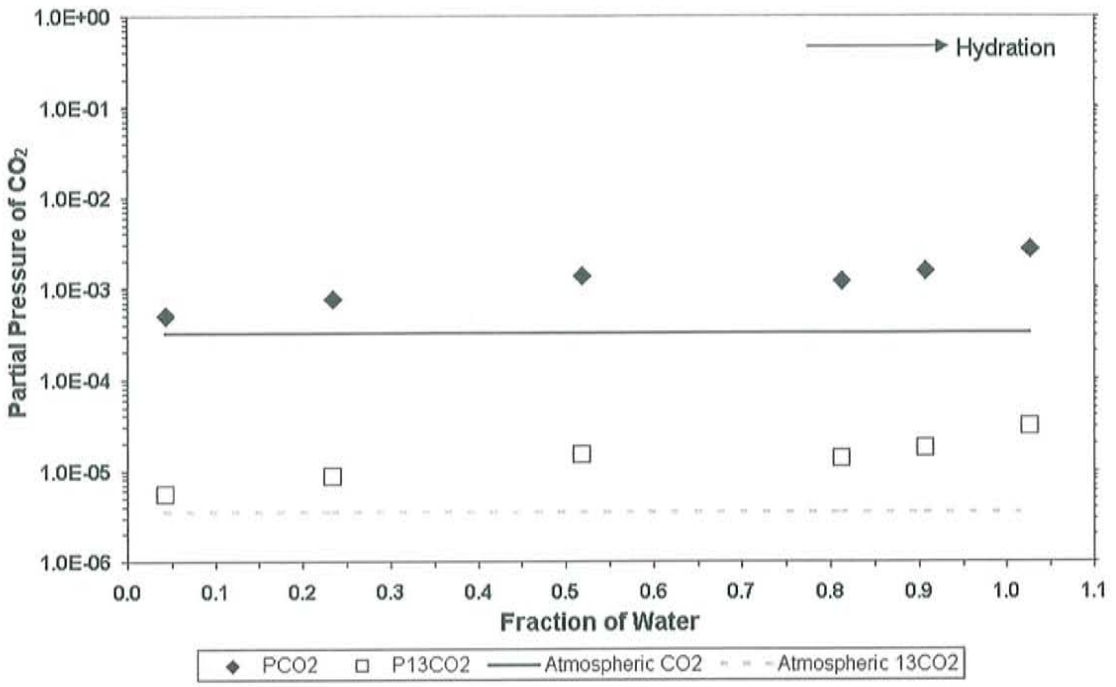

Figure 51 Calculation of the partial pressure of carbon dioxide in the hydrating Na-HCO_3 solution. Partial pressures for both $^{12}CO_2$ and $^{13}CO_2$ are shown as symbols with the atmospheric values shown as lines.

K.4. Calculation of HCO_3 to Gaseous Carbon Dioxide Enrichment Factors in the Ca-Na-HCO_3-Cl Solution during the Hydration Phase

The chemistry of the Ca-Na-HCO_3-Cl solution during hydration is consistent with the Na-HCO_3 solution. The total carbon, HCO_3, carbonic acid and aqueous carbon dioxide all increase during the hydration. The CO_3 decreases to below detection shortly after the first hydration step. The carbon distributions for both carbon-12 and carbon-13 are shown in Figure 52 and Figure 53, respectively. The fractional increase in HCO_3 above the initial HCO_3 at the end of the hydration is shown in Figure 54. The fraction of total carbon increased by 0.8.

The enrichment factors for the atmospheric carbon dioxide to HCO_3 in the Ca-Na-HCO_3-Cl solution were not highly variable during the hydration phase. The curve-fitting technique required for the evaporation phase was not required for the hydration. The average enrichment factor calculated was 11.4‰, with a standard deviation of 0.99‰ (Figure 55). The published equilibrium value is 7.9‰ (Mook, et al., 1974).

In addition to the calculation of enrichment factors, the partial pressures of $^{12}CO_2$ and $^{13}CO_2$ were also calculated following the same method as for the evaporation phase. The partial pressures (Figure 56) indicate that Ca-Na-HCO_3-Cl solution during the hydration phase was not in equilibrium with the atmosphere with respect to carbon dioxide. As for the Na-HCO_3 solution, the partial pressures of both species show an increase during the hydration phase above the equilibrium partial pressures.

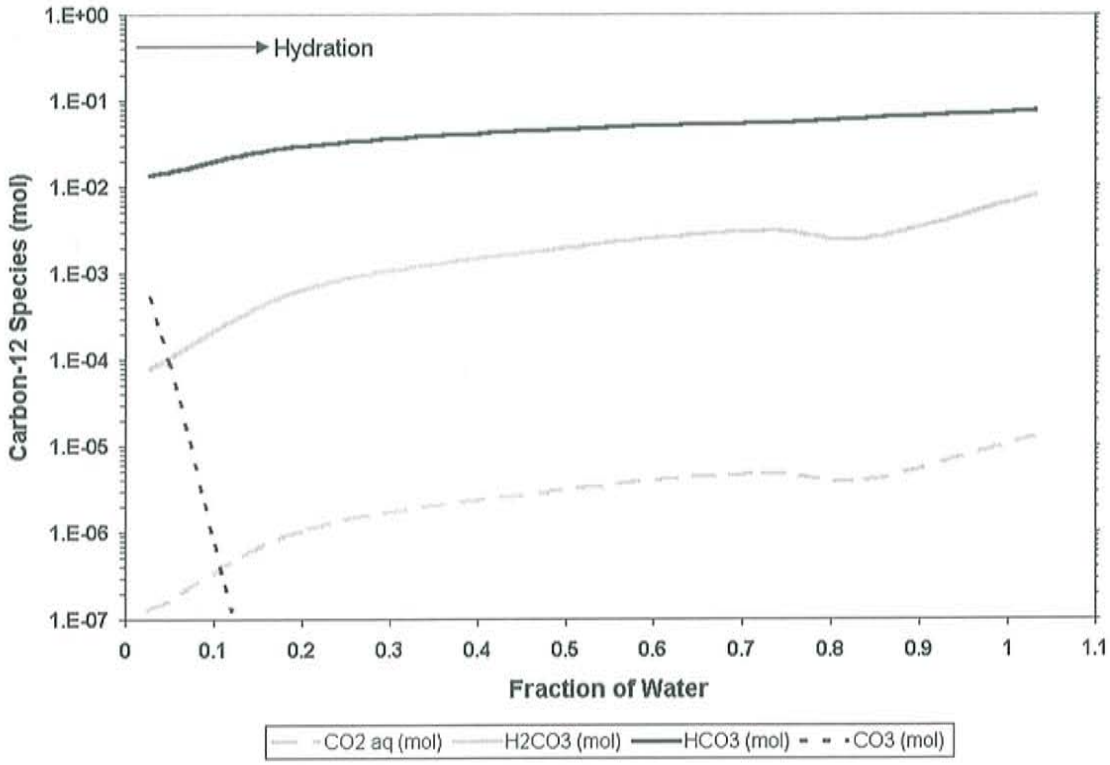

Figure 52 Calculations for each carbon-12 species at every sampling point during the hydration of the Ca-Na-HCO_3-Cl solution.

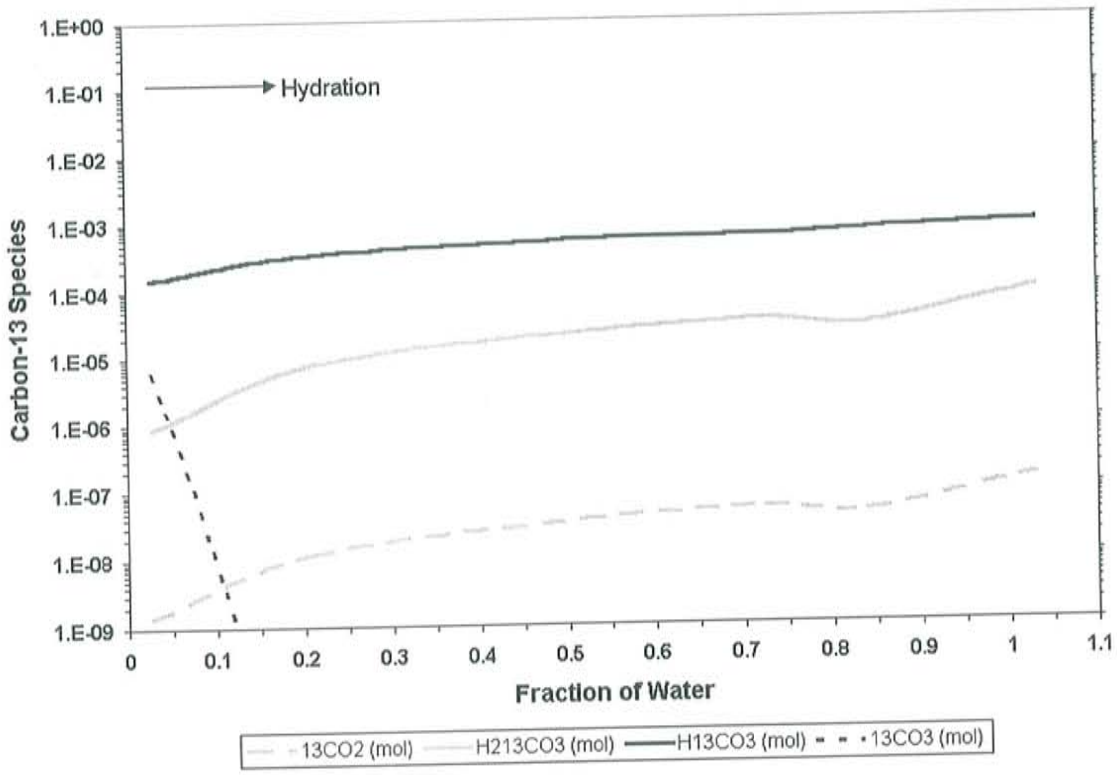

Figure 53 Calculations for each carbon-13 species at every sampling point during the hydration of the Ca-Na-HCO_3-Cl solution.

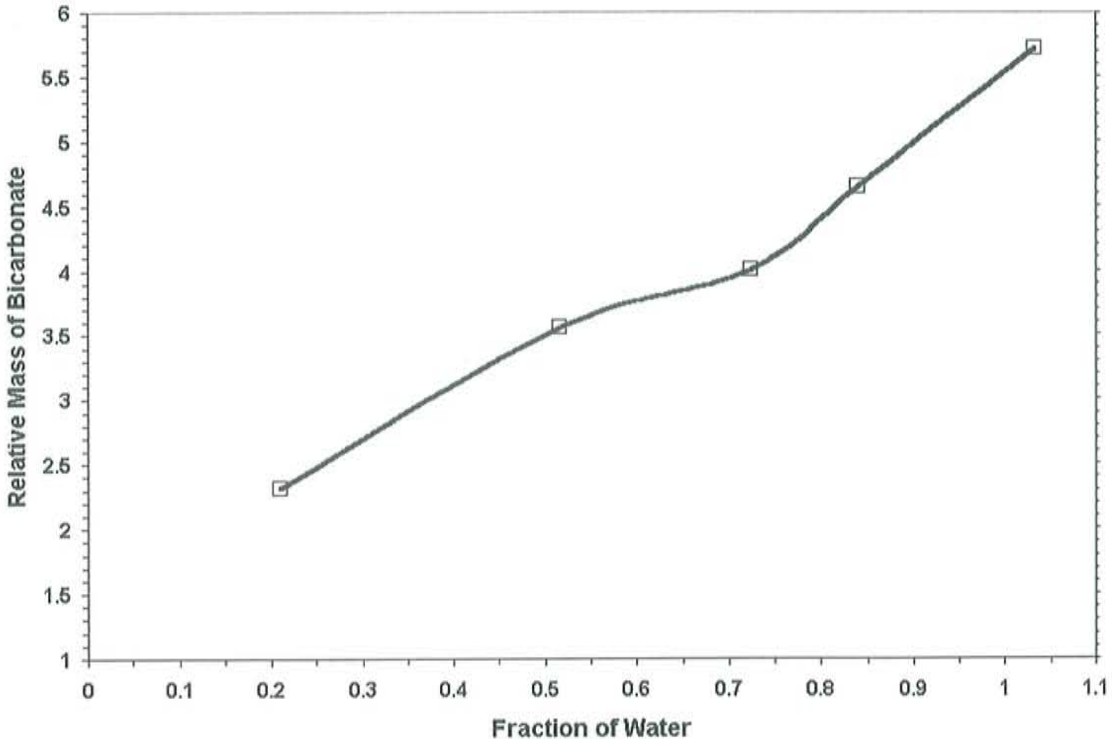

Figure 54 Relative mass of HCO_3 during the hydration of the Ca-Na-HCO_3-Cl solution. At the end of the evaporation, the HCO_3 is counted as the initial condition for hydration, so that at the end of the hydration this solution has increased the HCO_3 in solution by a fraction of 4.5.

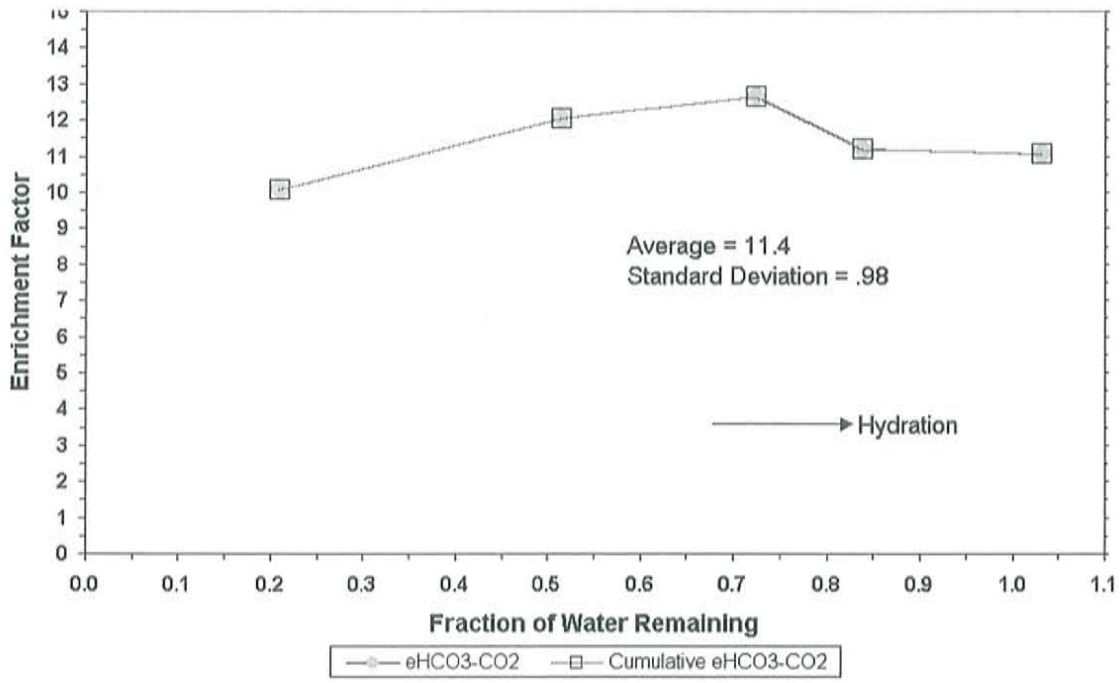

Figure 55 Enrichment factors for HCO_3 to CO_2 from the hydration of the Ca-Na-HCO_3-Cl solution. The average enrichment factor is 8.17‰. The equilibrium value is 7.9‰ (Mook et al., 1974).

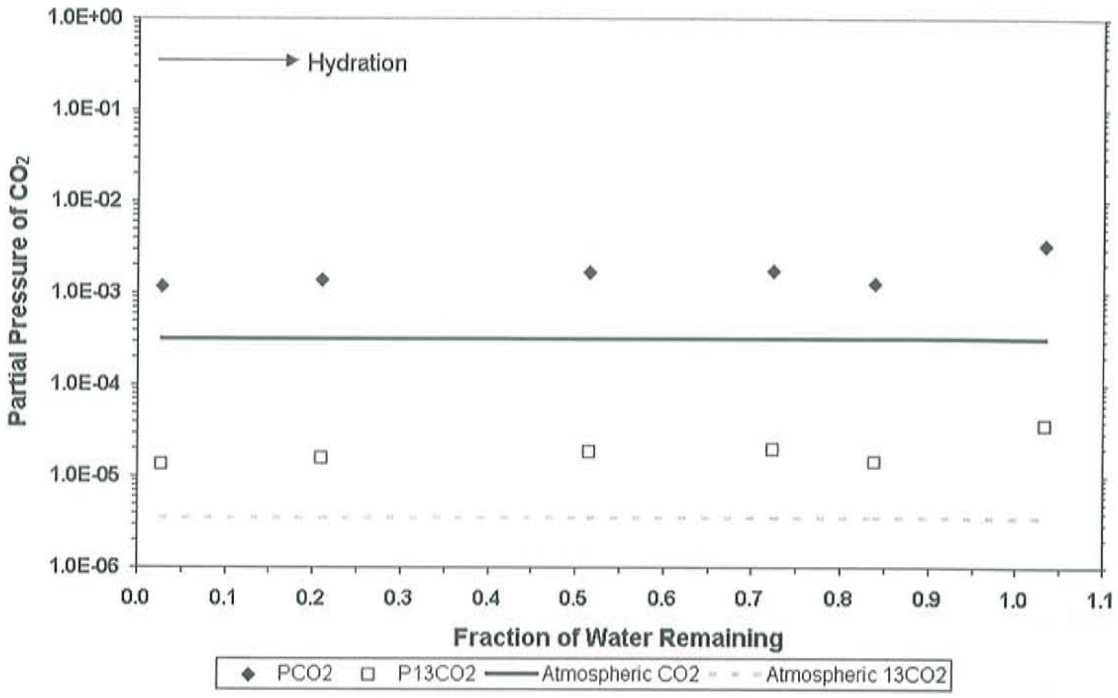

Figure 56 Calculation of the partial pressure of carbon dioxide in the hydrating Ca-Na-HCO_3-Cl solution. Partial pressures for both $^{12}CO_2$ and $^{13}CO_2$ are shown as symbols with the atmospheric values shown as lines.

K.5. Oxygen-18 Isotopic Difference between Water and CO_3 Ions

The Na-HCO_3 solution yielded smooth trends for oxygen-18 measured in the water itself and in the DIC samples, with a relatively uniform separation between them (Figure 57). Similarly, the Ca-Na-HCO_3-Cl solution also shows a relatively uniform separation (Figure 58). The oxygen-18 isotopic difference between water and DIC for the Na-HCO_3 solution (Figure 59) averaged –31.0‰ with a standard deviation of 1.8‰. There was quite a bit of scatter in the data early in the evaporation, but the isotopic difference tended toward a smaller value at the late stages of evaporation. In addition to

data for oxygen-18 in water and DIC, oxygen-18 values were measured in calcite for the Ca-Na-HCO_3-Cl solution. Similar to the Na-HCO_3 solution, the Ca-Na-HCO_3-Cl solution also shows a smooth trend for the water and DIC reservoirs, with a large separation between the two. The oxygen-18 values for the precipitate were increasingly different from the solution DIC and quite different from the water measurements. The increasing difference between the oxygen-18 in the precipitate is largely due to the re-mixing of precipitate during sampling. The isotopic difference for the Ca-Na-HCO_3-Cl solution (Figure 60) was calculated between the water to DIC, the water to the calcite, and the DIC to calcite. The average for the water to bulk DIC isotopic difference was –28.0‰ with a standard deviation of 3.8‰. The isotopic differences for the water to DIC in the Na-HCO_3 and Ca-Na-HCO_3-Cl solutions were not statistically different since the populations overlap, but the shape of the trends were different. The Ca-Na-HCO_3-Cl solution had a much larger standard deviation. The decrease in the isotopic difference was much larger at the later stages of evaporation than in the Na-HCO_3 solution. The decrease in the isotopic difference toward the late stages of evaporation may represent the change in solution composition from mostly HCO_3 to more CO_3. The isotopic differences between the water-to-calcite as well as between the DIC-to-precipitate have much larger changes than between the water and DIC. Because of these large changes, averages were not computed for either. The DIC-to-calcite isotopic difference increased 32‰ and the water-to-calcite isotopic difference increased 42‰ during evaporation of the Ca-Na-HCO_3-Cl solution. These large changes in isotopic difference are caused by the lack of evolution of the oxygen-18 measured in the calcite. The lack of similarity

between the solution chemistry at the precipitate suggests that the calcite was re-mixed during sampling. The data show a cumulation of the isotopic values.

The isotopic difference, as defined in chapter 3, can approximate an enrichment factor assuming that $\delta_b/1000 << 1$. The average enrichment for oxygen-18 between the water and DIC is –31.0‰ and –28.0‰ for the Na-HCO_3 and Ca-Na-HCO_3-Cl solutions, respectively. These values are close to those published by Usdowski et al. (1991) and shown in Table 2. Usdowski reports the enrichment from water to HCO_3 is –34‰ and from water to CO_3 is –18‰. The majority of the DIC is in the form of HCO_3 with a minor component of CO_3 considering the pH and the previous calculations of CO_3 distribution at each sampling step of the evaporation. It is unlikely that the difference between Usdowski's values and the values reported here were due to the presence of CO_3 with a lower enrichment value.

The measurements during the hydration phase for oxygen-18 in the CO_3 and water compare well with the evaporation measurements with the exception of the initial hydration step in both solutions (Figure 57and Figure 58). The isotopic difference calculated for the Na-HCO_3 hydration measurements was -30.2‰ with a standard deviation of 1.1‰. This value was similar to the evaporation measurement of -31.0‰. Figure 61, shows the isotopic differences for the Ca-Na-HCO_3-Cl solution during the evaporation and hydration phases. Unlike the Na-HCO_3 solution, the data from two experimental phases do not overlap. The average isotopic difference during the hydration phase was -23.6‰ with a standard deviation of 1.5‰.

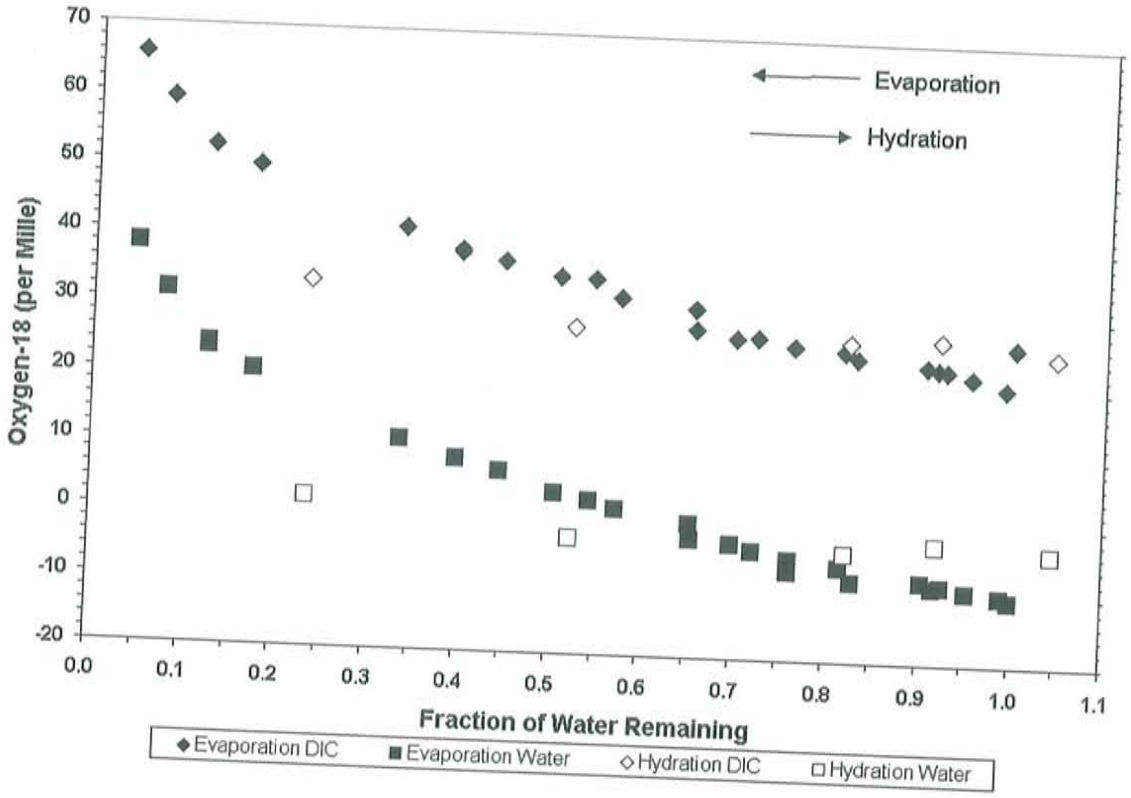

Figure 57 Comparative plot of delta Oxygen-18 measurements from the water ions and the CO_3 ions from the evaporating and hydrating Na-HCO_3 solution.

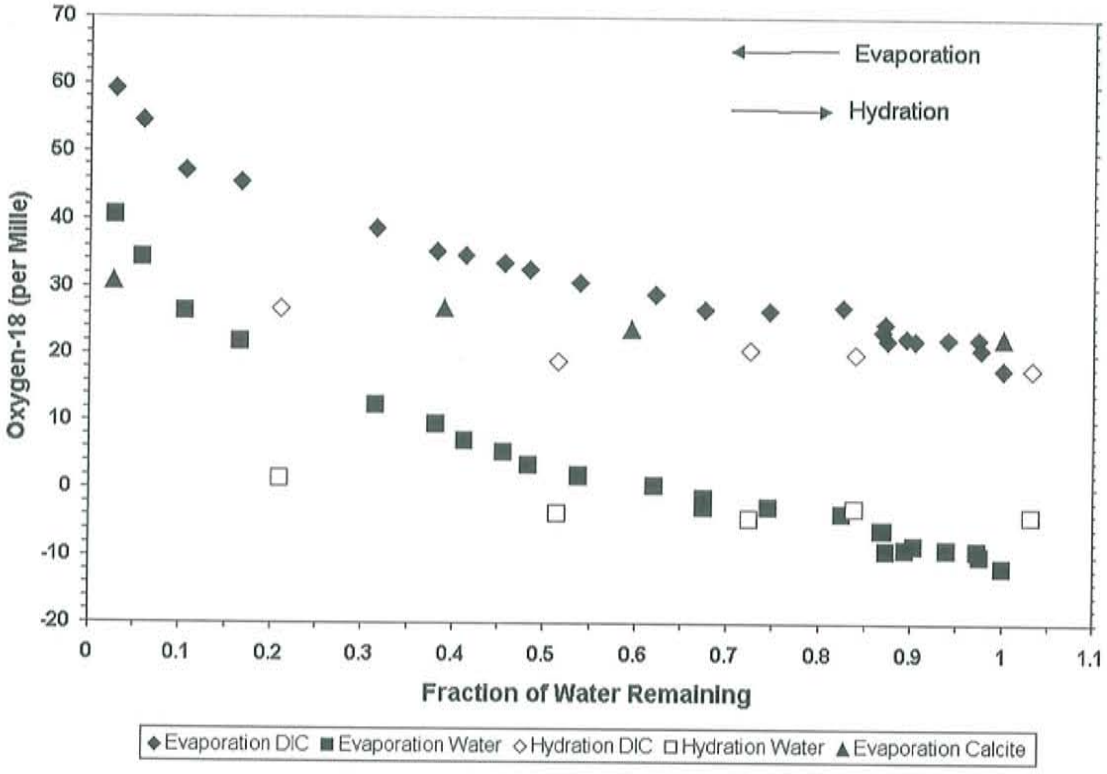

Figure 58 Comparative plot of delta oxygen-18 measurements from the water ions and the CO_3 ions from the Ca-Na-HCO_3-Cl solution during evaporation and hydration. The oxygen-18 measurements from the collected precipitate are also shown.

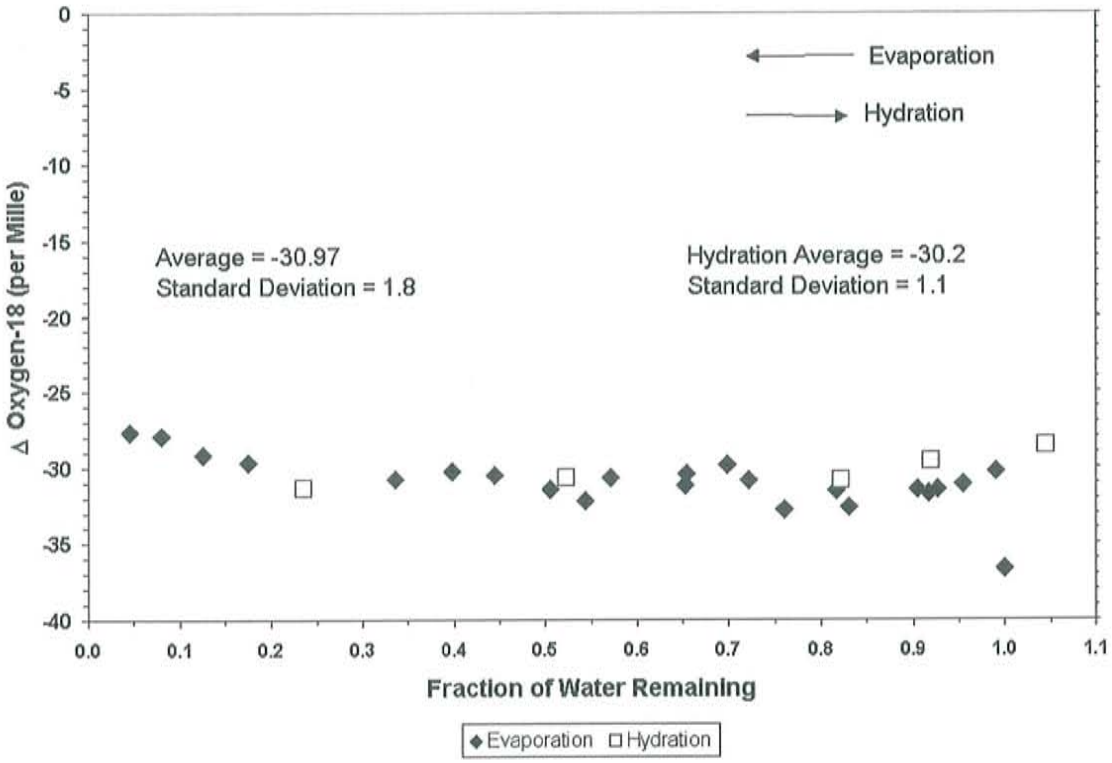

Figure 59 Calculation of the isotopic difference Δ(water oxygen-18 → DIC oxygen-18) for the evaporating and hydrating Na-HCO_3 solution.

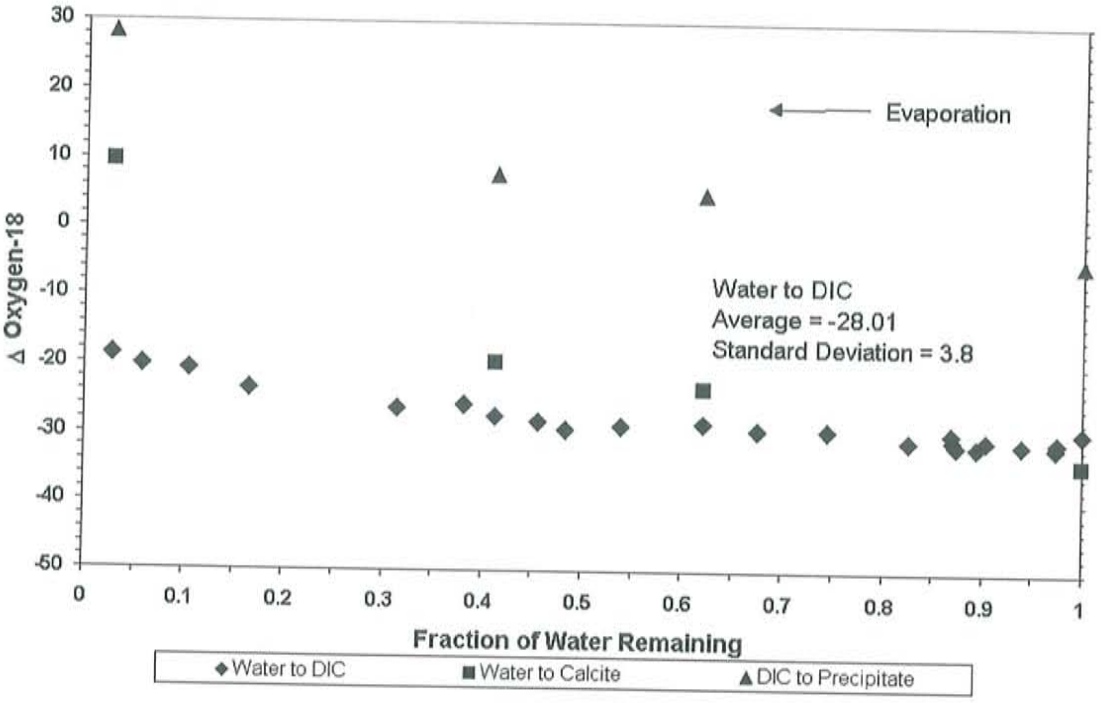

Figure 60 Calculation of Δ (water oxygen-18 → DIC oxygen-18) for the evaporating Ca-Na-HCO_3-Cl solution. Also shown is the water to precipitate and bulk CO_3 to precipitate differences.

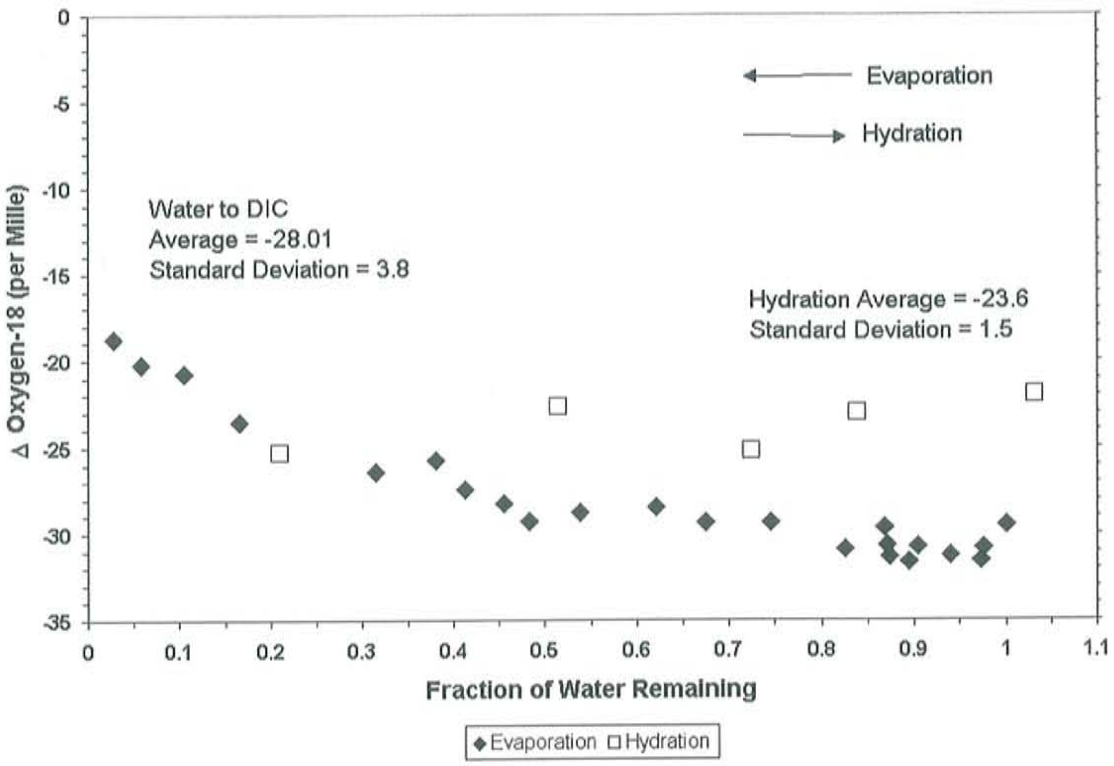

Figure 61 Calculation of Δ (water oxygen-18 → CO_3 oxygen-18) for the evaporating and hydrating Ca-Na-HCO_3-Cl solution.

L. Additional Isotopic Relationships

L.1. Rayleigh Distillation of Oxygen and Deuterium

The weather data in Appendix E were used to find the minimum, maximum, average, and mode values for temperature and humidity (Table 26). The mode value is the value that appeared the most in the data set. The range of temperatures recorded in this experiment were from 2°C to 25°C with an average value of 15°C. The range of recorded relative humidities was from 2% to 48%, with an average of 18.4%.

	Minimum Temperature, and Humidity	Maximum Temperature and Humidity	Average Temperature and Humidity	Mode Temperature and Humidity
Value	4.0°C, 2%	25.6°C, 48%	15.7°C, 18.4%	16.2°C, 16%

Table 26 Temperature and Humidity statistics for the duration of the experiment.

The enrichment factors for oxygen-18 and deuterium can be calculated using the average humidity information and equations (9) through (14). Two curves were calculated using the average temperature and humidity for the upper and lower bounds provided by Gat (1981) and Merlivat and Jouzel (1979) respectivly. The parameter of Gat's equation ($\Delta\varepsilon$)was then adjusted until the calculated curve fit the data set. The calculated oxygen-18 curves with the data sets for the deionized water, Na-HCO_3, and Ca-Na-HCO_3-Cl solutions are in Figure 62, through Figure 64. In all three solutions, the measured oxygen-18 data was between the upper and lower bounds and the adjusted parameters were similar. The deuterium data showed similar trends (Figure 65, through Figure 67). The deuterium adjusted parameter for the deionized water was markedly different from the two chemical solutions because of the difference in tank geometries.

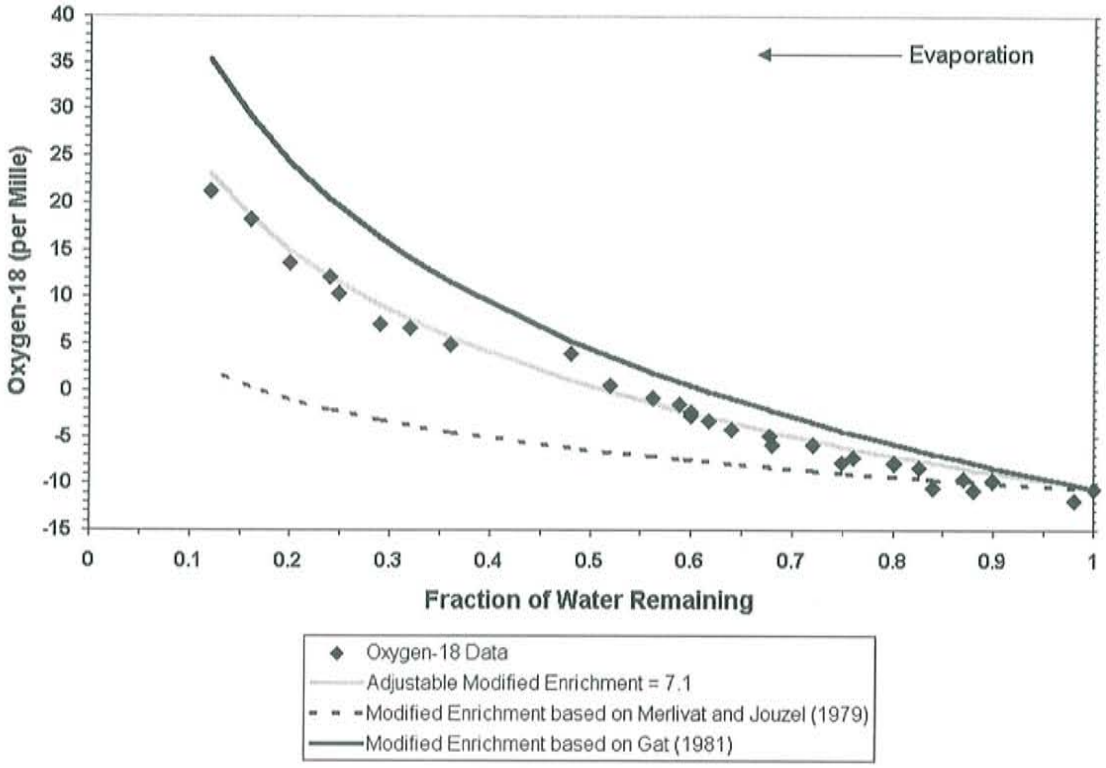

Figure 62 Oxygen-18 data from the deionized water plotted with calculated enrichments bounds based upon the work of Merlivat and Jouzel (1979) and Gat (1981).

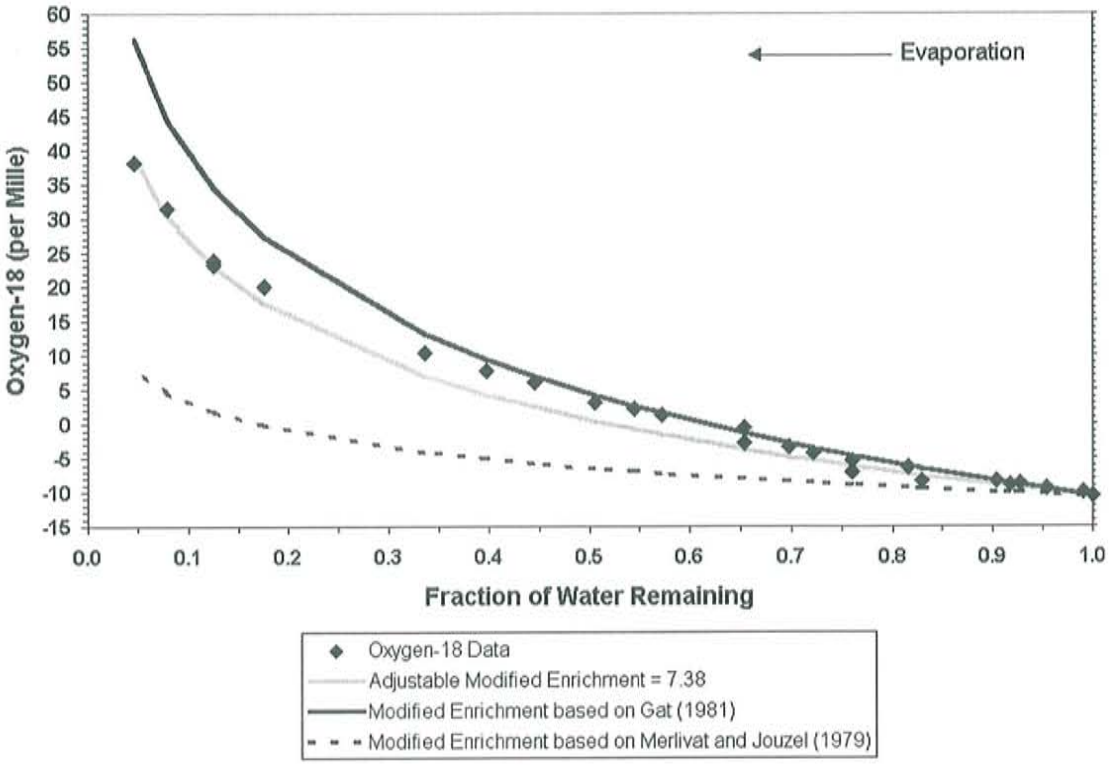

Figure 63 Oxygen-18 data from the Na-HCO_3 solution plotted with calculated enrichments bounds based upon the work of Merlivat and Jouzel (1979) and Gat (1981).

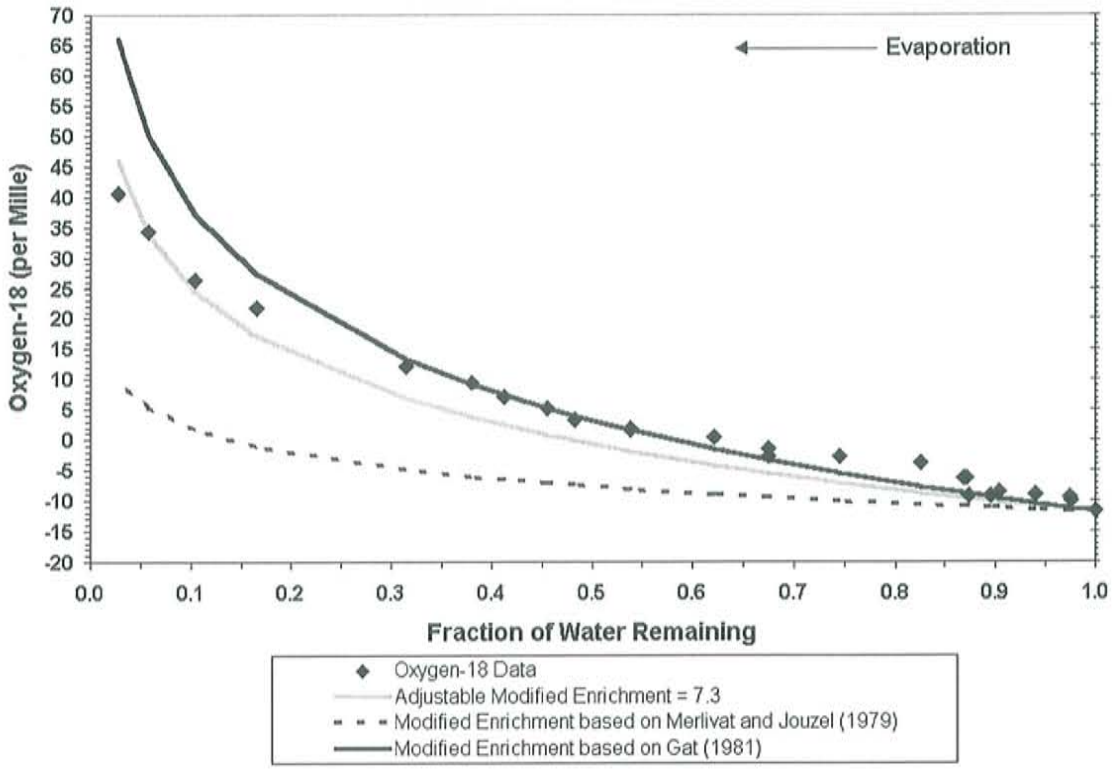

Figure 64 Oxygen-18 data from the Ca-Na-HCO_3-Cl solution plotted with calculated enrichments bounds based upon the work of Merlivat and Jouzel (1979) and Gat (1981).

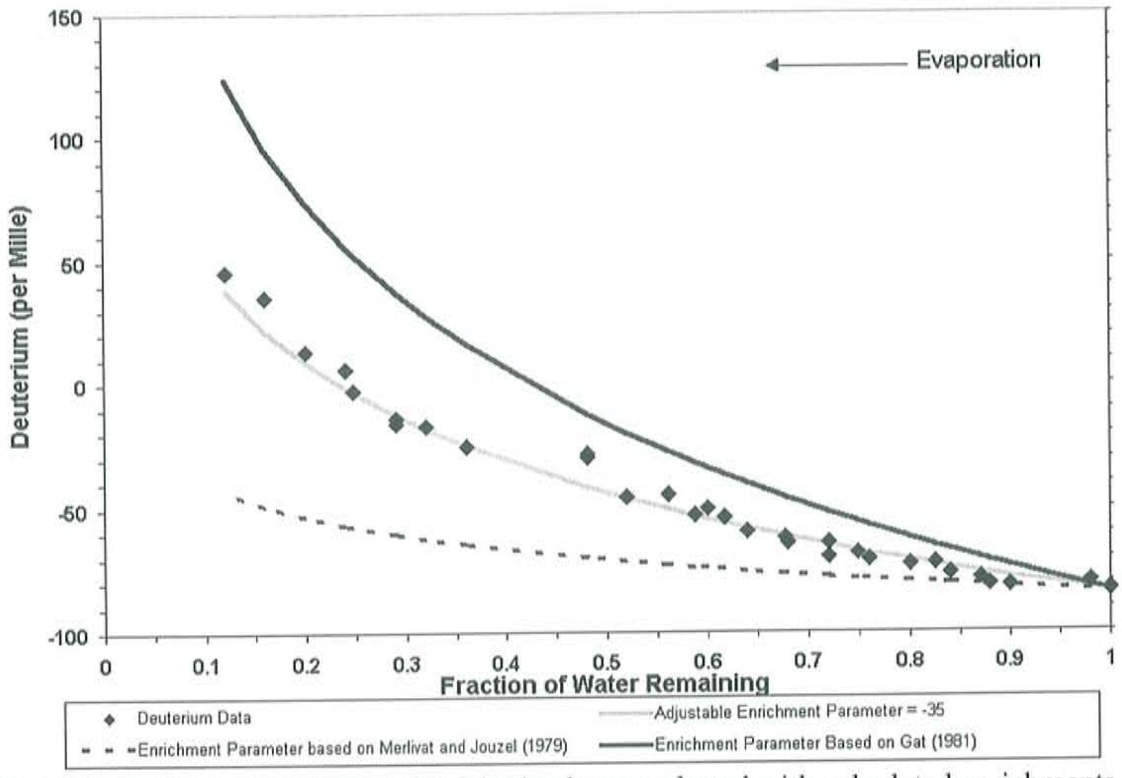

Figure 65 Deuterium data from the deionized water plotted with calculated enrichments bounds based upon the work of Merlivat and Jouzel (1979) and Gat (1981).

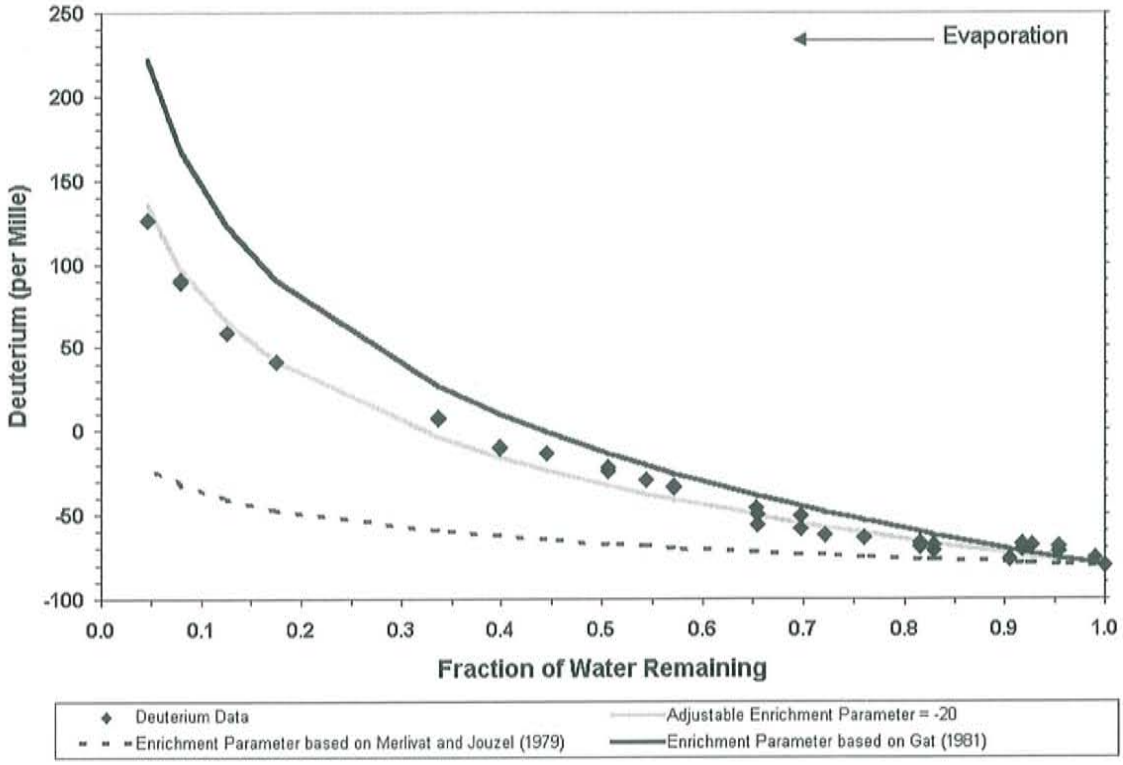

Figure 66 Deuterium data from the Na-HCO_3 solution plotted with calculated enrichments bounds based upon the work of Merlivat and Jouzel (1979) and Gat (1981).

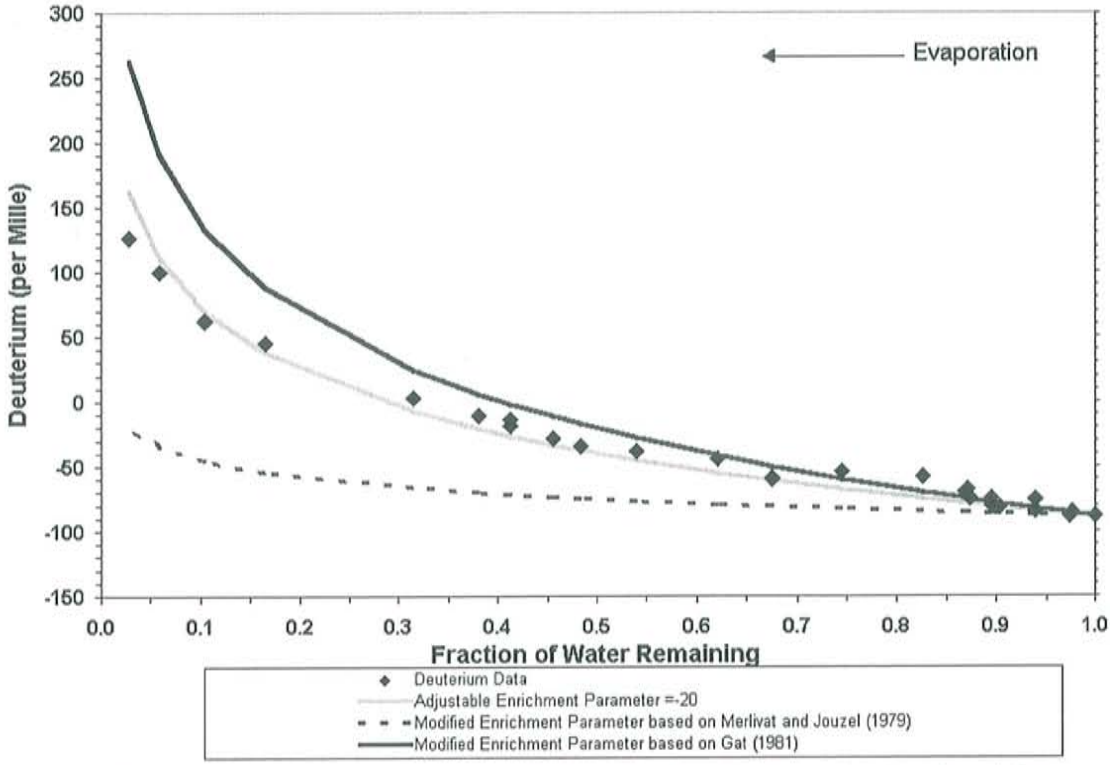

Figure 67 Deuterium data from the Ca-Na-HCO_3-Cl plotted with calculated enrichments bounds based upon the work of Merlivat and Jouzel (1979) and Gat (1981).

L.2. Oxygen-18 and Deuterium Mixing Solutions during Hydration

The model detailing the mixing calculations was described in section 3.2.2. The oxygen-18 data and the mixing calculation results match reasonably well with less than a ±2‰ difference over the entire hydration phase for both the Na-HCO_3 and Ca-Na-HCO_3-Cl solutions (Figure 68 and Figure 69). The 2‰ difference is most likely due to errors in estimating the volume. However, the deuterium data are more complex (Figure 70 and Figure 71). Model calculations exceed the data by 20‰ in some cases. This difference suggests that deuterium may be more sensitive to small errors in volume or evaporation than oxygen-18.

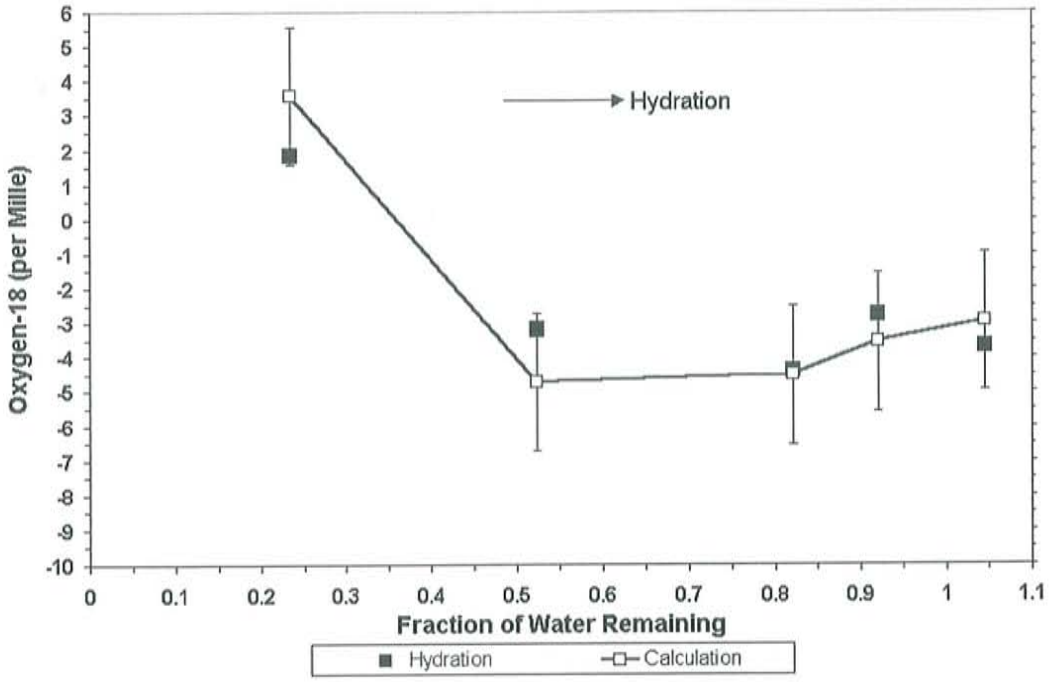

Figure 68 Oxygen-18 measurements during the hydration of the Na-HCO_3 solution compared with the calculation results. The ±2‰ error bars on the calculation result demonstrate the fit of the calculation to the data and do not represent the error associated with the data measurement.

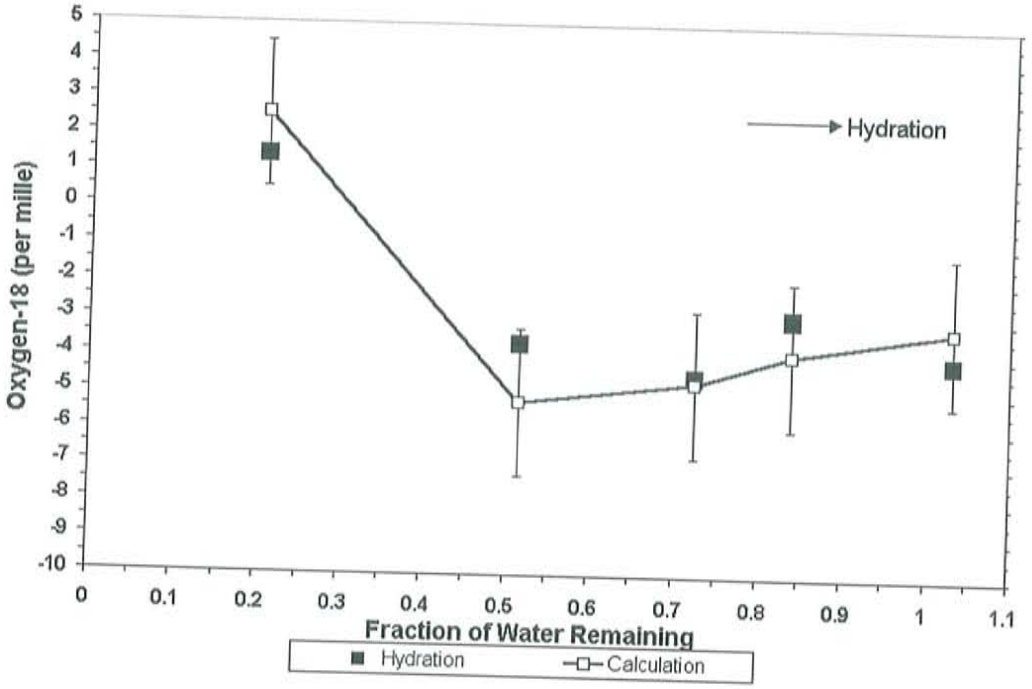

Figure 69 Oxygen-18 measurements during the hydration of the Ca-Na-HCO_3-Cl solution compared with the calculation results. The ±2‰ error bars on the calculation result demonstrate the fit of the calculation to the data and do not represent the error associated with the data measurement.

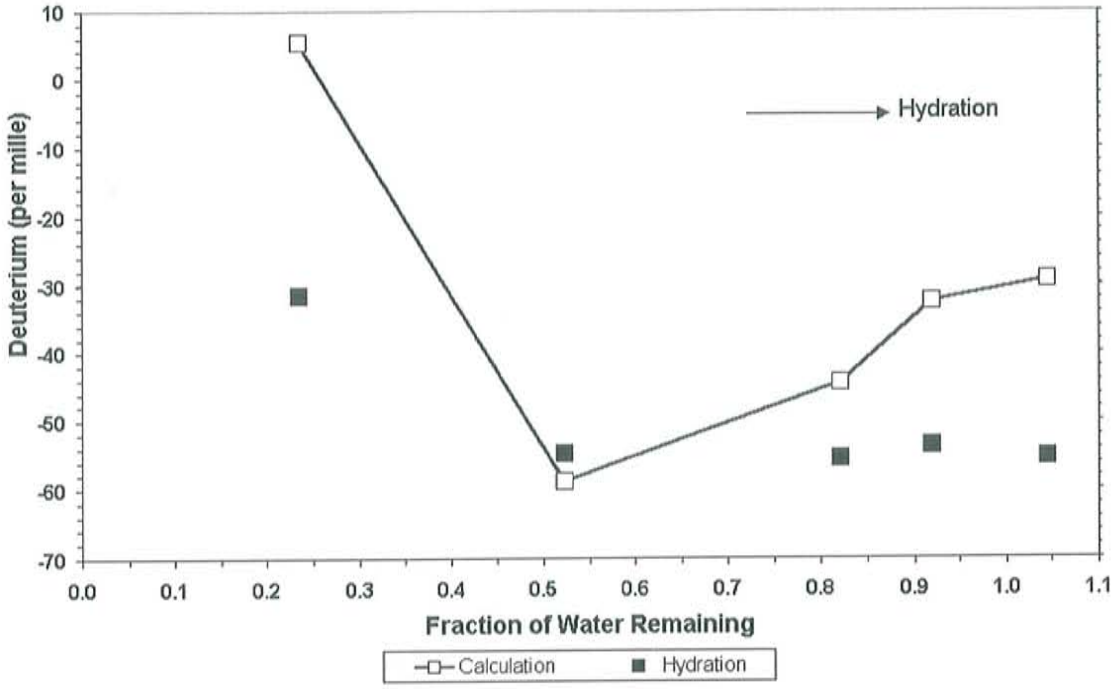

Figure 70 Deuterium measurements during the hydration of the Na-HCO_3 solution compared with the calculation results.

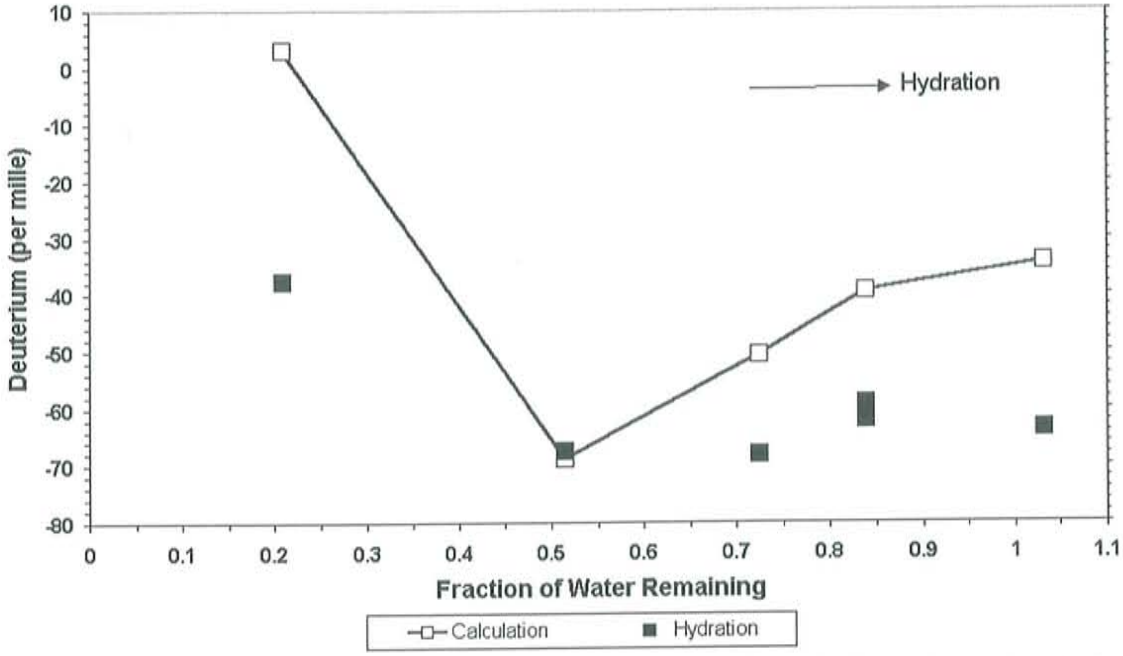

Figure 71 Deuterium measurements during the hydration of the Ca-Na-HCO_3-Cl solution compared with the calculation results.

L.3. Relationship of Oxygen-18 and Deuterium to the Global Meteoric Water Line

The oxygen-18 and deuterium data for all three solutions do form a straight line, with an initial value on the GMWL. The slope values from both the hydration and evaporation data set were between 3.9 and 4.1 (Figure 72 through Figure 74), suggesting that the relative humidity was lower than 85% (Clark and Fritz, 1997). This is consistent with the average measured humidity of 18.4% during the experiment.

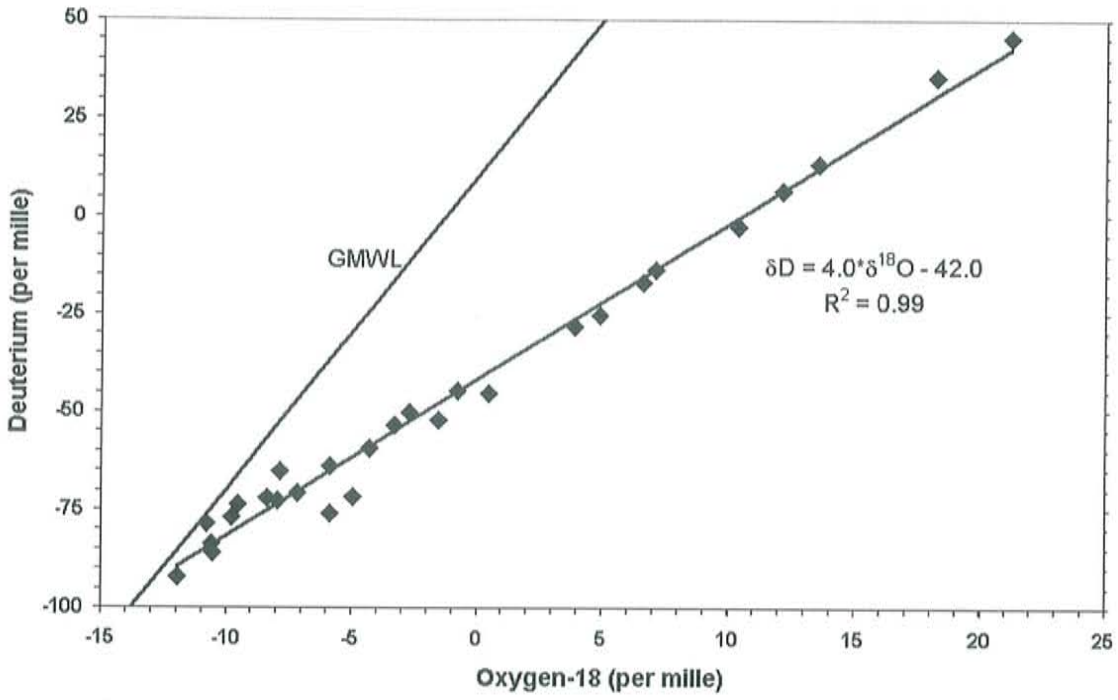

Figure 72 Relationship between Oxygen-18 and Deuterium from the deionized water.

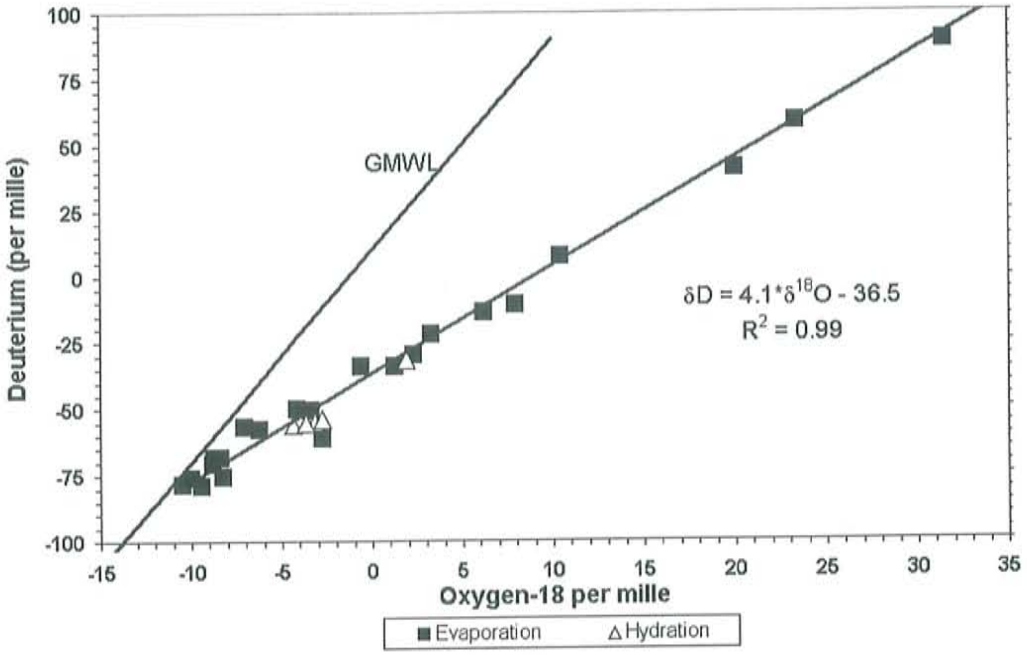

Figure 73 Relationship between Oxygen-18 and Deuterium from the Na-HCO_3 solution.

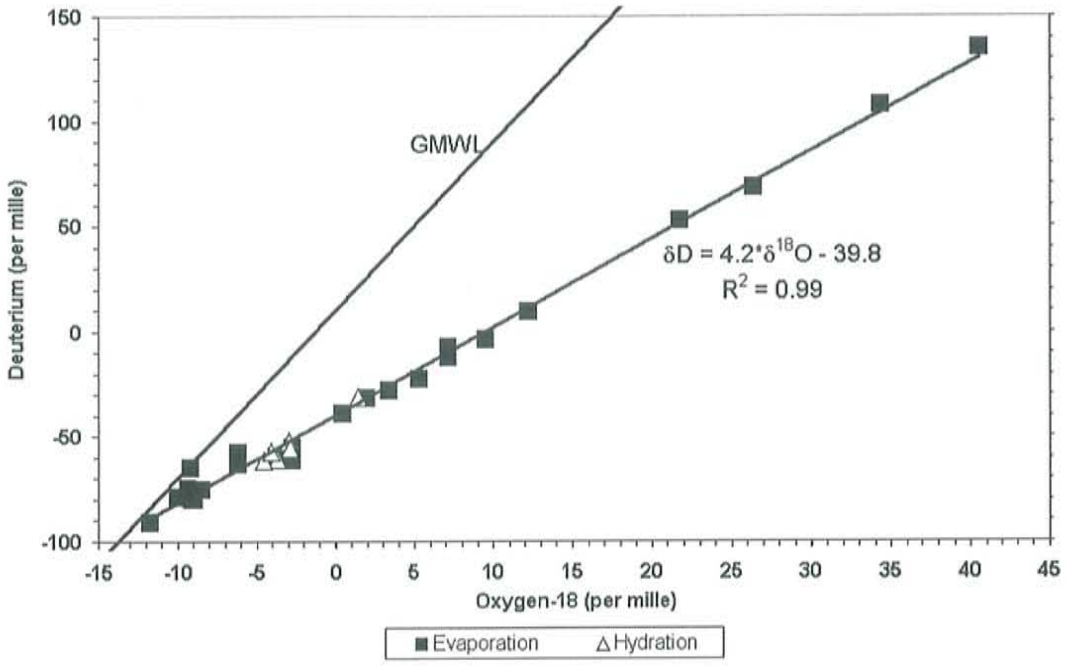

Figure 74 Relationship between Oxygen-18 and Deuterium from the Ca-Na-HCO_3-Cl solution.

L.4. Carbon-13 Evolution with Changing Total Carbon

Some interesting trends resulted from examining the evolution of carbon-13 against the fraction of total carbon remaining in the solution during the evaporation of the Na-HCO_3 and the Ca-Na-HCO_3-Cl solution. The Na-HCO_3 solution (Figure 75) degassed less than 50% of the total carbon, although 90% of the water evaporated. The large enrichment in carbon-13 did not follow a pattern consistent with Rayleigh distillation (logarithmic curve). The majority of the enrichment of carbon-13 occurred with little loss of total carbon. In other words, the water vapor was removed while carbon-12 was exchanged for carbon-13, but total carbon mass decreased little.

The evolution of the Ca-Na-HCO_3-Cl solution (Figure 76) differed somewhat from the Na-HCO_3 solution, as the carbon was lost either to degassing or calcite precipitation. There was a 20% loss of carbon during the initial stages of evaporation that coincided with ~15‰ enrichment in carbon-13. The next 50% resulted in a 5‰ increase in delta carbon-13. As the final ~30% of the total carbon were removed; the delta carbon-13 showed minimal change. The Ca-Na-HCO_3-Cl solution was similar to the Na-HCO_3 solution in that the majority of enrichment occurred with little loss in total carbon again indicative of an exchange process. However, unlike the Na-HCO_3 solution, the Ca-Na-HCO_3-Cl solution had multiple episodes of enrichment that coincided with little loss in total carbon. These periods suggest that exchange of carbon-12 with carbon-13 was occurring in both solutions despite the fact that the solutions were supersaturated with respect to carbon dioxide and in contact with the atmosphere.

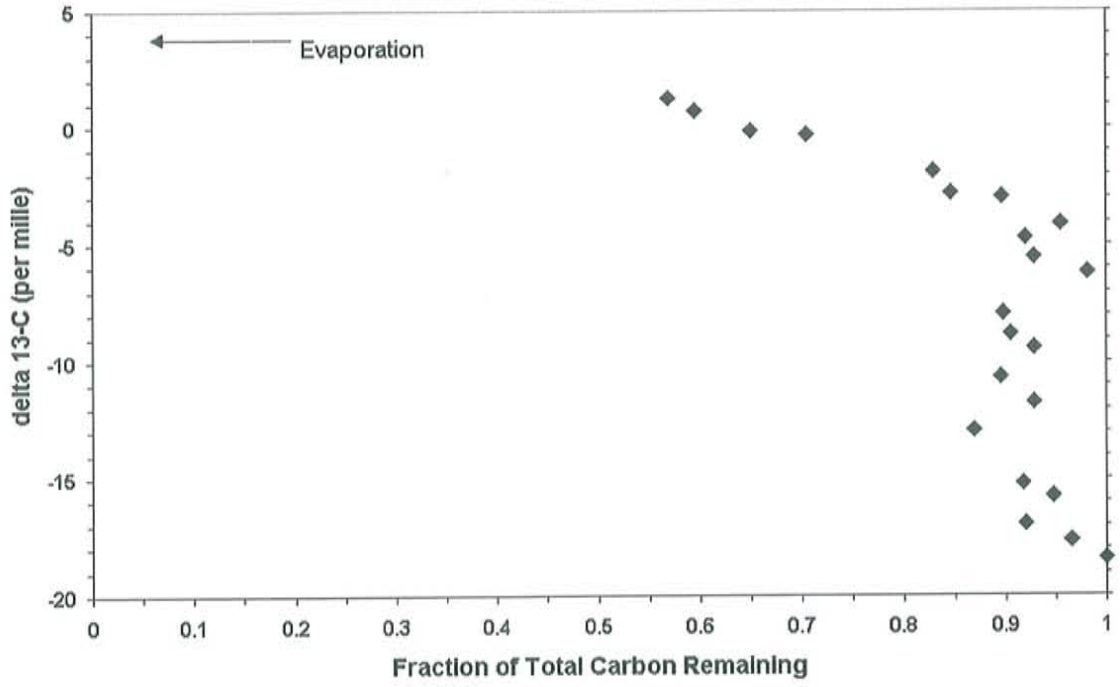

Figure 75 Delta carbon-13 measured in DIC versus fraction of total carbon during the $NaHCO_3$ solution evaporation.

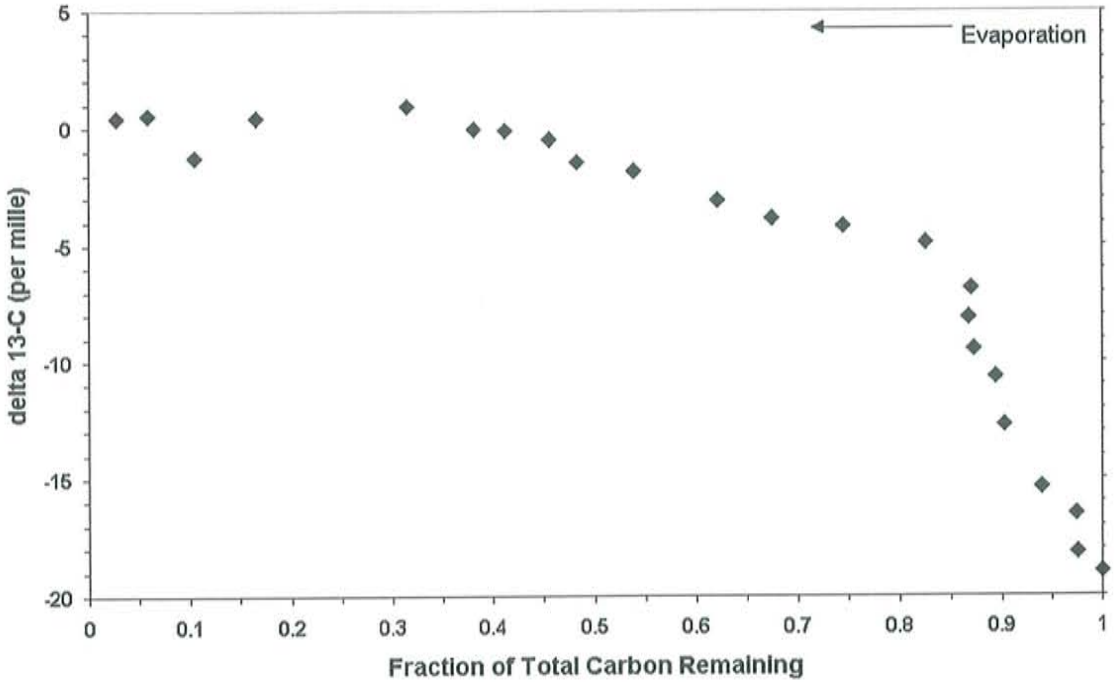

Figure 76 Delta carbon-13 measured in DIC versus fraction of total carbon during the Ca-Na-HCO_3-Cl solution evaporation.

M. Examination of Calculated Carbon Dioxide Supersaturation

The apparent supersaturation in both of the chemical solutions with respect to dissolved CO_2 poses several problems for the interpretation of other pieces of chemical and isotope data. For instance, the evolution of $\delta^{13}C$ when compared to the fraction of total carbon shows periods of exchange rather than CO_2 degassing. The calculated P_{CO2} values indicate that the solution should have been degassing throughout the entire evaporation phase. This contradiction is explored through examination of the data from the Na-HCO_3 solution in the following subsections.

M.1 Calculation Error

One possible explanation for the apparent CO_2 supersaturation is an error in calculation of the P_{CO2} values. Corrections were made for temperature and solution activity but these provided for only minor shifts in the calculated P_{CO2} values. The geochemical code PHREEQC was used to calculate the P_{CO2} at each sampling point based on the measured solution chemistry. Figure 77 shows the P_{CO2} values calculated based on equation (53) and the values calculated by PHREEQC. The overlap between the two approaches confirms that an error was not made during the calculation of P_{CO2}.

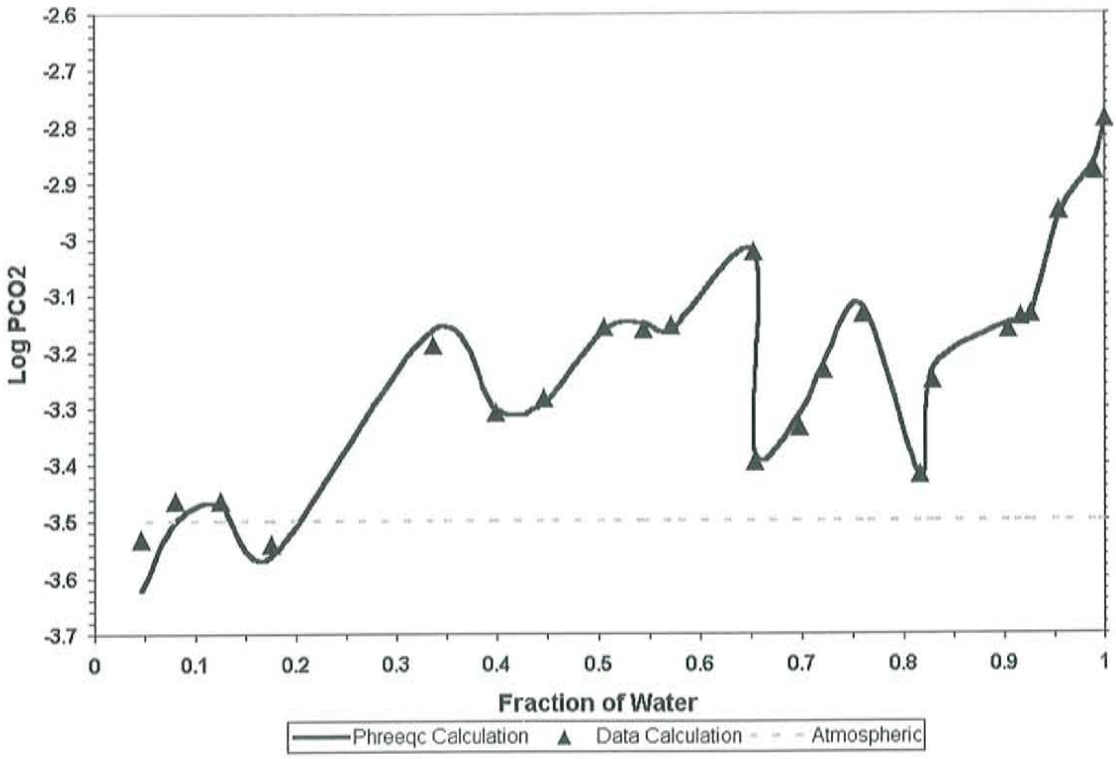

Figure 77 P_{CO2} values calculated using equation (53) and by the geochemical code PHREEQC.

M.2. Error Propagation

The P_{CO2} calculation is most sensitive to changes made in the pH measurement, which has an error of ±0.2 pH units. Calculation of the error (Bevington and Robinson, 1992, pg. 47) introduced to the P_{CO2} calculation shows that the lower bound does periodically cross the globally averaged atmospheric equilibrium line of $10^{-3.5}$ (Figure 78). However, the periodic crossing of the lower bound does not explain the supersaturated nature of the mean value.

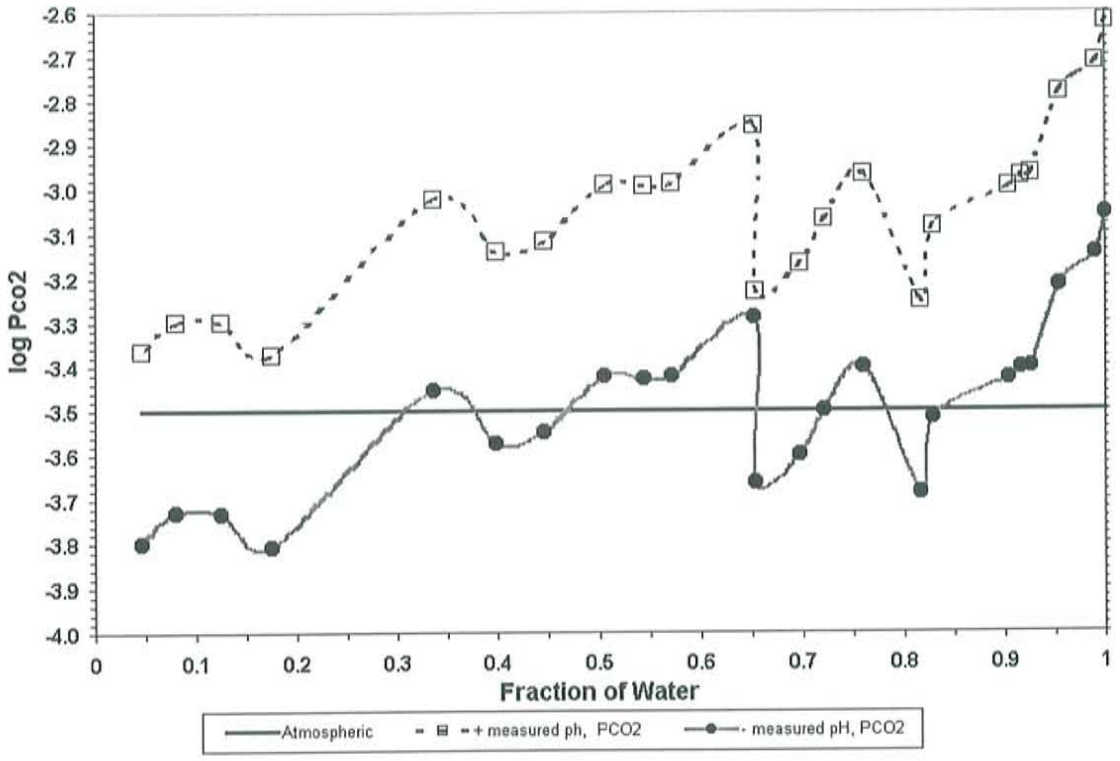

Figure 78 Upper (dashed) and lower (solid gray) P_{CO2} uncertainty bounds from the propagation of pH measurement error.

M.3. Boundary Layer Diffusion

The boundary layer at the surface of a solution can influence the flux of gases into and out of the solution by diffusion. An excessively thick boundary layer (>2000μm) can significantly impede the equilibration of a solution with the atmosphere because of the slow diffusion process. Boundary layer depths in ocean waters are generally considered to be between 20 and 200 μm (Asher and Wanninkhof, 1998). The boundary layer (z_d) was calculated following Asher and Wanninkof (1998)

$$F = \frac{D}{z_d} * (K_h P_a - C_w) \tag{60}$$

where F is the flux at the surface, K_h is the inverse of the Henry's law solubility, P_a is the atmospheric partial pressure, C_w is the concentration near the surface of the water, and D is the diffusion coefficient of the species in water. In the case of the Na-HCO_3 solution, the calculated boundary layer was no greater than 3-μm thick and decreased as the total water decreased (Figure 79). Clearly, a boundary layer thickness of less than 3-μm should not significantly limit diffusion of CO_2 to the atmosphere.

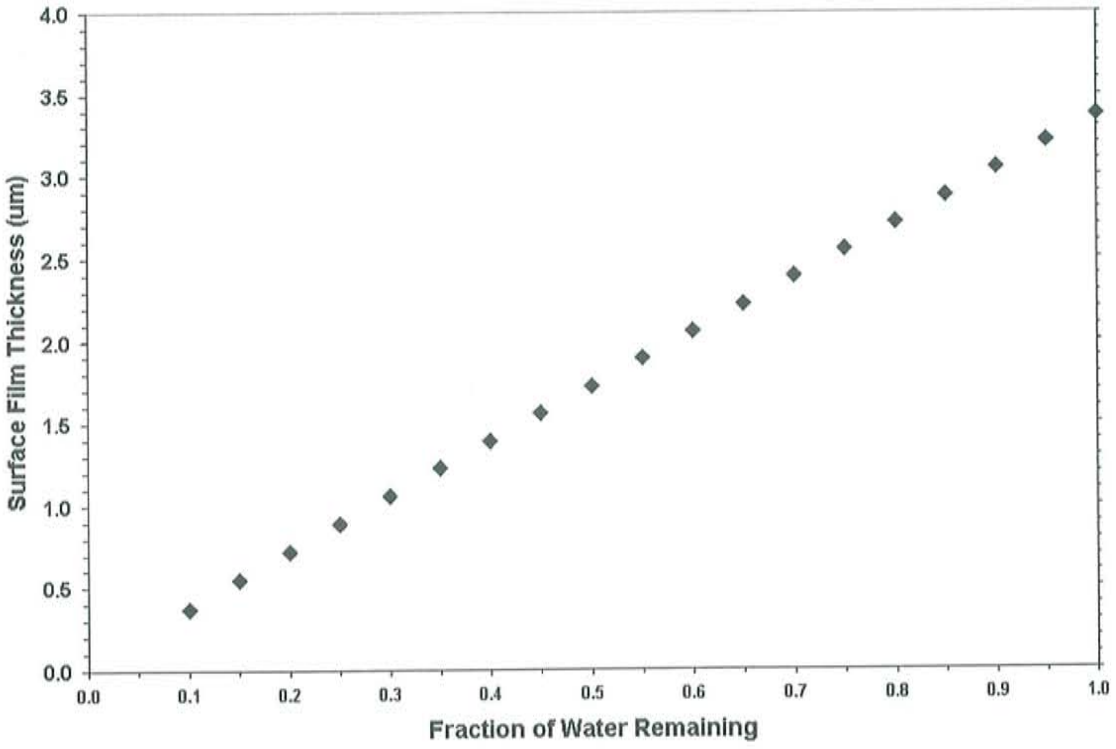

Figure 79 Boundary layer thickness calculations from the evaporating Na-HCO_3 solution.

M.4. Atmospheric Carbon Dioxide

It was initially assumed that the atmospheric carbon dioxide concentration was $10^{-3.5}$ atm. However, atmospheric carbon dioxide records collected as part of the NOAA/CMDL air sampling network show steady long term increases (Figure 80) and short term cyclic behavior (Figure 81). Air samples collected in flasks and analyzed for CO_2 at the Niwot Ridge sampling station in Colorado provided data that are consistent with other stations in the United States. The data show an annual minimum of P_{CO2} between August and September and a maximum between March and May (Conway et al., 1994). The seasonal variations average 8 to 9 ppm (v) (parts per million by volume) and were too small to cause a noticeable change in the solution P_{CO2}. Extrapolating the long

term average increase of 1.4 ppm (v) per year to 1998 suggest that the average atmospheric concentration would be on the order of 365 ppm (v). This changes the P_{CO2} from $10^{-3.5}$ to $10^{-3.43}$. While this conservative estimate does not account for the consistent supersaturation within the solutions, it calls into question the validity of using the global average value of P_{CO2} for these experiments.

The evolution of carbon-13 compared with the change in total carbon suggests that, contrary to the P_{CO2} calculations, the solution was in equilibrium and responding to changes in the atmosphere. Without direct measurements of CO_2 concentration above the solutions during the experiment, further analysis is not possible.

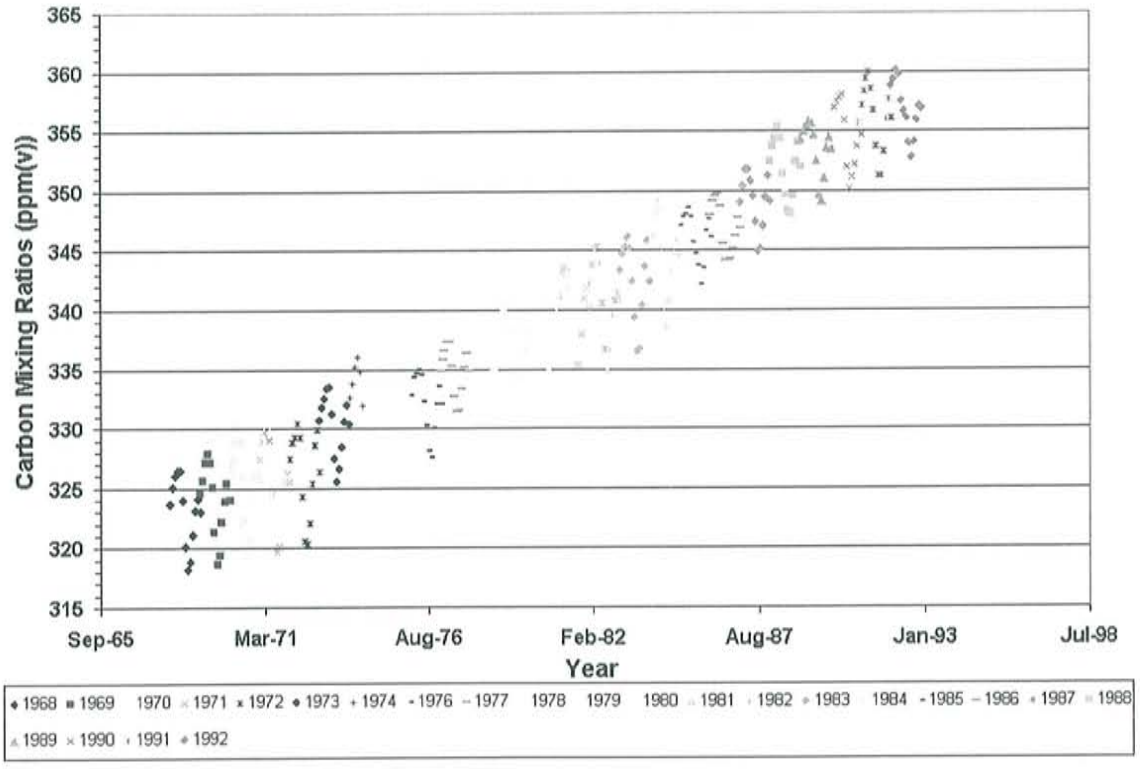

Figure 80 Carbon mixing ratios from 1968 to 1992 at the Niwot Ridge station in Colorado. The data show long-term increases in the average Carbon dioxide of 1.4 ppm (v) per year and short term seasonal variations averaging 8 to 9 ppm (v) per year.

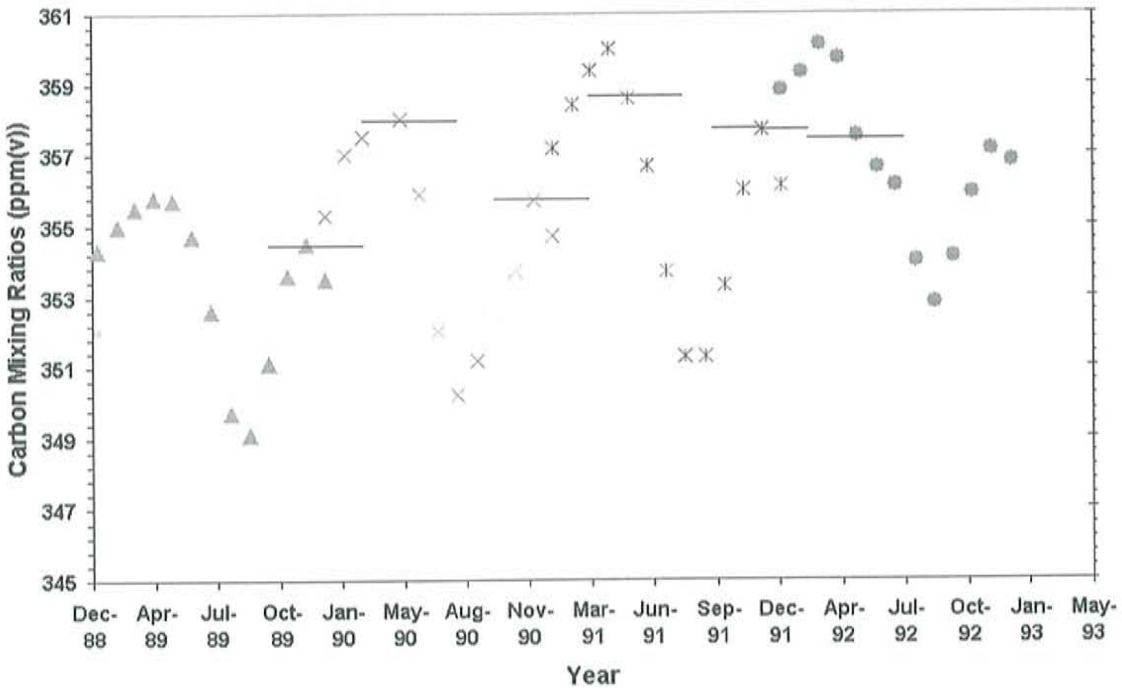

Figure 81 Example of the short-term variations in carbon dioxide concentrations from 1988 to 1992 measured at the Niwot Ridge station in Colorado. The black lines mark the beginning of the experiment in December and the ending in May.

M.5. pH Meter Measurement Bias

The pH meter used to collect all of the direct pH measurements from the solution tanks and the alkalinity measurements was checked for equipment bias. The pH meter used during the experiment (referred to as the experimental meter) was compared to a Triple Check meter (model number A55220, serial number B807828142 referred to as the comparison meter). The comparison meter is maintained by the New Mexico Bureau of Mines and Mineral Resources Chemistry Laboratory. Both meters were independently calibrated using different pH buffer solutions. Each meter was then used to measure all

of the buffered solutions. These measurements showed good agreement, with the exception of the pH 4.0 buffer. This was due to the difference in calibration. The comparison meter used a three-point calibration (pH 10.0, pH 7.0 and pH 4.0) and the experimental meter has only a two-point calibration (pH 10.0 and pH 7.0). A difference of ~0.1 pH units was observed on an independent water sample. The experimental meter produced pH measurements 0.1 pH units lower than the comparison meter. This difference was within the measurement error of the meter (±0.2 pH units). However, adding 0.1 pH units to the pH measurements collected during the evaporation/hydration experiments did lower the uncertainty bounds calculated by error propagation analysis and lowered the calculated P_{CO2} (Figure 82). The overall atmospheric P_{CO2} value was also increased based upon section 4.5.4. At this point, the two bounds bracket the atmospheric line almost entirely. Although the high mean P_{CO2} value is not completely explained, statistically the Na-HCO_3 solution is in equilibrium with the atmosphere during the experiment.

Standard	Experimental Meter	Comparison Meter
Experimental Buffer 4	4.0	4.09
Experimental Buffer 7	6.98	6.98
Experimental Buffer 10	10.4	9.98
Experimental Buffer 7	6.99	6.98
Experimental Buffer 10	10.3	9.98
Comparison Buffer 4	3.92	4.0
Comparison Buffer 7	7.01	7.0
Comparison Buffer 10	10.05	10.01
Field Sample	8.17	8.29
Field Sample	8.2	8.3

Table 27 Results of examination of experimental pH meter bias when measuring standards and a field sample.

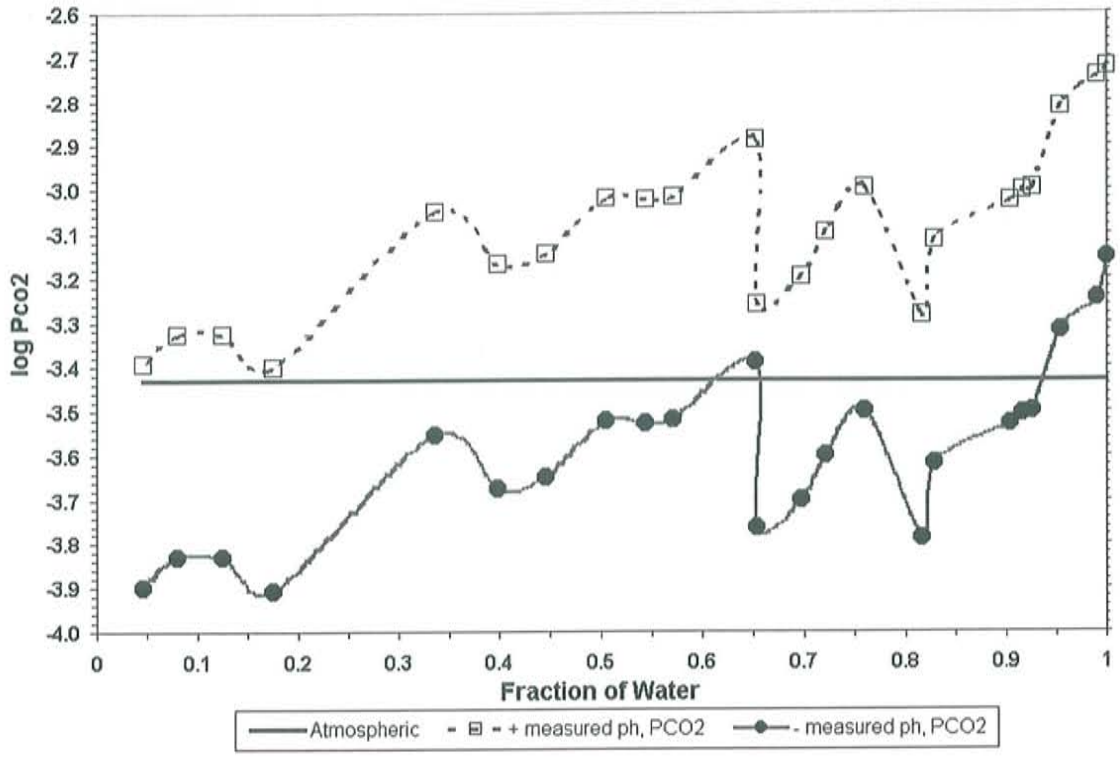

Figure 82 Adjusted P_{CO2} uncertainty bounds and an increased atmospheric P_{CO2} based on increasing trends.

N. Calcium Saturation

The Ca-Na-HCO_3-Cl solution was designed to be saturated with respect to calcite at the start of the experiment. The changes in calcium concentration are due to the formation of calcite. The amount of precipitated calcite during the evaporation is calculated based on the assumption that changes in calcium concentration reflect the formation or dissolution of calcite. This kind of precipitation-dissolution history has proven difficult to model using PHREEQC for this case. PHREEQC simulated calcium concentration based on the assumption that once the water was saturated with respect to

calcite, precipitation would occur and continue as long as the solution composition was in equilibrium with calcite. The geochemical code did not allow for the dissolution of calcite when the solution was saturated with respect to calcite. The model assumed that the Ca-Na-HCO_3-Cl solution started evaporating at the calcite solubility and should have formed a precipitate immediately. However, calcite precipitate was not visible in the solution at the time corresponding to f = 0.95. The lack of immediate precipitation and the apparent dissolution of calcite are in direct conflict with the geochemical model. However, supersaturation of $CaCO_3$ without precipitation is commonly observed in natural waters worldwide. Adjustment of the saturation index within in the model resulted in variable changes in calcium concentration during the evaporation, but none of the adjustments provided a good match to the entire data set (Figure 83). The adjustments to the saturation index changed the onset of precipitation and the concentration of calcium during the evaporation. However, the changes in the saturation index did not change the final values at the end of each model run.

The change in calcium concentration from the evaporation and hydration phases of the Ca-Na-HCO3-Cl solution was not expected to behave in the same conservative manner as sodium. The calcium evaporation data show a complex precipitation and dissolution pattern that resulted in an overall decrease in calcium concentration. The geochemical model was unable to model the evaporation or hydration changes in calcium concentration. The geochemical model assumes that all of the calcium was used to form calcite during the evaporation, and so the modeled calcium value was below detection in the hydration phase and most of the evaporation phase. Increasing the saturation indices

(SI) allows for better matches to portions of the calculated amounts of precipitated calcite (Figure 84).

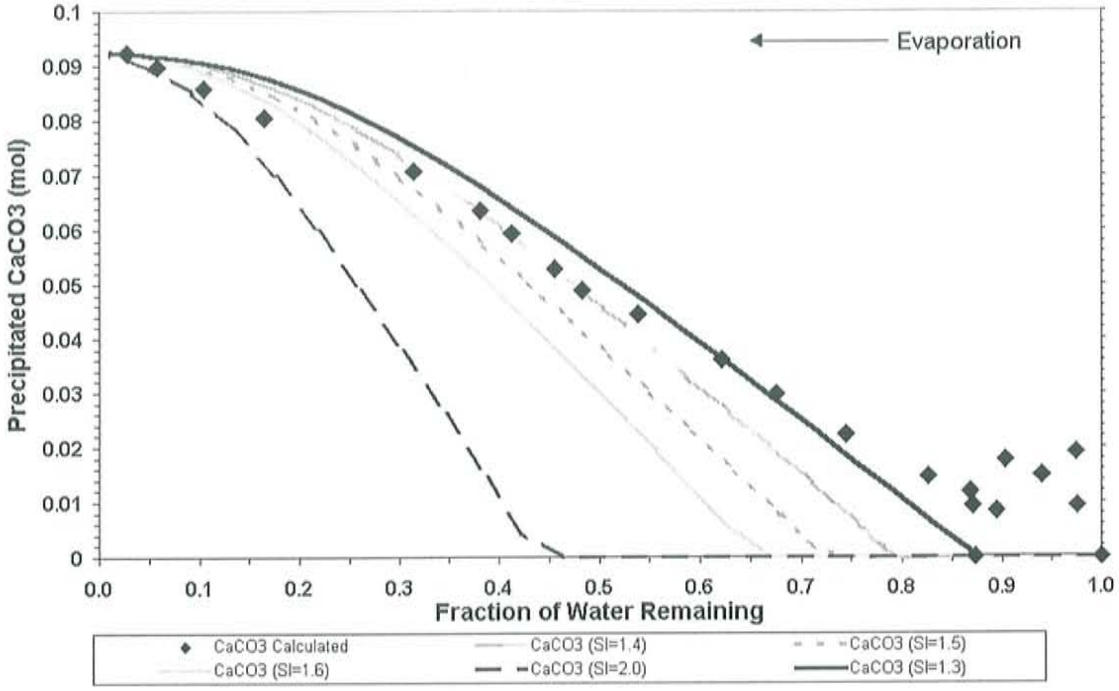

Figure 83 Calculated amounts of precipitated calcite with curves of precipitated calcite from PHREEQC. No one SI matches the entire data set.

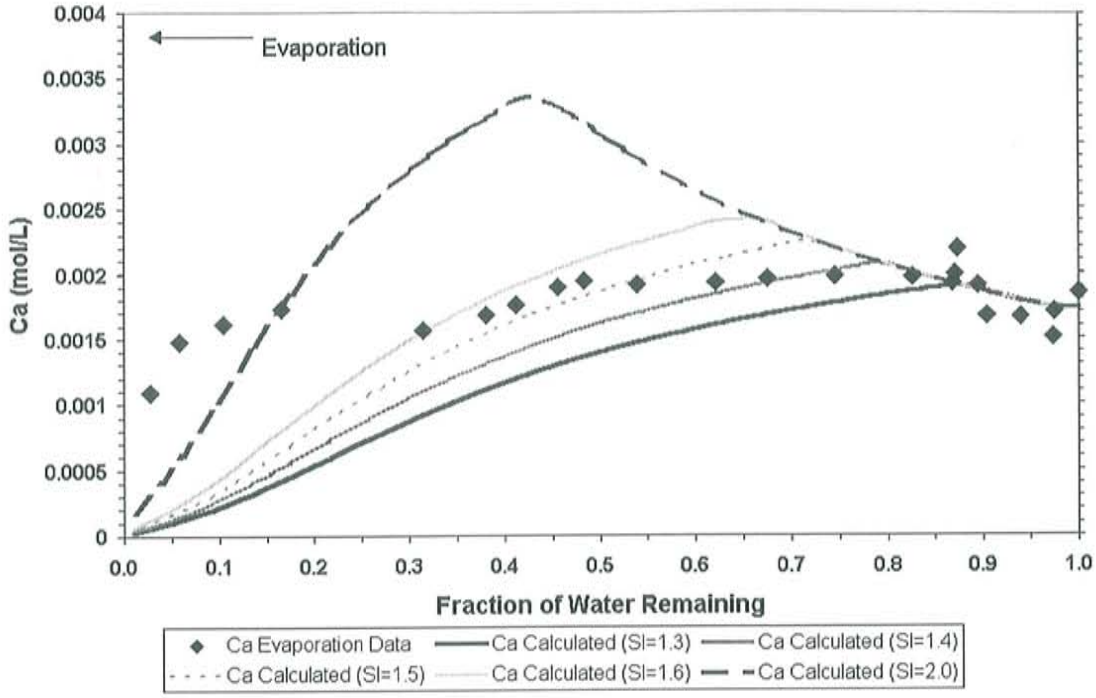

Figure 84 Modeled and measured calcium for the evaporating Ca-Na-HCO_3-Cl solution. The family of curves generated by different saturation indices (SI) does not produce one curve that fits a majority of the measured data.

O Examination of Intermediate Na-HCO_3 Data

The evaporation of the Na-HCO_3 solution shows three phases: a early phase of CO2 degassing, and intermediate phase where the pH increases but DIC remains approximately constant, and the final phase of evaporation-driven degassing. Initially, the intermediate phase appeared quite anomalous because of the relatively constant DIC compared to the 50% reduction in water volume. However, the intermediate Na-HCO3 data by comparison with PHREEQC model runs are not anomalous. The PHREEQC model runs show small regular changes in DIC during the same period. The pH increases

are also small in both the experiment and the model. Carbon dioxide is being degassed but in small quantities (~0.001 mol per water removal step) relative to the early and late phases. Figure 85 shows the bicarbonate data compared with the PHREEQC. The data points are in good agreement with the PHREEQC calculated line (dashed) except around an f of 0.5. The error bars show +/- 5% as a guide for the eye not any assessment of error.

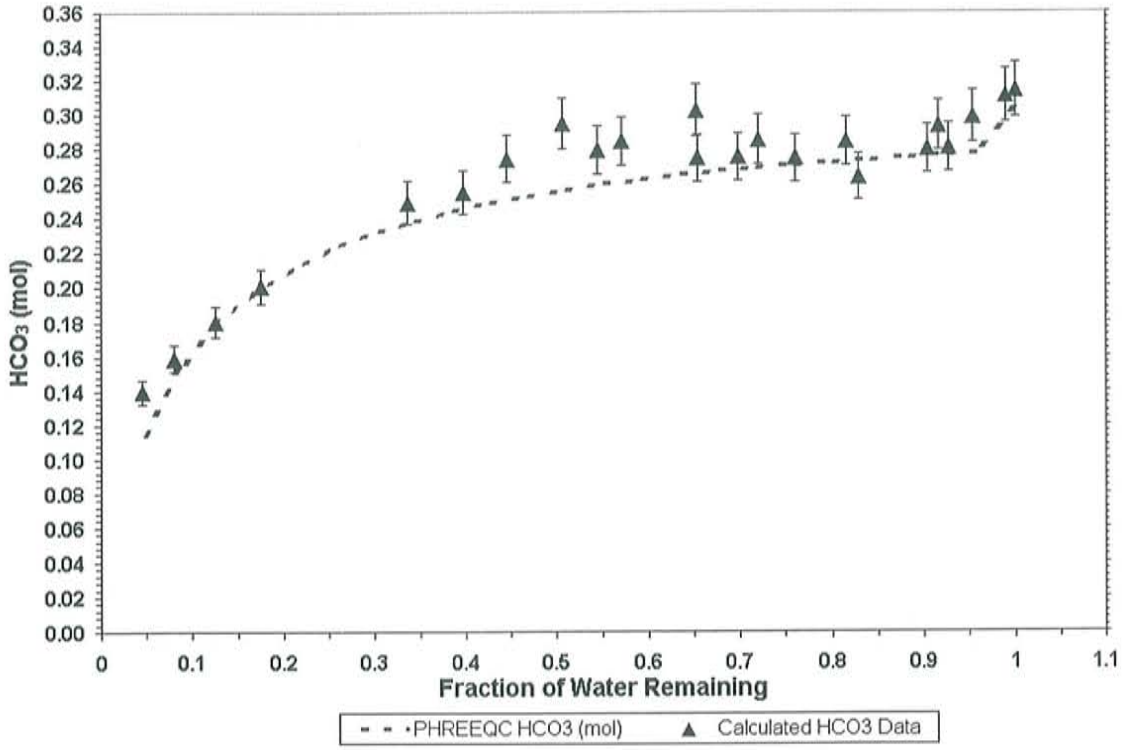

Figure 85 Na-HCO_3 evaporation Bicarbonate data and model comparisons.

This thesis is accepted on behalf of the
Faculty of the Institute by the following committee:

Fred M Phillips
Advisor

Robert A. Sanford

Andrew Campbell

MAY 3, 2007
Date

I release this document to the New Mexico Institute of Mining and Technology.

Alyssa J Olson
Student's Signature

5-16-02
Date

verbal authorization